ASPECTS OF THE MICROMAGNETIC LAGRANGIAN: DUALITIES, GAUGE STRUCTURE AND SPIN WAVE THEORY

by

Sayak Dasgupta

A dissertation submitted to The Johns Hopkins University in conformity with the requirements for the degree of Doctor of Philosophy

Baltimore, Maryland

November 2020

Abstract

Our work deals with developing effective Lagrangian descriptions to capture the dynamics of excitations in magnetically ordered systems. Working in the continuum limit of micromagnetism, where spins in ordered systems can be expressed as classical vectors, we study the nature of discrete soliton structures (domain walls and vortices) and spin waves. In this thesis we present the field theories developed for a planar ferromagnet and vortices, for the two sublattice antiferromagnet and the three sublattice antiferromagnet. For the planar ferromagnet we show that the spin-field theory is dual to a theory of electromagnetism in 2+1 dimensions with vortices acting as centres of charge and flux. We argue that these charge-flux particles can exhibit quantum statistics that switches between fermions and bosons. For the two sublattice antiferromagnet we devise a method to obtain a gauge connection for the Neel field, which does not carry spin angular momentum, and use it to generate a Magnus force (Hall effect) on antiferromagnetic vortices. We end with a description of the three sublattice triangular antiferromagnet in terms of normal modes of a triangle. We explicitly derive the spin wave spectrum for these systems and extend it

to more complicated stacked systems such as Mn_3Ge. Our field theory reveals some interesting connections including a mapping of the spin modes to an emergent theory of elasticity. We end by deriving the additions made by external fields like magnetic fields, strains and local anisotropies to the Lagrangian density.

Primary Reader and Advisor: Oleg Tchernyshyov

Secondary Reader: Collin Broholm

Acknowledgments

Frist and foremost I would like to express my sincere gratitude to my advisor Prof. Oleg Tchernyshyov whose guidance in matters physics and life in general, has been invaluable. Oleg is patient and careful listener and has given me the opportunity to grow as a researcher, encouraging, often insisting on original thought. His approach to the philosophy of doing science is something I am going to lean on for a while to come. I would also take this opportunity to thank my collaborators Prof. Se Kwon Kim, Shu Zhang, Allen Scheie, Prof. Ibou bah, Youzhe Chen, Jonathan Gaudet, Prof. Collin Broholm, Dipanjan Chaudhuri, and Prof. Peter Armitage. It was an immense pleasure working with them and learning physics from them. In particular I thank Collin for his patient hearing of ideas as I navigated the tricky world of neutron scattering in magnetic systems. I also thank Prof. Serra and Kirsten for sharing their work on nematics. Thanks is owed to Reid Mumford, Kelley Key, Pam McCullough for the amount of behind the scenes work they have put in.

Thank you to my fellow physicists who lit up the concrete dreariness that is Bloomberg with their passionate defence of the (un ?)physical world. Specially Anir-

ban da, Hitesh, Fahad, Eric, Canon, Kim and Mike. Fahad it would give you great pleasure to know that you will soon have a fellow chicken (you know what) joining the ranks at UBC. An immense debt of thanks is owed to the student community of Johns Hopkins University without whom I would never have realized how much I love teaching and engaging in science education. Thank you to Maddy, Sarah R, Erini, Heena, Eric, Alice, Zubia, Matthew, Vedant for making the onerous task of teaching pleasurable. If I end up teaching professionally it will be because of you folks. A very special thank you to Fran for successfully distracting me from the global pandemic through tutoring her in physics.

And finally to my friends and family here and back home. A Ph.D. is less of a destination and more of a journey and without you the wheels would have come off a long while ago. To mom and dad who (begrudgingly at first) admitted that a 'Dr' in physics might be a doable thing after all ! And then made every effort to support me through it. To my sister thank you for being the repository of all my anguish. To Suzy who happily shared her research, and life with me. In an academic (and possibly very real sense) we are siblings. Thanks to Indu, Purba, Swap, Shayoree, Abhinav, Nitica who are always there to hear me out on my rants especially Indu, Swap and Shayoree who have been around forever. And my house-mates (life-partners ?) Dipen and Keisuke, what can I say ? Should we do this again ? Maybe somewhere with access to a good biriyani and actual mangoes..

Contents

Abstract **ii**

Acknowledgments **iv**

List of Tables **x**

List of Figures **xi**

1 Introduction to micromagnetism **1**

1.1 Dissertation outline 1

1.2 A (very) brief review of microscopics 6

1.3 The micromagnetic approach 10

1.3.1 Topological Defects - Solitons 14

1.3.1.1 Planar Vortex 15

1.3.1.2 Uniaxial domain wall 17

1.3.2 Collective coordinates and zero modes 18

1.4 Dynamics of magnetic moments 19

1.4.0.1 Domain wall dynamics 22

1.4.0.2 Vortex dynamics 24

1.4.1 The micromagnetic Lagrangian 25

1.5 Spin-waves 28

2 The planar ferromagnet and its electromagnetic dual 31

2.1 Introduction 31

2.2 The planar Heisenberg ferromagnet 37

2.3 Electromagnetism in 2+1 dimensions 40

2.4 The dual theory at low energies 43

2.4.1 Gauge field 44

2.4.2 Coupling field and current 46

2.4.3 Duality via an auxiliary field 47

2.5 The dual theory near the vortex core 48

2.6 Quantum statistics of vortices 50

3 Two-sublattice antiferromagnets 55

3.1 Introduction 55

3.2 The kinetic term and spin wave spectrum 59

3.3 Moving antiferromagnetic solitons 63

3.3.1 Magnetic field 65

3.3.2 Spin Transfer Torque 72

3.3.3 Dzyaloshinski-Moriya Interaction 74
3.3.4 Crossed Interactions 75
3.3.5 Antiferromagnetic vortices and (re)emergence of Berry curvature 78
3.4 Discussion 81

4 Three sublattice antiferromagnets 83

4.1 Introduction 83
4.2 Lattice and geometry 86
4.2.1 Local geometry of the normal modes 88
4.2.2 Hard and soft modes 92
4.3 Field theory for the soft modes 93
4.3.1 Singlet 95
4.3.2 Doublet 96
4.3.3 Six-fold symmetric terms 98
4.4 Testing the theory on the triangular and kagome lattices 100
4.4.1 Triangular antiferromagnet 100
4.4.2 Kagome antiferromagnet 102
4.5 Stacked Kagome 104
4.5.1 Intralayer interactions 110
4.5.2 Interlayer interactions 111
4.5.2.1 In-plane velocities 113
4.5.2.2 Out-of-plane velocities 114

4.5.3 Symmetry features of the interplane interactions 114

4.6 Gapping the Goldstones 117

4.7 Coupling to external fields 120

4.7.1 Net spin in the ground state 121

4.8 Discussion 122

5 Discussion **130**

Bibliography **132**

Vita **147**

List of Tables

4.1 List of exchange parameters for Mn_3Ge 120

List of Figures

1.1 Examples of magnetic order 8
1.2 Examples of topological solitons 11
1.3 Spin wave in one dimension 28

2.1 Vortices as charge duals 33
2.2 Simulated vortex profiles using OOMMF 34
2.3 Exchange statistics of vortices 51

3.1 Uniaxial two sublattice antiferromagnet 57
3.2 Magnetic monopoles in ferromagnetic domain walls 58
3.3 Square-lattice antiferromagnet 60
3.4 Magnus force in the Antiferromagentic vortex 79

4.1 Triangular lattice prototypes 88
4.2 Ground state spin and normal modes of 120° order 89
4.3 Ground-state chirality 91
4.4 Spin wave spectrum examples 104
4.5 Comparison of model to experiment. 126
4.6 Heisenberg exchanges in Mn_3Ge. 127
4.7 Comparison of the effect of J_4 and J_1 on dispersion. 128
4.8 Local symmetry for six fold interactions. 129

Chapter 1

Introduction to micromagnetism

"If there was no spin there would be no physicists..."
- S Zhang (Suzy-speaks).

1.1 Dissertation outline

Magnetism is one of the oldest directions of scientific enquiry and was at least pondered on in qualitative terms by the ancients in their account of lodestones and their latter use in the science (and art) of navigation [1]. It also is perhaps one of the most fruitful. Its study in conjunction with developments in electronic and materials physics has been critical to the development of modern technology from the ubiquitous electric motor to the trapping of information on plastic real estate. More importantly, for the purpose of modern theoretical physics, electromagnetism is one of the fundamental components of the standard model of physics and forms one of

the pillars on which our constructions rest. Maxwell's formulation of the theory in terms of electric and magnetic fields is the prototypical field theory construction [2] whose accuracy forms the benchmark of any new field theoretic construction.

The microscopic picture of magnetism arrived on the heels of quantum theory with the realization that magnetism in materials is derived from the magnetic moments of electrons and their quantum statistics (fermions). This mechanism is simple enough to state but its details, in actual materials, are more often than not very complicated and intricate; depending heavily on the lattice and its surrounding constituents. One of the biggest current thrusts in the study of materials is to effectively understand their magnetic orders, or lack therein, and the governing mechanism.

While a problem of tremendous theoretical and practical importance, we shall not focus on this microscopic ordering in this thesis. Here our concern lies with systems below a critical temperature T_c where they are already ordered. In the ordered regime the individual magnetic moments can be taken to be classical angular momentum vectors in spin/moment space. In this thesis the approach we take is to promote these vectors to a vector field that lives on a sphere in 3 dimensions (or a circle in 2), embedded in space-time $(\mathbf{r}, t)$. This forms the basis of micromagnetic field theory.

In the classical field theory that describes the dynamics of these spin vector fields what is unique is the kinematic term. Unlike the field theory for classical angular momentum which have a quadratic kinetic term originating from a moment of inertia, the kinematic terms of spins are pure geometric phases [3, 4]. This has a profound

effect on the continuum field theory for spins, giving rise to theories where the particles (charges) of the theory can interpolate between fermions and bosons.

The questions that people in the community want to address in these ordered systems are primarily of two kinds. The first category relates to the creation and control of magnetic textures through external electronic currents aptly categorized as 'Spintronics'. The other question deals with the kind of magnetic order that forms in a particular material/lattice that and its characterization through an analysis of the spin-wave (disturbances from the ordered state) spectra. We provide instances of both in this body of work.

1. Spintronics, where our goal is to study the energetics of ferromagnets and antiferromagnets in terms of the vector fields, in order to identify topologically stable distortions in the order, and develop effective ways of moving them in space. Typical examples of such defects are domain walls and vortices. The term topological is used here in the sense that these solitons cannot be unwound/destroyed locally by rotating the moments.

In addition to the implications for device design and data storage [5] there are some basic mathematical and physical motives guiding this study. Firstly, the defects themselves are mathematically interesting solutions to the underlying field theory and secondly their dynamics often leads to a better appreciation of the system Lagrangian and how it can be extended to accommodate perturbations. We shall see examples of both the features in Chapters 2 and 3.

In Chapter. 2 we study the $O(2)$ field theory of ordered ferromagnetic moments confined (mostly) to the xy plane. We show, in some detail, how the theory can be mapped onto a dual theory. The dual is the theory of electromagnetism in 2+1 dimensions with vortices acting as electric charges. The spins in a vortex core cant out of the plane endowing these charges with attached magnetic flux lines. The geometric phase kinematic term then forces these charge-flux complexes to have a statistics that interpolates between fermionic and bosonic. In Chapter. 3 we study solitons in antiferromagnets. These are magnetic systems where locally the magnetic moments cancel each other leading to a suppression of the Berry phase. However, we show how to revive this geometric kinematic term and provide a generic recipe for electromagnetic gauge field like couplings in antiferromagnetic systems.

2. Materials study, where we use field theoretic models to study the local fluctuations of ordered spins in ferro and antiferromagnets. The fluctuations are created by probes like neutrons which can deposit momentum and angular momentum on the ordered spins. Our job lies in predicting the dispersions of these fluctuations through the derivations of an effective field theory, to get a better idea of the underlying order.

We shall look into one of these analyses in detail in Chapter. 4. This chapter features the spin wave theory for antiferromagnets with a local D_3 (triangular) symmetric environment. The magnetic unit cell involves three sublattices with the spins locked in a 120° order. In a surprising addition, our theory for the spin waves reveals a map to an emergent elasticity theory. We extract the parameters for the spin

Hamiltonian from our analytical theory.

To set the stage, in this chapter we shall briefly dwell on the microscopic picture of magnetism and the dynamics of its local components, the individual spins. Our motivation is to set up a framework to discuss various forms of magnetic order and deviations from the order that exist in magnetic systems and analysing the associated dynamics.

In the first part we familiarise the reader with the concepts and forms of magnetic ordering. We discuss the nature of excitations away from the magnetic ground state. In particular we pay special attention to a class of defects which are topologically protected, using the opportunity to introduce the language of collective coordinates [6].

We move on to a discussion of the equations governing dynamics of the magnetic moments. We shall work out such an example using the opportunity to introduce the notion of collective coordinates. We finish the chapter by setting up the methods to study gentle undulations of spins in an ordered system– 'spin-waves'. Spin wave dispersions are a much used probe in studying magnetic order and a sizeable part of this thesis will focus on their study.

1.2 A (very) brief review of microscopics

Magnetic systems that we shall look into in this thesis come in two varieties. Systems in which the local moments point along the same direction over a broad region in space (domains) called ferromagnets, see Fig. 1.1(a). The order is defined through a vector order parameter, the local magnetic moment. The tendency to order is driven by an exchange interaction whose origin lies in the combined effect of Coulomb interactions between electrons and the Pauli exclusion principle which forces the wave-function of the electrons to be antisymmetric.

Consider the situation: a two site - two electron system. The two electron wave-function ψ_{2e} has two parts: a spinor and a spatial part, $\psi_{2e} = \sigma_{2e} \otimes \phi_{2e}(\mathbf{r})$ where σ_{2e} is the spinor. Now ψ_{2e} has to be antisymmetric by the Pauli principle. This can be achieved through a symmetric spinor and an antisymmetric ϕ_{2e} or vice versa. To minimize Coulomb repulsion among themselves the electrons would like to occupy different spatial sites and would hence energetically favour an antisymmetric ϕ_{2e}. This forces the spinor to be symmetric which is achieved through the spins aligning, producing the required ferromagnetic unit. The exchange coefficient of typical ferromagnets such as Fe, Ni, and Co is of the order of 0.1 eV [7] which is the characteristic electronic excitation in atomic systems. This can be encapsulated in the Hamiltonian:

$$H = \sum_{i,j} J_{ij} \mathbf{S}_i \cdot \mathbf{S}_j \tag{1.1}$$

where $J_{ij} < 0$ are the exchange coefficients. Given the sign of the exchange it is easily seen that this model would prefer alignment of neighbouring spins. This model was derived by Heisenberg [8] and refined further by Dirac [9] in order to explain the multiplet structure of atoms, for instance the large energy difference between the singlet and triplet states of Helium. The exchange coefficients are representative of an overlap integral between the electronic wavefunctions at the two sites i and j and in general decays exponentially with $|\mathbf{r}_i - \mathbf{r}_j|$. The range of the interaction is thus limited to a few neighbouring sites.

Then there are ordered spin systems where there is zero net moment inside a domain see Fig. 1.1(b,c), called antiferromagnets. In this case one might define another vector order parameter out of the constituent moments of a magnetic unit cell. For instance in the case of a two sublattice system we can define the difference of the magnetic moments in a unit cell as the Neel order parameter $\mathbf{n} = \mathbf{m}_1 - \mathbf{m}_2$ where $\mathbf{m}_i$ is the magnetic moment of the i^{th} sublattice.

The mechanism for antiferromagnetism is more complicated than ferromagnetism, involving an exchange pathway called a super-exchange, where the two magnetic sites interact through an intermediary non-magnetic ion, often Oxygen [10, 11]. They too can be in most cases modelled using the Heisenberg exchange in Eq. (1.1) with $J_{ij} > 0$. Notable exceptions occur when the local spins are spin - 1/2 and the lattice is frustrated (triangular for instance) [12]. Such situations require a more quantum treatment involving the singlet dimer comprising of two spin-1/2 moments.

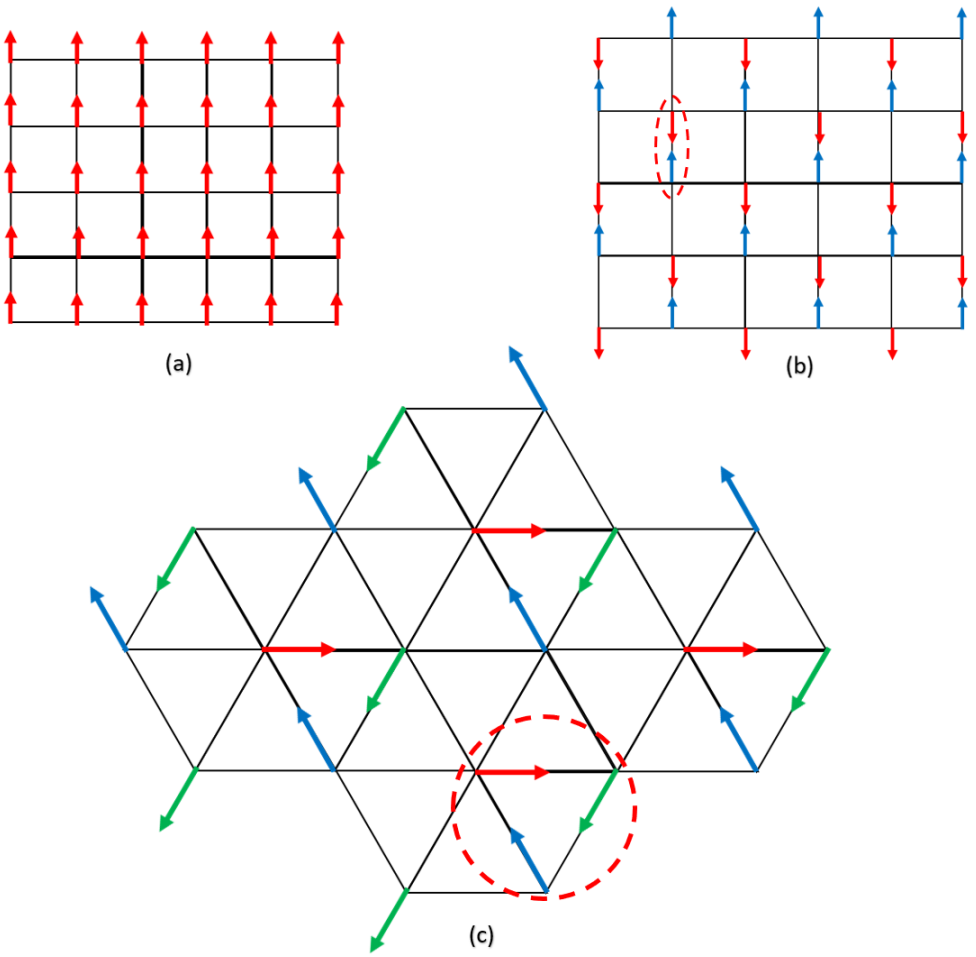

Figure 1.1: This image shows three typical examples of ordered systems: a ferromagnet on a square lattice (a), an antiferromagnet on a square lattice (two sublattice) (b) and an antiferromagnet on a triangular lattice (three sublattice) (c). The red dotted regions show how the spins add to produce a zero net moment per unit cell in the antiferromangets

Transition-metal oxides such as MnO and FeO make a large group of antiferromagnetic insulators [11]. In these compounds, the d-orbitals of magnetic atoms are so localized that hopping cannot occur between two magnetic ions which are next nearest neighbours. Instead electrons occupying the localized d-orbitals of magnetic ions can hop to the next-nearest neighbour magnetic atoms via the p-orbitals of the intermediate oxygen atoms.

Besides exchange interactions there are other lattice anisotropies which affect the local magnetic order. They are usually the result of the local electronic charge distribution expressed through a crystal field. In general the anisotropies are in the form of a tensor:

$$H_{\text{aniso}} = \sum_{(ab),i} S_i^a K^{ab} S_i^b \tag{1.2}$$

where (a, b) runs over spin components and (i) over lattice sites. The tensor K^{ab} is dictated by the symmetries of the crystal field. For instance, when the crystal field possesses a uniaxial symmetry along the z-axis, then the interaction can be written as:

$$H_{\text{axial}} = K^{zz}(S^z)^2 + K^{xx}(S^x)^2 + K^{yy}(S^y)^2. \tag{1.3}$$

The uniaxial symmetry forces $K^{xx} = K^{yy} \equiv K$. The easy-axis case is described by the condition $K^{zz} - K < 0$. The opposite sign presents the other commonly encountered

situation of an easy-plane anisotropy. The plane in question here is the xy plane.

There is an additional energy term from the dipolar interactions between the magnetic moments. It can be written using the standard magnetic dipole dipole interaction potential in three dimensional space as [13]:

$$H_{\text{dipole}} = \frac{\gamma^2}{2} \sum_{i \neq j} \frac{\mathbf{S_i} \cdot \mathbf{S}_j - 3(\mathbf{S}_i.\hat{\mathbf{r}}_{ij})(\mathbf{S}_j.\hat{\mathbf{r}}_{ij})}{|\mathbf{r}_{ij}|^3}, \tag{1.4}$$

where γ is the gyromagnetic ratio and $\mathbf{r}_{ij}$ is the vector connecting the two sites (i, j).

1.3 The micromagnetic approach

The magnetic systems which we study have their spins or moments ordered at temperatures below the ordering temperature T_c (Curie temperature). Exciting these systems, like for instance scattering spin-full particles off of the sample, result in deviations from this uniform order. In addition, the uniform order is broken by competing ordered states with the same energy cost but with different patterns of moment orientation each forming a domain with domain walls interpolating between the differently oriented ordered states, see Fig.1.2(a) for a 1-d example. The number of such domains depends on the local symmetries of the lattice and anisotropies. In certain other systems, like Cr_2O_3 chiral terms like the Dzyaloshinski-Moriya (DM) interaction[14, 15] can induce textures like helical spin arrangements [16].

The energetics in the ordered systems are described by a collection of lattice terms,

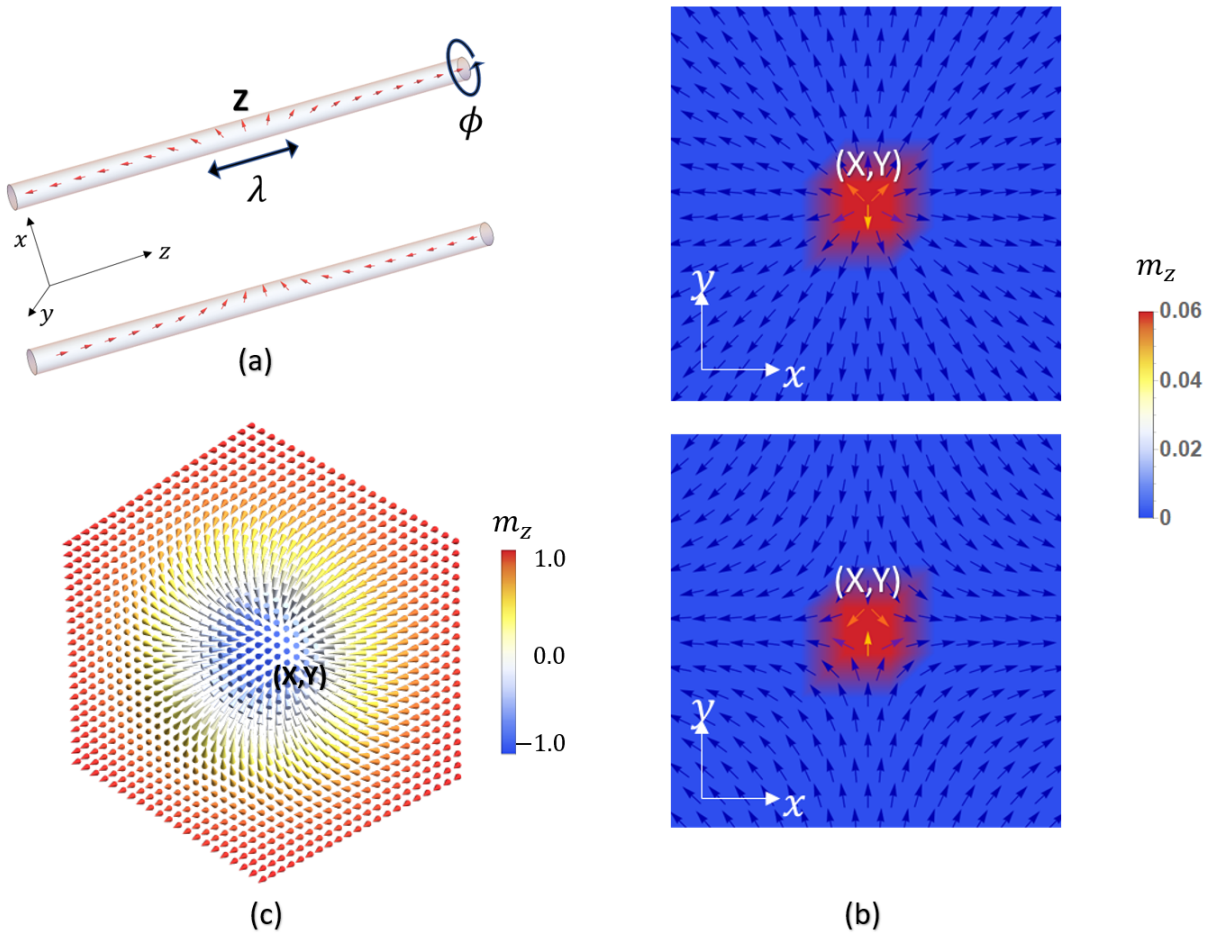

Figure 1.2: This image shows the three most common types of topological soltions. We have a uniaxial domain wall on the left (a). The two images are the two possible boundary conditions $\sigma = \pm 1$ refereed to in Eq.(1.17), we mark the two zero modes: the domain wall centre Z and the wall plane Φ. The domain wall length λ is set by material parameters. It also serves as an example of a mode that is not a zero mode as the energy of the system depends on λ. On the right (b) we have the $n = 1$ vortex at the top and $n = -1$ anti-vortex at the bottom. The vortex centre (X, Y) are the zero modes here.(c) Bottom right we have a two dimensional magnetic skyrmion. The spins at the centre point into the plane (blue) while the spins far away point out (red).

usually dominated by the exchange interaction:

$$H = H_{\text{exchange}} + H_{\text{anisotropy}} + H_{\text{DM}} + \dots \tag{1.5}$$

We can take this Hamiltonian for a particular lattice and solve for stationary modes subject to boundary conditions. It is a computationally hard problem when expressed in terms of individual spins on a discrete lattice and solutions to defect structures can be obtained for highly symmetric, simple situations like a one dimensional chain. The analytical approach, at least in systems where the ordered moment size is large (classical), is to convert the discrete spins into a magnetization field: $\mathbf{S}_i = S\mathbf{m}(\mathbf{r}_i)$, where $\mathbf{m}(\mathbf{r}_i)$ is a unit vector field. We then expand the energy densities in terms of this uniform field. Using these formulation for the ferromagnet the Heisenberg exchange, can be rewritten as follows:

$$H_{\text{exchange}} = -J \sum_{\langle ij \rangle} \mathbf{S}_i \cdot \mathbf{S}_j = J \sum_{\langle ij \rangle} \frac{1}{2} (\mathbf{S}_i - \mathbf{S}_j)^2 - S^2. \tag{1.6}$$

The energy is minimized by a uniform state with all spins $\mathbf{S}_i$ pointing in the same direction. In the continuum limit, the spin difference in the exchange energy is approximated by a spatial gradient,

$$\mathbf{S}_i - \mathbf{S}_j \approx (\mathbf{r}_i - \mathbf{r}_j) \cdot \nabla S\mathbf{m}. \tag{1.7}$$

As an example of this let us look into the uniaxial ferromagnet in one dimension along $\hat{\mathbf{z}}$, Fig. 1.2 (a). The energy density is given by a Heisenberg exchange H_{exchange} and an easy axis anisotropy $H_{\text{anisotropy}}$. Consider the situation where the strength of the Heisenberg exchange is uniform J and the easy axis along $\hat{z}$. Since the system extends along a single direction the magnetization density $\mathbf{m} = \mathbf{m}(z)$. This implies $\nabla S\mathbf{m} \to S(\partial_z \mathbf{m})$ with

$$\mathbf{m}(z) = (\sin\theta(z)\cos\phi(z), \sin\theta(z)\sin\phi(z), \cos\theta(z)) \tag{1.8}$$

Now we can expand the total energy in terms of the unit vector field and its gradient. The energy functional $U[\mathbf{m}(z)] = \int dz\, \mathcal{U}$ has the energy density:

$$\begin{aligned} \mathcal{U} &= \frac{\mathcal{J}}{2}(\partial_z \mathbf{m})^2 + \frac{\mathcal{K}}{2} m_z^2 \\ &= \frac{\mathcal{J}}{2}\left[(\partial_z\theta)^2 + \sin^2\theta(\partial_z\phi)^2\right] + \frac{\mathcal{K}}{2}\cos^2\theta. \end{aligned} \tag{1.9}$$

The coupling constants of the continuum theory are related to those of the lattice model. For the one dimensional lattice, $\mathcal{J} = JS^2$ and $\mathcal{K} = KS^2/a$. Another important quantity is the density of angular momentum (spin) $\mathcal{S} = S/a$ on the 1-d lattice. Here a is the nearest neighbour distance on the lattice.

We can see that the uniaxial anisotropy favours two ground states with $\mathbf{m} = \pm\hat{\mathbf{e}}_z$ and the exchange interaction penalises spatial variations of the magnetic moment. In situations where both ground states are present we have a domain wall interpolating

between them, see Fig.1.2(a). This can be easily extended to higher dimensions for a ferromagnet but higher dimensions allow for a greater variety of topological defects as we shall see.

1.3.1 Topological Defects - Solitons

Among variations in order, the ones that are particularly of interest to the spintronics community are the topological solitons. These are defects in the moment order which cannot be unwound/straightened by a local rearrangement of spins and are hence protected, see Fig. (1.2). Examples of such solitons are domain walls in uniaxial systems, vortices and skyrmions in planar systems and Bloch points in three dimensional systems [17].

To solve for the profiles of a soliton we start with the energy density written out in terms of the fields whose solitons we want to find. For example, if we want to find solitons of the magnetization field $\mathbf{m}(\mathbf{r})$ we start with energy density for $\mathbf{m}$. In most cases one would include just the nearest neighbour exchange and the local anisotropy since these are the dominant energetic terms. However, in certain situations we might need to add terms like the Dzyaloshinski Moriya interaction [14, 15] to solve for chiral textures. As pedagogical examples let us solve for the two most common solitons in ferromagnets, the planar vortex and the uniaxial domain wall. Starting with the energy density in Eq. (1.9):

$$\mathcal{U} = \frac{\mathcal{J}}{2}\left[\sin^2\theta(\boldsymbol{\nabla}\phi)^2 + (\boldsymbol{\nabla}\theta)^2\right] + \frac{\mathcal{K}}{2}\cos^2\theta. \tag{1.10}$$

As before $\mathcal{J} = \eta J S^2$ and $\mathcal{K} = \eta K S^2$ where η depends on the local lattice structure ($\eta = 1/a^2$ for the square lattice). $K > 0$ denotes an easy plane (xy) anisotropy and $K < 0$ denotes an easy axis ($\hat{z}$) anisotropy. We shall use this functional to derive the profiles for two of the most commonly encountered topological defects: a planar vortex, and an uniaxial domain wall, Fig. 1.2 (b) and (a).

1.3.1.1 Planar Vortex

For the planar vortex, $K > 0$ and the ground state of the magnetic system prefers $\theta = \pi/2$. Deviations in the θ from this are energetically costly, penalized by the easy plane anisotropy. This is our first encounter with a 'hard' mode. These modes (say ζ) are characterized by a positive mass term $a\zeta^2$ ($a > 0$) in the energy density. They have dynamical timescales which are much smaller than 'soft' modes (soft modes are not energetically costly, for example the ϕ mode here). When a system is perturbed, the long-time dynamics is mediated through the soft modes with the hard mode following. Gradients of hard modes, are for this reason, dropped from the energetics. For the planar system we can then neglect $\nabla\theta$ and set $\theta = \pi/2$ everywhere else to minimize the energy from the θ sector. This leaves an energy functional:

$$\mathcal{U}_{\text{planar}} = \frac{\mathcal{J}}{2}(\boldsymbol{\nabla}\phi)^2. \tag{1.11}$$

Minimizing this gives the Laplace equation $\nabla^2\phi = 0$ with generic solutions:

$$\phi(x, y) = n \arctan\left(\frac{y - Y}{x - X}\right) + \phi_0 \tag{1.12}$$

Solutions with $n = 0$ are uniform ground states, while solutions with $n \in \{\pm 1, \pm 2 \ldots\}$ are vortices centred at (X, Y) with vorticities given by n. The vorticity is defined through the equation

$$n = \frac{1}{2\pi} \oint_c (\boldsymbol{\nabla}\phi) \cdot \mathbf{dl} \tag{1.13}$$

where the contour c encloses the vortex centre and is traversed in a counter-clockwise direction. At the centre of the core the moment can no longer stay in plane as the exchange energy cost is too high, hence it cants out, defining a vortex polarisation $p = \pm 1$, see Fig. 1.2(b). We shall see in Chapter.2 that the vorticity maps onto an electric charge in a dual description of the XY ferromagnet in terms of electromagnetism. The vorticity cannot be changed in a continuous manner; and is determined entirely by the topology of the magnetization. In other words, a vortex is a topological object which cannot be created or removed by continuous deformation of magnetization.

1.3.1.2 Uniaxial domain wall

Let us now look at the uni-axial domain wall extended along $\hat{z}$:

$$\mathcal{U}_{\text{uniaxial}} = \frac{\mathcal{J}}{2}\left[\sin^2\theta(\partial_z\phi)^2 + (\partial_z\theta)^2\right] - \frac{\mathcal{K}}{2}\cos^2\theta. \tag{1.14}$$

Since the potential depends on $\phi(\mathbf{r})$ only through gradients, on minimizing it with respect to ϕ, $\delta_\phi\mathcal{U} = 0$, we find $\partial_z(\sin^2\theta\partial_z\phi) = 0$. This is solved with $\phi = \Phi$ a constant azimuthal angle plane which the domain wall occupies.

To solve for the $\theta(z)$ profile we have to contend with a second order differential equation. This is not ideal and we would like to reduce it to a first order equation. There is a route to this, notice that since the energy density is not explicitly coordinate $(\mathbf{r}, t)$ dependent we have a conserved quantity. This is analogous to the conserved energy (Hamiltonian) when the corresponding Lagrangian is time independent.

$$\mathcal{H} = \frac{\mathcal{J}}{2}\left[\sin^2\theta(\partial_z\phi)^2 + (\partial_z\theta)^2\right] + \frac{\mathcal{K}}{2}\cos^2\theta. \tag{1.15}$$

To fix $\mathcal{H}$ we need to pick a set of boundary conditions. Consider at $z \to \infty$, $\theta = 0$ and $\partial_z\theta = \partial_z\phi = 0$. Then we have $\mathcal{H} = \mathcal{K}/2$. This also implies that to have a domain wall we need $\theta = \pi$ as $z \to -\infty$. This leads to the equation:

$$\partial_z\theta = \pm\frac{1}{\lambda}\sin\theta, \tag{1.16}$$

where $\lambda = \sqrt{J/K}$ is the characteristic length scale of the domain wall. This is now a first order differential equation in θ, which can be solve to obtain the profile:

$$\cos\theta(z) = \sigma \tanh\left(\frac{z-Z}{\lambda}\right), \quad \phi(z) = \Phi \tag{1.17}$$

where $\sigma = \pm 1$ depending on the boundary conditions, in our case $\sigma = 1$. Z is the location of the domain wall centre, see Fig. 1.2(a).

1.3.2 Collective coordinates and zero modes

In both the defect profiles we solved for, we had the location (or orientation) of the defects identified by coordinates: (X, Y) for the vortex and (Φ, Z) for the domain wall. Note that the energy of the system is independent of shifts in these coordinates $(q_i \to q_i + \delta q_i)$, as they can be absorbed into a shift (or rotation for Φ) of the system coordinates which are present in $\mathcal{U}$ only as gradients. These are called zero modes of the defect. They are representative of the continuous degrees of freedom that a soliton spontaneously breaks, translation in the plane for the vortex, and translation + rotation (in ϕ) for the domain wall. The zero modes are the dynamical components in these systems and much of spintronics is devoted to effectively manipulating them through external controls [6, 18].

In the study of defect dynamics we restrict our analysis to a study of these coordinates, referred to as collective coordinates. We can represent a generic texture $\mathbf{m}(\mathbf{r})$

in terms of a set of coordinates $\mathbf{m}[q_i, q_j, \ldots]$ and only retain the collective coordinates associated with the zero modes in our analysis. This does not imply that they are the only collective coordinates, for instance in the 1-d domain wall we can take the wall length λ as a collective coordinate. However the coordinates which are not zero modes have dynamical time scales that are much shorter than the zero modes. The zero modes of the defect locations say (q_1, q_2) for ferromagnetic solitons turn out to be conjugate momenta of each other [19, 20], i.e $P_{q_{1,2}} = n_{sk}\ q_{2,1}$. Here n_{sk} is the Skyrmion index of the coordinates (q_1, q_2) which we define in the next section. This results from the Berry phase kinematic term of the spins.

1.4 Dynamics of magnetic moments

We move on to a discussion of dynamics unique to magnetic moments. Locally the moments behave as angular momentum vectors. They have no inertial mass and hence no moment of inertia [4]. Hence, the local dynamics is purely precessional. In this the local magnetic moment behaves like a gyroscope. However, as we shall see in an example, this can lead to translation of defects that are composed out of these local spins, like a domain wall. Let us first look at the dynamics of a single spin, $\mathbf{S}$, in a magnetic field along the $\hat{z}$ axis, $\mathbf{h}$. The Hamiltonian has a single term:

$$H = \gamma \mathbf{S} \cdot \mathbf{h} \tag{1.18}$$

where $\gamma = g|e|/2mc$ is the gyromagnetic ratio. The equations of motion are given by:

$$\partial_t S_i = \{S_i, H\} = \gamma h_j \{S_i, S_j\} = \gamma \epsilon^{ijk} h_j S_k = -\gamma (\mathbf{S} \times \mathbf{h})_i, \tag{1.19}$$

where we have used the regular angular momentum Poisson bracket relation $\{S_i, S_j\} = \epsilon^{ijk} S_k$. Thus it is evident that for an individual spin (where the size of the moment/spin is fixed) the dynamics is precessional. Note the absence of a moment of inertia for the individual spin. This phenomena also goes under the name of Larmor precession in classical mechanics. In that case if one has a magnetic moment $\boldsymbol{\mu}$ in a magnetic field $\mathbf{B}$, there is a torque on the moment $\boldsymbol{\tau} = \boldsymbol{\mu} \times \mathbf{B}$. This leads to a precession of the moment about the magnetic field axis.

This equation is extended to the unit vector magnetization field ($\mathbf{m} = \mathbf{S}/S$) in the Landau-Lifshitz-Gilbert (LLG)[21, 22] equation:

$$\mathcal{J} \dot{\mathbf{m}} = \mathbf{h}_{\text{eff}} \times \mathbf{m} + \alpha \mathcal{J} \mathbf{m} \times \dot{\mathbf{m}}, \tag{1.20}$$

where $\mathcal{J} = M/\gamma$, and $\mathbf{h}_{\text{eff}}$ is an effective magnetic field derived from the energy functional $\mathbf{h}_{\text{eff}} = -\delta \mathcal{U}[\mathbf{m}(\mathbf{r})]/\delta \mathbf{m}(\mathbf{r})$. The second term on the RHS is a damping term introduced by Gilbert and serves as a proxy for various losses in a material which slowly damps the precession of the moment and aligns it with the field. It can be explicitly added to the dynamics of a single spin through a term $-\alpha \dot{\mathbf{S}}$, it dictates the number of precessions needed ($\sim 1/\alpha$) needed to align with the field direction. In

most materials $\alpha \ll 1$.

The LLG equation discretized on a lattice forms the basis for numerical simulations of magnetization dynamics with several popular platforms like OOMMF [23]. The programs calculate the potential energy $U[\mathbf{m}(\mathbf{r}_i)]$ per unit area of the lattice and hence determine the effective field $\mathbf{H}_{\text{eff}}$ through a numerical gradient. While widely used it is most effective in cases of finite sample geometry where due to magnetic charges at the boundaries ($\sigma = \mathbf{m} \cdot \hat{n}$) an analytical determination of energy is not feasible.

In Spintronics, since we are mostly interested in the dynamics of solitons we project the LLG equation onto the manifold of a few collective coordinates, representing the zero modes in the system $\mathbf{q} = [q_i(t), \ldots]$, $\mathbf{m}[\mathbf{r}, t] = \mathbf{m}[q_i(t)]$. One can express the time derivative through $\dot{m} = \dot{q}_i(\partial \mathbf{m}/\partial q_i)$. Taking the scalar product of Eq. 1.20 with $\mathbf{m} \times (\partial \mathbf{m}/\partial q_j)$, followed by a spatial integration gives us the equations of motion for the collective coordinates q_i: [18]

$$F_i + G_{ij}\dot{q}_j - D_{ij}\dot{q}_j = 0. \tag{1.21}$$

Here F_i is a conservative force conjugate to the coordinate q_i, $G_{ij}\dot{q}_j$ is a gyrotropic force with an antisymmetric tensor G_{ij}, and $D_{ij}\dot{q}_j$ is a viscous force with a symmetric

dissipation tensor D_{ij}. Explicitly:

$$\begin{aligned} F_i &= -\int dV\ \frac{\delta U}{\delta \mathbf{m}} \cdot \frac{\partial \mathbf{m}}{\partial q_i} = -\frac{\partial U}{\partial q_i}, \\ G_{ij} &= \mathcal{J} \int dV\ \mathbf{m} \cdot \left(\frac{\partial \mathbf{m}}{\partial q_i} \times \frac{\partial \mathbf{m}}{\partial q_j} \right), \\ D_{ij} &= \alpha \mathcal{J} \int dV \frac{\partial \mathbf{m}}{\partial q_i} \cdot \frac{\partial \mathbf{m}}{\partial q_j}. \end{aligned} \tag{1.22}$$

1.4.0.1 Domain wall dynamics

Let us now use these equations of motion to work out the effect of applying a magnetic field along the long axis of a uniaxial domain wall, see Fig.1.2(a). The domain wall has two zero modes (Z, Φ) as previously noted and a profile derived in Eq. (1.17). This can be used to obtain the gyrotropic and disspational tensors as:

$$\begin{aligned} G_{Z\Phi} &= 2\sigma\mathcal{J} = -G_{\Phi Z}, \\ D_{ZZ} &= \frac{2\alpha\mathcal{J}}{\lambda}, D_{\Phi\Phi} = 2\alpha\mathcal{J}\lambda. \end{aligned} \tag{1.23}$$

A magnetic field along z, $\mathbf{H} = h_0\hat{z}$, introduces an additional potential energy $U = -2Mh_0Z$. This produces a conservative force $F_Z = 2Mh_0$. Since this force is along the Z collective coordinate we can think of it as a 'push' on the domain wall. The

equations of motion:

$$2Mh_0 + 2\sigma\mathcal{J}\dot{\Phi} - \frac{2\alpha\mathcal{J}}{\lambda}\dot{Z} = 0 \tag{1.24}$$
$$\sigma\mathcal{J}\dot{Z} + \alpha\mathcal{J}\lambda\dot{\Phi} = 0$$

Note that in the absence of a dissipation $\dot{Z} = 0$, while $\dot{\Phi} = \sigma\frac{Mh_0}{\mathcal{J}}$, i.e the domain wall only has a precession. This 'push to rotate' dynamics is ubiquitous in ferromagnets where the dynamics is controlled by a gyrotropic tensor [24]. This will become more explicit when we construct the Lagrangian for this theory, directly manifest in the type of kinematic term we write down. A finite dissipation gives a steady state velocity to the domain wall $\mathcal{J}\dot{Z} = \frac{\alpha}{1+\alpha^2}\lambda Mh_0$. Since $\alpha \ll 1$ the steady state velocity is proportional to α.

We can also see from Eq. (1.24) that to effectively move a domain wall we need to apply a torque F_Φ. This can be achieved through application of a spin transfer torque [25, 26]. There an external electronic current carrying a spin moment which adiabatically aligns with the local magnetization field is used to transfer angular momentum on to the domain wall($\Delta\mathbf{L}$), providing the necessary torque $\tau = \Delta\mathbf{L}/(\Delta t)$. The LLG equation is modified to:

$$\mathcal{J}\dot{\mathbf{m}} = \mathbf{h}_{\text{eff}} \times \mathbf{m} + \alpha\mathcal{J}\mathbf{m} \times \dot{\mathbf{m}} - \mathcal{J}(\mathbf{u}\cdot\boldsymbol{\nabla})\mathbf{m} + \beta\mathcal{J}\mathbf{m} \times (\mathbf{u}\cdot\boldsymbol{\nabla})\mathbf{m}, \tag{1.25}$$

where the adiabatic term is expressed through the gradient term $(\mathbf{u}\cdot\boldsymbol{\nabla})\mathbf{m}$ and β

characterizes the misalignment between the electron spin and the local magnetization field. In materials β is known as the 'field' term and is usually small. For the adiabatic spin transfer torque the time derivative ∂_t is modified into a convective derivative $\partial_t \to \partial_t + \mathbf{u}\cdot\boldsymbol{\nabla}$, where $\mathbf{u} = \hbar P\mathbf{j}/(2|e|\mathcal{J})$. $\mathbf{j}$ is the electronic current and P is the spin polarization of the carriers. We shall revisit this term in Chapter. 3 where we study the effects of the adiabatic spin transfer torque on antiferromagnetic defects.

1.4.0.2 Vortex dynamics

For the ferromagnetic vortex the soft mode collective coordinates are the locations of the vortex core (X, Y). The gyrotropic tensor in Eq. (1.21) is given by $G_{XY} = -G_{YX} = 4\pi q\mathcal{J} \equiv G$. Here $q = p/2$ is the skyrmion index of the vortex with $p = m_z$ the magnetization at the vortex core [6]. The equations of motion are given by:

$$\begin{aligned} F_X + G\dot{Y} + D_{XX}\dot{X} + D_{XY}\dot{Y} = 0 \\ F_Y - G\dot{X} + D_{YX}\dot{X} + D_{YY}\dot{Y} = 0. \end{aligned} \tag{1.26}$$

The gyrotropic force on the vortex core moving with a velocity $\mathbf{V}$ is given by $\mathbf{F} = G\mathbf{V}\times\hat{\mathbf{z}}$. This is analogous to the Lorentz force on a particle, with electric charge $Q = q$, moving in the xy plane with the magnetic field $\mathbf{B} = 4\pi\mathcal{J}\hat{\mathbf{z}}$.

It is also clear that a conservative force (an electric potential for the electric

charge analogue) along any of the coordinates x_i will result in a steady velocity in the perpendicular direction. This stems from the absence of an inertial term ($= m\ddot{X}_i$) which is present in the equation of motion for charges in electromagnetism.

1.4.1 The micromagnetic Lagrangian

In this thesis we shall not use the Landau-Lifshitz-Gilbert (LLG) equations in the form written down in Eq. (1.20) and Eq. (1.21). We shall instead construct a continuum Lagrangian for the magnetization fields $\mathbf{m}(\mathbf{r})$. There are two reasons why this approach was taken. Firstly the functional energy derivative $-\left(\frac{\delta \mathcal{U}}{\delta \mathbf{m}}\right)_i$ makes the equation a coupled partial differential equation which is very hard to solve analytically. This problem can be circumvented in a continuum theory by the assumption of slowly varying $\mathbf{m}$ and hence a non-singular slowly varying energy density $\mathcal{U}$. Secondly we shall mostly deal with antiferromagnets which combine two or more magnetic sublattices. The traditional approach forces you to write down the LLG equations separately for each sublattice in the hope that you can combine them going forward (a very confusing endeavour in most cases). In the field theory approach if the fields $\mathbf{m}_i$ (i denotes the sublattice index) are expressed through a judiciously chosen basis drawn from the point group symmetry of the lattice the task of combining the sublattices into one theory is fairly straightforward. We shall show this in Chapter. 4 for the three sublattice antiferromagnet.

The Landau-Lifshitz equation can be obtained from a Lagrangian, with the den-

sity:

$$\mathcal{L} = \mathcal{J}\mathbf{a}(\mathbf{m}) \cdot \dot{\mathbf{m}} - \mathcal{U}[\mathbf{m}] \tag{1.27}$$

where we define a vector potential $\mathbf{a}(\mathbf{m})$ on a magnetization sphere ($\mathbf{m}$ - sphere) through $\boldsymbol{\nabla}_{\mathbf{m}} \times \mathbf{a} = -\mathbf{m}$ [27]. In this construction the tip of the local magnetization unit vector $\mathbf{m}(\mathbf{r})$ is an electric charge fixed to the surface of the $\mathbf{m}$-sphere, which has a magnetic monopole of strength $\mathbf{b} = -\mathbf{m}$ sitting at the origin. The electric charge responds to the monopolar magnetic field through the magnetic Lorentz force which limits the dynamics to the surface of the sphere. Any additional energetic interaction $\mathcal{U}$ forces the charge to favour regions of the sphere, as stable.

Now although our monopole field is spherically symmetric, that does not translate to the generating vector potential $\mathbf{a}$ [19]. In particular to maintain the zero divergence condition, which is necessary for the $\mathbf{b}$ field to be even defined through the curl of a vector potential, we need to thread the flux emanating from the monopole out through a point (or points) on the spherical surface. These threads are the Dirac strings. Keeping these considerations in mind two popular choices for the vector potential are:

$$a_\theta = 0, \qquad a_\phi = \frac{\cos\theta \pm 1}{\sin\theta}. \tag{1.28}$$

In these gauge choices, the vector potential is singular at the south and north pole, $\theta = \pi$ and 0, respectively. The singularity is associated with the Dirac string which carries the monopole flux $+4\pi$ though the singular pole. Special care must be taken to

ensure that our electric charge (magnetization vector) does not encroach upon these regions of singularity.

Minimizing the Lagrangian with respect to the magnetization yields, $\mathcal{J}(\mathbf{m}\times\dot{\mathbf{m}}) = -(\delta\mathcal{U}/\delta\mathbf{m})$ which can be rewritten into Eq. (1.20) since $|\mathbf{m}| = 1$. The Gilbert term has to be incorporated through a separate Rayleigh like dissipation function:

$$\mathcal{R} = \frac{\alpha\mathcal{J}}{2}\dot{\mathbf{m}}^2 \tag{1.29}$$

The Lagrangian can be written out in terms of collective coordinates starting with the definition of the vector potential:

$$\mathcal{J}\int dV\,\mathbf{a}(\mathbf{m})\cdot\dot{\mathbf{m}} = \mathcal{J}\int dV\,\mathbf{a}(\mathbf{m})\cdot\left(\frac{\partial\mathbf{m}}{\partial q_i}\right)\dot{q}_i = \mathbf{A}\cdot\dot{\mathbf{q}}, \tag{1.30}$$

where we have collected the coordinates into the vector $\mathbf{q} = (q_1, q_2, \ldots)$. The Lagrangian can then be written as:

$$L[\mathbf{q}] = \mathbf{A}\cdot\dot{\mathbf{q}} - U[\mathbf{q}]. \tag{1.31}$$

The link between the magnetization field and an electrical charge is now explicit. Note that the curvature of the gauge field $A_i = \int dV\,\mathbf{a}\cdot(\partial\mathbf{m}/\partial q_i)$ in the collective coordinate space is what we had earlier defined as the gyrotropic tensor in E.(1.22), $G_{ij} = \partial_j A_i - \partial_i A_j$. Hence a topological defect, such as a vortex or a domain wall,

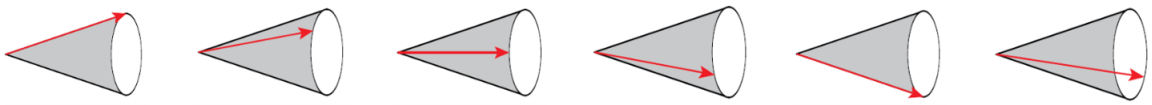

Figure 1.3: This image shows a spin wave propagating along the ordered axis in a one-dimensional ferromagnet. Note that the oscillation takes place in the plane perpendicular to the order direction.

behaves like a charge coupled minimally to a vector potential whose source is given by the local curvature of the magnetization field.

This tensor is known in literature as the skyrmion density of the magnetization when $i, j = x, y$. Integrating this density over the area gives the skyrmion charge of the area [28].

It might seem that we need a finite magnetization density to have this sort of emergent gauge theory and hence it would be absent for an antiferromagnet where locally the magnetization density is zero. However, as we shall show in Chapter 3 this form of gauge coupling can be induced in an antiferromagnet using an external magnetic field.

1.5 Spin-waves

A significant portion of the thesis deals with the continuum version of the magnetization field instead of the discrete collective coordinates of topological soltions. This method is useful to obtain the dispersions of spin waves which are gentle deviations of the magnetic order in space and time.

Among the spin waves the ones we shall be most interested in are the Goldstone modes. These are the modes which characterize the underlying order and the symmetries spontaneously broken by the ordered state. For instance the uniaxial ferromagnet spontaneously breaks the azimuthal (ϕ) degree of freedom. Spin waves in this system are hence rotations of the spin about the ordering vector in the azimuthal plane. For the planar antiferromagnet there are two degenerate Goldstone modes, representing oscillations of $\mathbf{n}$ in the two directions orthogonal to its ground-state orientation. In the last chapter we shall encounter triangular antiferromagnetic systems. Here the spins order into a coplanar 120° locked state forming a triangle. Any ordering of these spin triangles then spontaneously breaks $SO(3)$ rotations resulting in three Goldstone modes.

We end this chapter with a very simplistic derivation of the spin wave in a one dimensional ferromagnet from the Landau-Lifshitz equations see Fig.1.3. Let us consider a chain of spins with spins aligned along $\hat{\mathbf{z}}$. The net local magnetic field experienced by a spin at any site z_i is $\mathbf{H}_{\text{eff}} = \gamma\left(\mathbf{m}(z_i - a) + \mathbf{m}(z_i + a)\right)$ where a is the nearest neighbour distance. On expanding the magnetizations we end up with:

$$\mathbf{H}_{\text{eff}} \times \mathbf{m} = \gamma(2\mathbf{m} + a^2\partial_z^2\mathbf{m}) \times \mathbf{m} = \gamma a^2(\partial_z^2\mathbf{m}) \times \mathbf{m}. \tag{1.32}$$

Plugging this back into the Landau-Lifshitz equation and taking the continuum limit

we get the spin wave equation as:

$$\dot{\mathbf{m}} = \gamma(\partial_z^2 \mathbf{m}) \times \mathbf{m}. \tag{1.33}$$

As a simple situation let us consider the one shown in Fig.1.3 with $\theta(z) = \theta_0$ a constant and $\phi = \omega t + k_z z$. The L.H.S goes to $\dot{\mathbf{m}} = (\sin\theta_0)\dot{\phi}\hat{\mathbf{e}}_\phi$ and the R.H.S:

$$\partial_z^2 \mathbf{m} \times \mathbf{m} = \sin\theta_0 \left[(\partial_z^2\phi)\hat{\mathbf{e}}_\phi + (\partial_z\phi)(\partial_z\hat{\mathbf{e}}_\phi)\right] \times \hat{\mathbf{e}}_\mathbf{m}, \tag{1.34}$$

where $\hat{\mathbf{e}}_\theta$, $\hat{\mathbf{e}}_\phi$, and $\hat{\mathbf{e}}_\mathbf{m}$ are the spherical polar unit vectors. The first term drops out from the choice of solutions, resulting in an equation:

$$\dot{\phi} = \gamma \cos\theta_0 \ (\partial_z\phi)^2 \tag{1.35}$$

We can see from this that in this one dimensional ferromagnet the spin wave dispersion is quadratic in k_z, $\omega = \gamma k_z^2$.

Chapter 2

The planar ferromagnet and its electromagnetic dual

2.1 Introduction

In this chapter we shall take a closer look at the field theory of a planar (XY) ferromagnet. We study the Heisenberg ferromagnet in 2+1 dimensions and the solitons it hosts, magnetic vortices. In the course of which we map the XY theory onto a theory of electromagnetism in $d = 2 + 1$ space-time (t, x, y) where the vortices map to sources of electric charge and magnetic flux. The work was done in collaboration with Shu Zhang, Ibrahima Bah and Oleg. Tchernyshyov [29].

In the analogy between the XY ferromagnet and electrostatics in two spatial dimensions $d = 2$, vortices behave as electric charges [30]. The definition of the

vortex number n as the increment of the magnetization's azimuthal angle ϕ along the boundary of some region Ω, $\int_{\partial\Omega} d\mathbf{r}\cdot\nabla\phi = 2\pi n$, can be recast as Gauss's law for the electric charge Q, $\int_{\partial\Omega} d\mathbf{s}\cdot\mathbf{E} = 2\pi Q$, if we identify the vortex number with the electric charge, $Q = n$, and the spatial gradients of the angle with components of an electric field, $E_i = \epsilon_{ij}\partial_j\phi$, see Fig.2.1. Here Roman indices $i = 1, 2$ refer to spatial directions and ϵ_{ij} is the Levi-Civita symbol in $d = 2$.

Let us quickly revisit this construction. Since the azimuthal field $\phi(\mathbf{r})$ is well defined except at the cores of vortices we have $\partial_x\partial_y\phi - \partial_y\partial_x\phi = 0$. Now in the presence of the singular regions at the vortex cores we can split the azimuthal field up into:

$$\phi(\mathbf{r}) = \tilde{\phi}(\mathbf{r}) + \phi'(\mathbf{r}), \tag{2.1}$$

where $\tilde{\phi}$ is a gently varying well defined spin wave field and ϕ' is a singular field sourced from vortex cores. Let us consider the vorticity equation and expand it in the situation where we have a square contour around a single vortex, the xy blue contour in Fig. 2.1:

$$\int_{\partial\Omega} d\mathbf{r}\cdot\nabla\phi = \int dxdy(\partial_x\partial_y\phi' - \partial_y\partial_x\phi') = 2\pi n \tag{2.2}$$

Now we can use the map to the electric field, $E_i = \epsilon_{ij}\partial_j\phi$, to convert this to a Gauss law $\boldsymbol{\nabla}\cdot\mathbf{E} = -\rho$. Here ρ is the vortex number distribution, $\rho(\mathbf{r}) = \sum_i n_i\delta(\mathbf{r}-\mathbf{r}_i)$ which gets mapped to an electric charge distribution. The solution to this is Coulombs' law

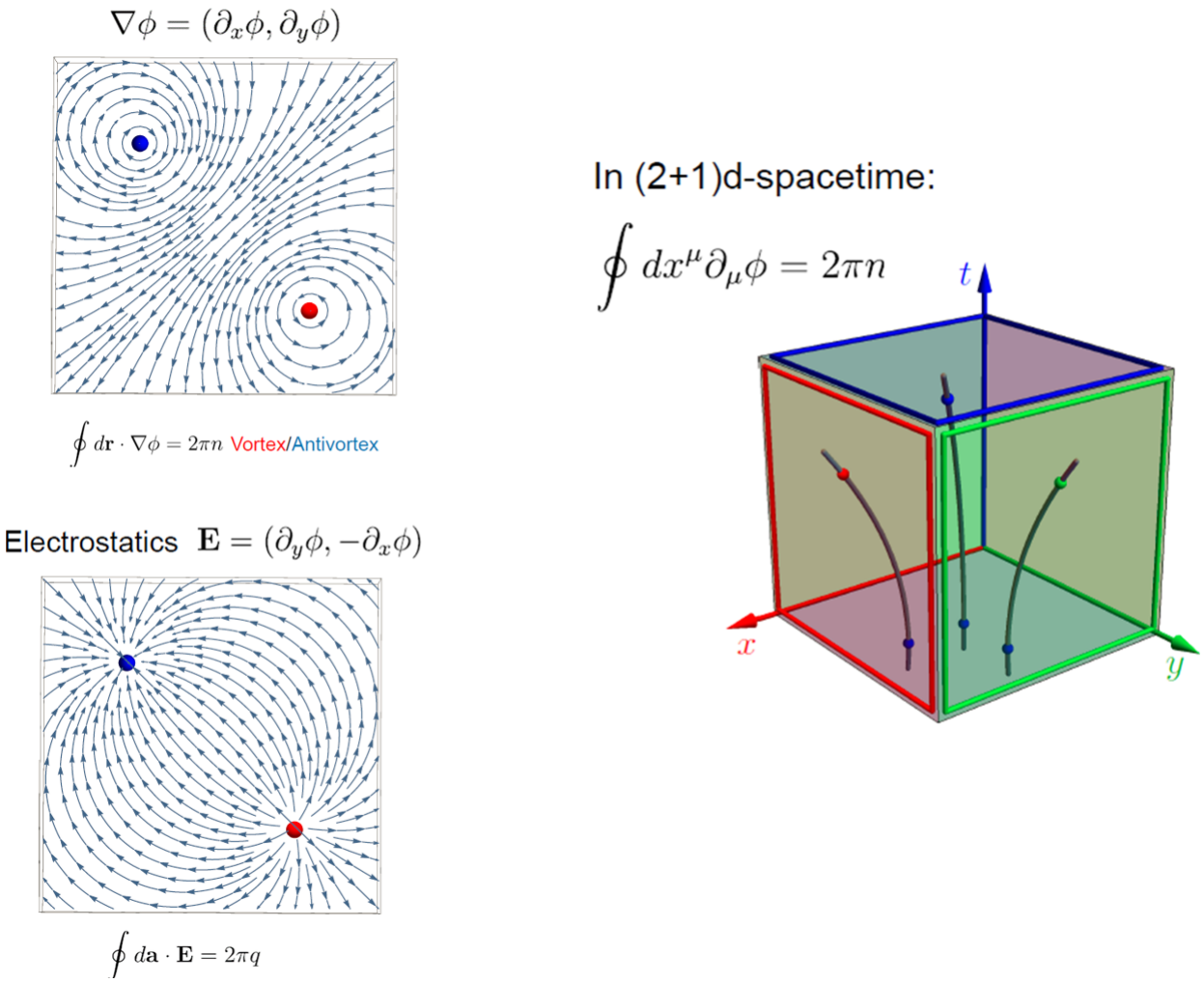

Figure 2.1: On the left we have the electrostatic duality in the xy plane for a vortex antivortex pair. One can see that the rotation of the vorticity gradient into the electric field produces the typical charge dipole pattern. On the right we have an extension of the duality picture in time. Vorticity, like charge is conserved and adds to zero over all space-time surfaces.

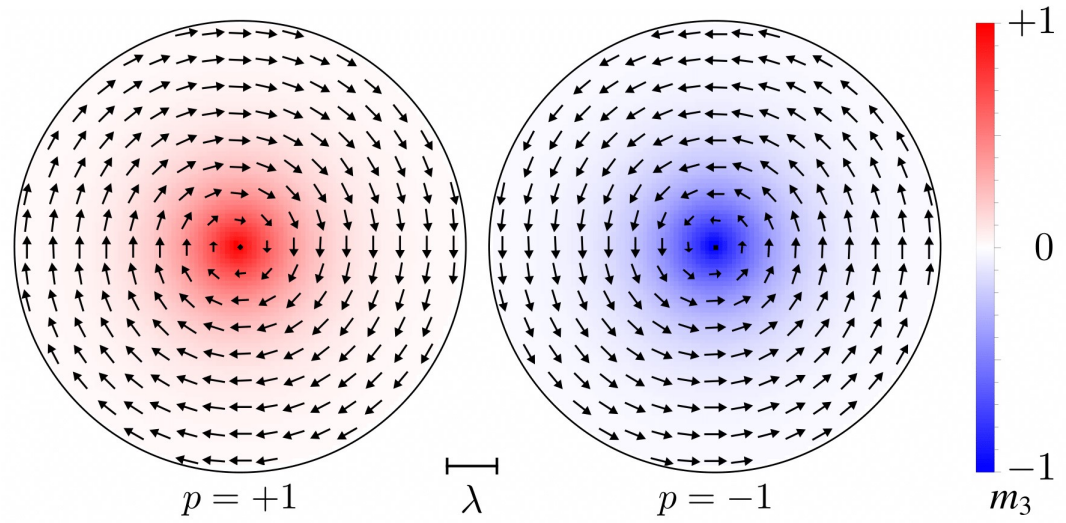

Figure 2.2: Vortices in a thin film of permalloy. Numerical simulation in OOMMF [23]. Color encodes m_3: positive (red), zero (white), and negative (blue). At a vortex core, magnetization leaves the easy plane and approaches the hard axis, $\mathbf{m} \to (0, 0, p)$, where $p = \pm 1$ defines the polarity of the vortex.

in d = 2 with a Greens function $g(r) = \log(r/r_0)$ with r_0 as the size of the charge core. In [30] an extra constraint is imposed at the boundary to cancel its contributions to the Green function: $\int d^2\mathbf{r}\rho(\mathbf{r}) = 0$. This imposes the conservation of vorticity (charge) in the system.

In a broader scenario the xy vector ($U(1)$ for complex wave functions) order parameter–electromagnetism duality has been extended to dynamical and quantum phenomena, which take place in a spacetime with $d = 2 + 1$. The addition of the time dimension promotes electrostatics to electrodynamics, vortices become quantum particles with Bose statistics, and the planar XY ferromagnet is mapped to a superconductor interacting with an electromagnetic field [31, 32]. Similar dualities have been investigated in the context of two dimensional superfluids [33, 34, 35].

CHAPTER 2. THE PLANAR FERROMAGNET AND ITS ELECTROMAGNETIC DUAL

In the course of this chapter we revisit the duality between the XY ferromagnet and electrodynamics in $d = 2 + 1$. In a realistic ferromagnet, the XY model with just two spin components represents a low-energy, long-wavelength limit of the *Heisenberg ferromagnet* with an easy-plane anisotropy. Although magnetization lies in the easy plane almost everywhere, it turns toward the hard axis at vortex cores, Fig. 2.2. This is an important feature that causes the Heisenberg ferromagnet to deviate from the pure XY systems. We shall see in the course of events that the core of the vortex and the angular momentum (Berry phase) it carries decides the quantum statistics of the vortex particles.

Despite its small radius (typically a few nanometers [36, 37]), the core plays a major role in the dynamics of a vortex. In particular, it is responsible for the gyroscopic (Magnus) force acting on a moving vortex [38, 39, 40]. One can see this is the case by checking that in the absence of a core the gyrotropic tensor $G_{XY} = 0$ in Eq. (1.22). Let us calculate this explicitly for a single vortex with vorticity n. We can choose a symmetric profile for the vortex in radial coordinates (r, ϕ):

$$\mathbf{m} = (\sin\theta(r)\cos\Phi(\phi), \sin\theta(r)\sin\Phi(\phi), \cos\theta(r)), \tag{2.3}$$

where we take the azimuthal profile of the magnetization field to be $\Phi = n\phi$+constant.

The gyrotropic tensor is then:

$$\begin{aligned} G_{XY} &= \mathcal{J}\int dxdy\ \mathbf{m}\cdot\left(\frac{\partial\mathbf{m}}{\partial x}\times\frac{\partial\mathbf{m}}{\partial y}\right) \\ &= \mathcal{J}\int drd\phi\ r\ \left(\frac{\sin\theta(\mathbf{r})\partial_r\theta(\mathbf{r})\partial_\phi\Phi(\phi)}{r}\right) \\ &= 2\pi\mathcal{J}\int d(\cos\theta(\mathbf{r})) = 2\pi np\mathcal{J}, \end{aligned} \tag{2.4}$$

where $p = \pm 1$ is the polarization of the spin at the vortex core. It is evident that in the absence of a canted centre the vortex will have no dynamics. The finite gyrotropic tensor is also responsible for the equations of motion of a vortex core in the presence of forces. The vortex behaves like an electrically charged massless (inertial mass) particle. A force along x (or y) produces a displacement of the core in the y (or x) direction, see Eq. (1.26) in Chapter 1.

It is noteable that the magnitude of the gyroscopic force is independent of the size and detailed structure of the core and is only sensitive to its topology and the density of angular momentum [41]. This is a rare example where high-energy physics (here the existence of a vortex core) crucially impacts low-energy dynamics.

The newly derived duality establishes an interesting connection between quantum statistics of vortices and the spin of the vortex core S_3 along the hard axis. In the dual description, vortices acquire not only the electric charge $Q = n$ but also a magnetic flux $\Phi = S_3$. Wilczek [42, 43] showed that in $d = 2 + 1$ the quantum statistics of particles carrying both an electric charge Q and a magnetic flux Φ is altered by the

Aharonov-Bohm phase. Generally, bosons turn into anyons with the braiding phase $\vartheta = 2\pi Q\Phi$. For magnetic vortices, this yields

$$\vartheta = 2\pi n S_3. \tag{2.5}$$

Simple vortices with $n = \pm 1$ and half-integer spin S_3 are therefore fermions. An even more exotic, anyon statistics is expected for vortices with a non-integer $2S_3$.

2.2 The planar Heisenberg ferromagnet

Switching to the continuum magnetization field $\mathbf{m}(\theta, \phi)$ where $\theta(x, y)$ and $\phi(x, y)$ are the polar and azimuthal angles of magnetization. The simplest model for the xy Heisenberg system without long-range dipolar interactions has the Lagrangian density

$$\mathcal{L}(\theta, \phi) = \mathcal{S}(\cos\theta - p)\partial_t\phi - \mathcal{U}(\theta, \phi). \tag{2.6}$$

The first term in the Lagrangian comes from the spin Berry phase and is responsible for the precessional dynamics of magnetization; $\mathcal{S}$ is the spin density, S/a^2 on a square lattice with a as the nearest neighbour distance. The number $p = \pm 1$ reflects a gauge choice and determines the location of a singularity of the spin wavefunction at $\cos\theta = -p = \mp 1$ [27]. Either choice of p would work if the spins stayed in the easy plane. However, a vortex configuration inevitably has a location where the spin

orientation approaches one of the poles, Fig. 2.2. To avoid the singularity, we have to make a specific choice of parameter p [44] by equating it to the vortex polarity, defined as the value of the out-of-plane magnetization at the center of the vortex core, $m_3 = \pm 1$ [45].

The lattice model of an easy-plane ferromagnet with nearest-neighbour Heisenberg exchange J and local anisotropy K has the potential energy

$$U = -J\mathcal{S}^2 \sum_{<ij>} \mathbf{m}_i \cdot \mathbf{m}_j + \frac{K\mathcal{S}^2}{2} \sum_i m_{iz}^2. \tag{2.7}$$

Here i and j denote lattice sites and $\langle ij \rangle$ a nearest-neighbour bond. In this simple form where we have ignored long range interactions like dipolar interactions, the energy functional $U[\mathbf{s}(\mathbf{r})] = \int d^2r\, \mathcal{U}$ has the energy density:

$$\begin{aligned} \mathcal{U} &= \frac{\mathcal{J}}{2}(\nabla \mathbf{m})^2 + \frac{\mathcal{K}}{2} m_z^2 \\ &= \frac{\mathcal{J}}{2}\left[(\nabla\theta)^2 + \sin^2\theta (\nabla\phi)^2\right] + \frac{\mathcal{K}}{2}\cos^2\theta. \end{aligned} \tag{2.8}$$

The coupling constants of the continuum theory are related to those of the lattice model. For a square lattice, $\mathcal{J} = JS^2$ and $\mathcal{K} = KS^2/a^2$. The natural unit of length $\lambda = \sqrt{\mathcal{A}/\mathcal{K}}$ sets the size of a vortex core; the natural unit of time is $\tau = |\mathcal{S}|/\mathcal{K}$. The Lagrangian (2.6) with the energy density (2.8) represents a full (high-energy) theory of magnetization dynamics, in which the magnetization field has three components.

In low-energy states, the magnetization field lies in the easy plane. The out-of-

plane magnetization $m_3 = \cos\theta \ll 1$ is suppressed and can be viewed as a hard mode. In the spirit of the gradient expansion, we may neglect the $(\nabla\theta)^2$ term in the exchange energy. With this simplification, the Lagrangian contains no gradients of the field θ and its (classical) equation of motion reads

$$\mathcal{K}\cos\theta = \mathcal{S}\partial_t\phi. \tag{2.9}$$

In static equilibrium, $\partial_t\phi = 0$ and thus $\cos\theta = 0$, the magnetization resides strictly in the easy plane. Slow dynamics of the azimuthal angle ϕ is accompanied by a small tilt of magnetization out of the easy plane. The hard polar angle is thus a slave of the soft azimuthal angle. Integrating out θ from the action yields a low-energy theory with just one field ϕ and an effective Lagrangian

$$\mathcal{L}(\phi) = -p\mathcal{S}\partial_t\phi + \frac{\rho}{2}(\partial_t\phi)^2 - \frac{\mathcal{A}}{2}(\nabla\phi)^2, \tag{2.10}$$

where $\rho = \mathcal{S}^2/\mathcal{K}$ quantifies the inertia of the azimuthal angle.

It is convenient to write the Lagrangian in a Lorentz-covariant form with the Minkowski metric $\eta_{\mu\nu} = \mathrm{diag}(+1, -1, -1)$ and in natural units,

$$\mathcal{L}(\phi) = \bar{\sigma}^\mu\partial_\mu\phi + \frac{e^2}{2}\partial_\mu\phi\,\partial^\mu\phi, \quad \bar{\sigma}^\mu = -pe^2\delta^\mu_0. \tag{2.11}$$

The dimensionless coupling constant $e^2 \equiv |\mathcal{S}|\mathcal{A}/\mathcal{K} \gg 1$ is roughly the net out-of-plane

spin S_3 of a vortex core.

The low-energy Lagrangian (2.10) has a global symmetry of rotations in the easy plane, $\phi \mapsto \phi + \text{const}$. The associated conserved global quantity is the hard-axis spin component S_3. The associated local conservation law, $\partial_\mu \sigma^\mu = 0$, is the continuity equation for the spin current defined as

$$\sigma^\mu \equiv \frac{\partial \mathcal{L}}{\partial(\partial_\mu \phi)} - \bar{\sigma}^\mu = e^2 \partial^\mu \phi. \tag{2.12}$$

Here we have separated a uniform background spin current $\bar{\sigma}$, whose only nonvanishing component $\bar{\sigma}^0 = -p\mathcal{S}$ is a background spin density, from the dynamical part σ. Although the linear term $\bar{\sigma}^\mu \partial_\mu \phi$ in the Lagrangian (2.11) does not influence the classical equation of motion,

$$\partial_\mu \partial^\mu \phi = 0, \tag{2.13}$$

it has a topological character and plays an important role in the dynamics of vortices, as we discuss below. Eq. (2.13) describes spin waves with a linear dispersion, $\omega = k$.

2.3 Electromagnetism in 2+1 dimensions

Before moving on to constructing the dual theory we present a brief summary of electromagnetism in a Minkowski spacetime with $d = 2+1$ dimensions along the lines of [13]. The metric tensor is $\eta_{\mu\nu} = \text{diag}(+1, -1, -1)$.

The electromagnetic field has three components, the scalar magnetic field B and an in plane vector electric field $\mathbf{E} = (E_x, E_y)$. The gauge field has three components, the scalar electrostatic potential ϕ and the vector potential $\mathbf{A} = (A_x, A_y)$. The vector potential can be sourced from a charge current $\mathbf{j}$ or flux lines that extend into the third spatial dimension.

In the relativistic notation, the gauge field has the following covariant and contravariant components:

$$A_\mu = \begin{pmatrix} \phi \\ -A_x \\ -A_y \end{pmatrix}, \quad A^\mu = \begin{pmatrix} \phi \\ A_x \\ A_y \end{pmatrix}. \tag{2.14}$$

The electromagnetic field is an antisymmetric tensor $F_{\mu\nu} = \partial_\mu A_\nu - \partial_\nu A_\mu$:

$$F_{\mu\nu} = \begin{pmatrix} 0 & E_x & E_y \\ -E_x & 0 & -B \\ -E_y & B & 0 \end{pmatrix}, \quad F^{\mu\nu} = \begin{pmatrix} 0 & -E_x & -E_y \\ E_x & 0 & -B \\ E_y & B & 0 \end{pmatrix}. \tag{2.15}$$

The field strength tensor $F_{\mu\nu}$ can also be represented by its dual [46, 13], which in

$d = 2 + 1$ is a 3-vector

$$*F^{\mu} = \frac{1}{2}\epsilon^{\mu\nu\rho}F_{\nu\rho} = \begin{pmatrix} -B \\ -E_y \\ E_x \end{pmatrix}. \tag{2.16}$$

The homogeneous Maxwell equation, $\partial_x E_y - \partial_y E_x + \partial_t B = 0$, reads $\partial_\mu *F^\mu = 0$ in the relativistic notation and is resolved by expressing the dual field as a 3-curl of the gauge field, $*F^\mu = \epsilon^{\mu\nu\rho}\partial_\nu A_\rho$, or $F_{\mu\nu} = \partial_\mu A_\nu - \partial_\nu A_\mu$.

The inhomogenous Maxwell equations, $\partial_\mu F^{\mu\nu} = 2\pi j^\nu$, can be derived from the Lagrangian:

$$\mathcal{L}(A, j) = -A_\mu j^\mu - \frac{1}{8\pi}F^{\mu\nu}F_{\mu\nu}. \tag{2.17}$$

The second term in the Lagrangian (2.17) represents the kinetic and potential energy densities of the electromagnetic field, $\mathbf{E}\cdot\mathbf{E}/(4\pi)$ and $B^2/(4\pi)$, respectively. The first term expresses the coupling between the electromagnetic field and electric current. For a point particle with spacetime coordinates x^μ and electric charge q, it generates the action term

$$S = -q\int A_\mu dx^\mu = q\int(\mathbf{A}\cdot d\mathbf{r} - \phi\, dt). \tag{2.18}$$

This action term is responsible for the 3-force $f_\mu = qF_{\mu\nu}\dot{x}^\nu$, where the dot means the derivative with respect to proper time τ, $d\tau^2 = dx^\mu dx_\mu$. Its spatial components, $f_x = qB\dot{y}$ and $f_y = -qB\dot{x}$, represent the Lorentz force.

2.4 The dual theory at low energies

Here we go through the details of the construction of the dual electromagnetic theory for the XY ferromagnet in the low energy limit 2.11, where we are focused on the regions away from the vortex cores. The duality can be revealed most efficiently in the language of differential forms. The electromagnetic field is represented by a 2-form $F = \frac{1}{2}F_{\mu\nu}dx^\mu \wedge dx^\nu$ and the electric current by a 1-form $J = J_\mu dx^\mu$ [46]. Maxwell's equations and current conservation read

$$d\,{}^*F = 2\pi\,{}^*J, \quad dF = 0, \quad d\,{}^*J = 0. \tag{2.19a}$$

Here d is the exterior derivative and * is the Hodge dual. In the theory of the XY ferromagnet, the spin and vortex currents are represented by 1-forms σ and j. The relation between them, and the conservation of the two currents read (in the low-energy limit)

$$d\sigma = 2\pi e^2\,{}^*j, \quad d\,{}^*\sigma = 0, \quad d\,{}^*j = 0. \tag{2.19b}$$

Comparing Eqs. (2.19) shows that the vortex current j maps to the electric current J and the spin current σ to the Hodge dual of the electromagnetic field $^*F$. We now unpack these details in the more explicit tensor notation, beginning with a list of ingredients that we expect to find in a theory of electrodynamics in $d = 2 + 1$.

2.4.1 Gauge field

An electromagnetic field should satisfy local constraints (Bianchi identities) in the form of the homogeneous Maxwell equations. These constraints are resolved by expressing the electromagnetic field as the curl of a gauge field, $F_{\mu\nu} = \partial_\mu A_\nu - \partial_\nu A_\mu$. The Bianchi identity in $d = 2 + 1$ reads

$$\partial_\mu {}^*F^\mu = 0, \quad {}^*F^\mu \equiv \frac{1}{2}\epsilon^{\mu\nu\rho}F_{\nu\rho}, \tag{2.20}$$

where $\epsilon^{\mu\nu\rho}$ is the Levi-Civita symbol in $d = 2 + 1$. Here ${}^*F$ is the Hodge dual of the electromagnetic field F [46, 13]. It corresponds to a conserved current for a global $U(1)_J$ symmetry, referred to as topological $U(1)$, which exist for Maxwell theories in $d = 2 + 1$. The theory admits monopole defect operators charged under $U(1)_J$.

The global symmetry in the ferromagnetic model is the symmetry of spin rotations in the xy plane. We identify the generator of this symmetry with that of the $U(1)_J$ of the Maxwell theory, and thus the current σ^μ maps to ${}^*F^\mu$ as follows:

$${}^*F^\mu \equiv -\sigma^\mu = -e^2\partial^\mu\phi, \quad {}^*\bar{F}^\mu \equiv -\bar{\sigma}^\mu. \tag{2.21}$$

Here quantities with a bar represent uniform background parts of the respective fields. The minus signs in Eq. (2.21) reflect the convention that a positive vortex number corresponds to a positive electric charge. This matching of the conserved currents onto

a Bianchi identity is the critical step in construction of the electromagnetic dualities. The symmetry group of the current decides the nature of the mapped gauge theory. For instance in elasticity theories where the conserved current (dislocations guided by Bergers vectors) is a tensor, the gauge theory is a tensor gauge theory characterised by A_{ij} [47].

With the physical units restored, the electric and magnetic fields are

$$E^i = \mathcal{A}\epsilon^{ij}\partial_j\phi, \quad B = \rho\partial_t\phi, \quad \bar{B} = -p\mathcal{S}. \tag{2.22}$$

As in $d = 2$ [30], the electric field comes from spatial gradients of ϕ, whereas the temporal gradient gives rise to the dynamical part of the magnetic field. The background magnetic field $\bar{B} = -p\mathcal{S}$ represents an effect well known in vortex dynamics. A particle with electric charge Q moving with velocity $\dot{x}^i$ should experience the Lorentz force $F_i = 2\pi Q\bar{B}\epsilon_{ij}\dot{x}^j$. With $Q = n$ and $\bar{B} = -p\mathcal{S}$, this exactly reproduces the gyroscopic force $F_i = -2\pi np\mathcal{S}\epsilon_{ij}\dot{x}^j$ acting on a moving vortex [38, 39, 44].

Electromagnetic waves. A hallmark of Maxwell's theory is the existence of transverse electromagnetic waves with a linear dispersion, $\omega = k$. Spin waves in the XY ferromagnet (2.13) seem like a good candidate. There is just one spin-wave mode for each wavevector, in accordance with a single transverse polarization expected for electromagnetic waves in $d = 2 + 1$. The transverse nature of the electric field in a spin wave can be checked with the aid of Eq. (2.22): $\partial_i E^i = \mathcal{A}(\partial_x\partial_y - \partial_y\partial_x)\phi = 0$ in

the absence of vortices.

2.4.2 Coupling field and current

To find a conserved matter current satisfying the continuity equation, $\partial_\mu j^\mu = 0$, we turn to vortices. They are indestructible and can only be annihilated with the conservation of the vortex number in pairs. In their presence, derivatives of ϕ are singular. This was earlier used to define the vortex density ρ in $d = 2$, $\partial_x\partial_y\phi - \partial_y\partial_x\phi = 2\pi\rho$. This definition of vortex density ρ generalizes to a vortex current j^μ in $d = 2+1$:

$$\epsilon^{\mu\nu\rho}\partial_\nu\partial_\rho\phi = 2\pi j^\mu. \tag{2.23}$$

With the help of the duality relation (2.21), this identity takes the form of the inhomogeneous Maxwell equations,

$$\partial_\mu F^{\mu\nu} = 2\pi e^2 J^\nu, \tag{2.24}$$

with the electric current J equal to the vortex current j.

Note that the entire dual theory can be obtained from the Lagrangian of Maxwell's electrodynamics with a matter current J coupled to both the dynamical and background electromagnetic gauge fields represented by the gauge fields A and $\bar{A}$, respec-

tively:

$$\mathcal{L}(J,A) = -2\pi(A_\mu + \bar{A}_\mu)J^\mu - \frac{F_{\mu\nu}F^{\mu\nu}}{4e^2}. \tag{2.25}$$

2.4.3 Duality via an auxiliary field

We now derive the dual theory (2.25) from the low-energy Lagrangian (2.11) in a standard formal way [48], through the introduction of an auxiliary vector field with components $^*F^\mu$. The Lagrangian of the two fields ϕ and $^*F$ is chosen to be

$$\mathcal{L}(\phi, {}^*F) = -({}^*F^\mu + {}^*\bar{F}^\mu)\partial_\mu\phi - \frac{{}^*F^\mu\,{}^*F_\mu}{2e^2}. \tag{2.26}$$

This choice assures that minimization of the action with respect to $^*F$ yields the conjectured relation (2.21). Integrating out the auxiliary field $^*F$ would lead to our effective theory (2.11). Instead, we will keep the auxiliary field $^*F$ and integrate out the angle field ϕ.

However, prior to that, we need to separate a singular vortex part of the field ϕ from the gentle spin waves along the same lines as it is done in $d = 2$ [30]. In the presence of vortices, the azimuthal angle ϕ is not a single-valued function of the spacetime coordinates and $\partial_\mu\phi$ is not, strictly speaking, a gradient. We separate this quantity into two parts, $\partial_\mu\phi = a_\mu + \partial_\mu\varphi$. The new gauge field a is defined by vortex world-lines,

$$\epsilon^{\mu\nu\rho}\partial_\nu a_\rho = 2\pi j^\mu. \tag{2.27}$$

The single-valued field φ represents spin waves in the original theory and generates gauge transformations for the vortex gauge field a. Put another way, the local conservation of the vortex current, $\partial_\mu j^\mu = 0$, can be viewed as the Bianchi identity for another electromagnetic field f, whose dual is identified with the vortex current, ${}^*f^\mu \equiv 2\pi j^\mu$. The Bianchi identity is resolved by the introduction of the gauge field a: ${}^*f^\mu = \epsilon^{\mu\nu\rho}\partial_\nu a_\rho$.

Integrating out the single-valued part of the field φ produces the Bianchi identity for F (2.20). Upon resolving it in the expected way, ${}^*F^\mu = \epsilon^{\mu\nu\rho}\partial_\nu A_\rho$, we obtain the Lagrangian for a gauge field A and the vortex current j parametrized by the vortex gauge field a:

$$\mathcal{L}(j, A) = -\epsilon^{\mu\nu\rho} a_\mu \partial_\nu (A_\rho + \bar{A}_\rho) - \frac{F_{\mu\nu}F^{\mu\nu}}{4e^2}. \tag{2.28}$$

Note that the first term in Eq. (2.28) is $a_\mu \sigma^\mu$, indicating that the role of the electric charge for the gauge field a is played by the spin S_3, whereas the electric charge for A is the vortex number n. Finally, we convert the first term in Eq. (2.28) via integration by parts and use the relation between a and j (2.27) to obtain the conjectured Lagrangian of the dual theory (2.25).

2.5 The dual theory near the vortex core

We can readily construct the electromagnetic fields following the familiar route. The Lagrangian (2.6) and potential energy (2.8) still have the global rotational sym-

metry. The spin current σ^μ has the following components:

$$\sigma^0 = \mathcal{S}\cos\theta, \quad \bar{\sigma}^0 = -p\mathcal{S}, \quad \sigma^i = -\mathcal{A}\sin^2\theta\,\partial_i\phi. \tag{2.29}$$

The dynamical temporal component σ^0 is the density of spin along the hard axis. Identification of the spin current with the electromagnetic field along the lines of Eqs. (2.21) and (2.22) yields

$$E^i = \mathcal{A}\sin^2\theta\,\epsilon^{ij}\partial_j\phi, \quad B = \mathcal{S}\cos\theta, \quad \bar{B} = -p\mathcal{S}. \tag{2.30}$$

where we have used the Bianchi identity to introduce the gauge fields $\sigma^\alpha = \epsilon^{\alpha\beta\gamma}\partial_\beta A_\gamma$. The low-energy result (2.22) is recovered if we set $\sin\theta = 1$ and use the low-energy equation of motion (2.9).In terms of the full spin current the full Lagrangian density in Eq.2.6 can be expressed, in a dimensionless form as:

$$\begin{aligned} \mathcal{L} &= S(\cos\theta - p)\partial_t\phi - \frac{\mathcal{A}}{2}\left[\sin^2\theta(\nabla\phi)^2 + (\nabla\theta)^2\right] - \frac{\mathcal{K}}{2}\cos^2\theta \\ &= \sigma^0\partial_t\phi + \bar{\sigma}^0\partial_t\phi - \sigma^i\partial_i\phi - \left(\frac{\boldsymbol{\sigma}\cdot\boldsymbol{\sigma}}{2\mathcal{A}\sin^2\theta}\right) - \frac{\mathcal{A}}{2}(\nabla\theta)^2 - \frac{\mathcal{K}}{2}\cos^2\theta \end{aligned} \tag{2.31}$$

where we can integrate out the (as of now) three-vector spin current field $\boldsymbol{\sigma}$ to obtain the original theory. Let us now look at the first three terms, they can be re-written

as:

$$\begin{aligned} \mathcal{L}' &= \sigma^\alpha \partial_\alpha \phi + \bar{\sigma}^0 \partial_t \phi \\ &= \sigma^\alpha (\partial_\alpha \varphi + a^\alpha) + \bar{\sigma}^0 (\partial_t \varphi + a_0) \end{aligned} \tag{2.32}$$

where we have introduced the slowly varying spin wave field φ and the vortex source field a^α. Form here we can integrate out the slowly varying spin wave field in the first term using the conservation of spin current $\partial^\alpha \sigma_\alpha = 0$, and integrating by parts. Note that as before the spin wave field φ is well behaved everywhere in space and vanishes at the boundaries and that $\partial_t \bar{\sigma}^0 = 0$. This leaves us with the Lagrangian density:

$$\mathcal{L}(J, A) = -2\pi (A_\mu + \bar{A}_\mu) J^\mu + \frac{1}{2e^2} \left(\frac{\mathbf{E} \cdot \mathbf{E} - (\nabla B)^2}{1 - (B/\bar{B})^2} - B^2 \right). \tag{2.33}$$

The Lorentz-covariant form (2.25) is recovered in the limit when the dynamical magnetic field is weak and varies slowly in space, $\nabla B \ll B \ll \bar{B}$.

2.6 Quantum statistics of vortices

Up to this point, our theory of the XY ferromagnet in $d = 2 + 1$, recast as electrodynamics, has faithfully reproduced what is already known. The electrostatic analogy goes back to 1974 [30]; the dynamical similarity with electric charges in a background magnetic field is also not new [49, 50, 51]. Can we glean something more

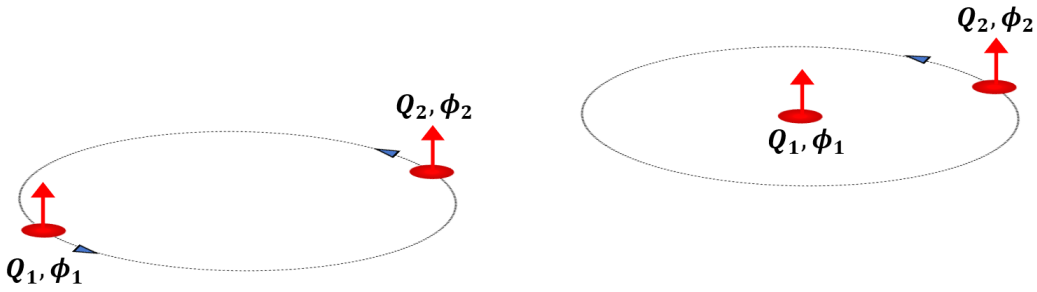

Figure 2.3: Each vortex acts as a localized center of charge and flux. The charge is given by the vorticity ($Q \equiv n$) and the flux by the net magnetic moment at the vortex core ($\Phi \equiv S_3$). In a situation where we have two such identical particles $Q_1 = Q_2$ and $\Phi_1 = \Phi_2$, we can imagine performing two different actions in the xy plane: exchange (shown on the left) and a braid (shown on the right). In either case we pick up two Berry phases one from each charge-flux winding, giving a statistical angle $\vartheta = 2\pi Q\Phi = 2\pi n S_3$.

from this duality ?

One interesting feature that, as far as we know, has not been previously pointed out is the presence of a magnetic field $B = \mathcal{S}\cos\theta$ localized at a vortex core, where $\cos\theta \neq 0$. The net magnetic flux of a vortex,

$$\Phi = \int d^2x\, B = \int d^2x\, \mathcal{S}\cos\theta = S_3, \tag{2.34}$$

is equal to the net spin S_3 of the vortex core. We thus find that a vortex behaves like a particle with both an electric charge $Q = n$ and a magnetic flux $\Phi = S_3$. The attachment of a well-localized magnetic flux does not influence the classical dynamics of a charged particle. However, it has important consequences at the quantum level because of the Aharonov-Bohm phase experienced by an electric charge moving

around a magnetic flux.

Wilczek [42, 43] pointed out that particles carrying both an electric charge q and magnetic flux Φ in $d = 2 + 1$, increment their statistical angle ϑ (0 for bosons and π for fermions) by $2\pi Q\Phi$. Viewed as a quantum particle, a vortex in a ferromagnet is ordinarily considered to be a boson [32]. The idea that a vortex carries both an electric charge $Q = n$ and a magnetic flux $\Phi = S_3$ means that its statistical angle is $\vartheta = 2\pi n S_3$. The most frequently encountered single vortices ($n = \pm 1$) can exhibit the fermion statistics if their spin S_3 is half-integer.

Are there vortices with a half-integer spin S_3? We do not know for sure. It is relatively easy to determine the spin of a vortex in a classical model such as the one defined by Eq. (2.8). The vortex core is well defined and its net spin is of the order of $e^2 = |\mathcal{S}|\mathcal{A}/\mathcal{K} \gg 1$. However, this classical answer varies continuously with the parameters of the model and is not quantized. More worryingly the compressibility of the size of the core itself raises the same issue that Haldane raised in the case of the superfluid vortices. What rescues our situation is that spins are quantized into integers and half-integers unlike the number of bosons trapped in a superfluid vortex core.

The problem needs to be solved at the quantum level. Aside from technical difficulties, such an endeavour runs into a conceptual problem. The transverse spin S_3 is a conserved quantity by virtue of the global O(2) rotational symmetry in the easy plane. However, in an ordered ferromagnet this symmetry is spontaneously broken

(even in a uniformly magnetized state). Therefore, the ground state of an ordered magnet is generally a superposition of (infinitely) many states with different values of S_3,

$$|\psi\rangle = \sum_{S_3} C_{S_3} |S_3\rangle, \tag{2.35}$$

and S_3 is not even a well-defined quantity. Fortunately, quantum statistics is determined not so much by the statistical angle ϑ but by its exponential $e^{i\vartheta} = e^{2\pi i n S_3}$. Because physical states are invariant under 2π rotations, the superposition (2.35) may only contain values of S_3 differing by integers, e.g., 1/2, 3/2, 5/2, ... or 0, 1, 2, ... The number $e^{2\pi i n S_3}$ is the same for all such S_3, so the quantum statistics of vortices is well defined even if S_3 is not.

We speculate that vortices with a half-integer spin could be found in single-layer ferromagnets. With two layers, the total spin would presumably double and give the trivial bosonic statistics. For the same reason, magnetic atoms with half-integer spin look more promising than ones with integer spin.

The attachment of fluxes to charges is absent in the naive dual theory (2.25). One could attempt to fix this deficiency by adding a Chern-Simons (CS) term, $\mathcal{L}_{\rm CS} = \pi k\, \epsilon^{\mu\nu\rho} A_\mu \partial_\nu A_\rho$ [52, 20]. Doing so would not affect the classical dynamics [48] and attach magnetic flux $\Phi = Q/k$ to an electric charge Q. However, this one-to-one correspondence between the charge and flux is too restrictive for our model. A magnetic vortex with "electric charge" $Q = n$ can have both positive and negative transverse "magnetic flux" $\Phi = S_3$, depending on the polarity $p = \pm 1$ of the core.

This $\mathbb{Z}_2$ degree of freedom is missing in the standard scenario of flux attachment via a CS term, thus requiring a more sophisticated approach.

Vortices in ferromagnets have been extensively studied for decades, both experimentally and theoretically. In practically all of these studies, vortices have been treated as *classical* objects. Only recently have theorists begun to ponder their unusual *quantum* properties. For example, Ivanov and co-workers [53, 54] considered the quantum mechanics of a single vortex in an atomic lattice with spins of length S. The single-vortex energy spectrum consists of $2S$ bands reminiscent of electron bands in a solid. Similar results for skyrmion energy bands were obtained by [55]. Noncommutativity of momentum components for vortices and skyrmions was pointed out by [56]; the same applies to their coordinates [57].

Thus we find that magnetic vortices, viewed as quantum particles, may exhibit nontrivial quantum statistics: vortices with a half-integer core spin S_3 are expected to be fermions. Even more exotic anyon statistics is expected for vortices with a non-integer $2S_3$. The existence of vortices with non-integer $2S_3$, also conjectured independently by Ivanov, would be a tantalizing possibility. However, it has been pointed out to us (by Prof. Feldman) that anyon statistics can probably be ruled out for vortices on account of the spin–statistics theorem [42, 58], which sets $e^{i\vartheta} = e^{-2\pi i S_3}$. This result is compatible with Eq. (2.5) for $n = 1$ only if $2S_3$ is an integer.

Chapter 3

Two-sublattice antiferromagnets

3.1 Introduction

In the previous chapter we presented the Lagrangian that produces the Landau-Lifshitz equations, for a ferromagnet on minimization with respect to the local magnetization field $\mathbf{m}(\mathbf{r}, t)$. In this chapter we extend this construction to the case of the antiferromagnets. In this case each magnetic unit cell comprises two or more magnetization fields $\mathbf{m}_i$ which are constrained by the exchange interaction to follow $\sum_i \mathbf{m}_i = 0$. To make this explicit note that we can convert the nearest neighbour exchange into:

$$H_{\text{exchange}} = J \sum_{<i,j>} \mathbf{S}_i \cdot \mathbf{S}_j = \frac{JS^2}{2} \sum_{\alpha} \left(\sum_i \mathbf{m}_i \right)_{\alpha}^2 - \frac{N}{2} \sum_{\alpha} S^2. \tag{3.1}$$

Here $\sum_i \mathbf{m}_i$ is a sum over all the spins that constitute the antiferromagnetic unit cell, if there are N sublattices then the sum is over N spins. The other sum α is over the lattice, broken down into the magnetic unit cell clusters. The second term is dropped as it is constant and does not enter equations of motion. To get to the continuum model we express the vector fields $\mathbf{m}_i$ in terms of the appropriate normal modes of the systems, dictated by the point group symmetry of the order, and expand the exchange interaction (and the other energies) in them.

The particular construction of the field theory depends on the specific lattice geometry. However, generically they all stem from labelling the sublattice magnetizations as individual fields and then putting them together by expressing the individual magnetization fields in terms of collective fields. The collective fields are of two kinds: soft modes which do not break $\sum_i \mathbf{m}_i = 0$, and hard modes which do break it and hence induce a net magnetization per unit cell.

In this chapter and the next we investigate two such constructions. We begin with more straightforward two-sublattice antiferromagnet. Here the meat of our discussion will focus on solitons (domain walls and vortices) of the order parameter field and induced dynamics in them. The spin wave theory will be briefly touched upon. A more detailed discussion is presented in seminal works by Anderson[59] and Haldane [60]. We then move on to the case of three-sublattice antiferromagnets on hexagonal lattices typified by the triangular lattice and the kagome lattice. There we focus on the spin wave theory, highlighting an alternate route to the magnon dispersions

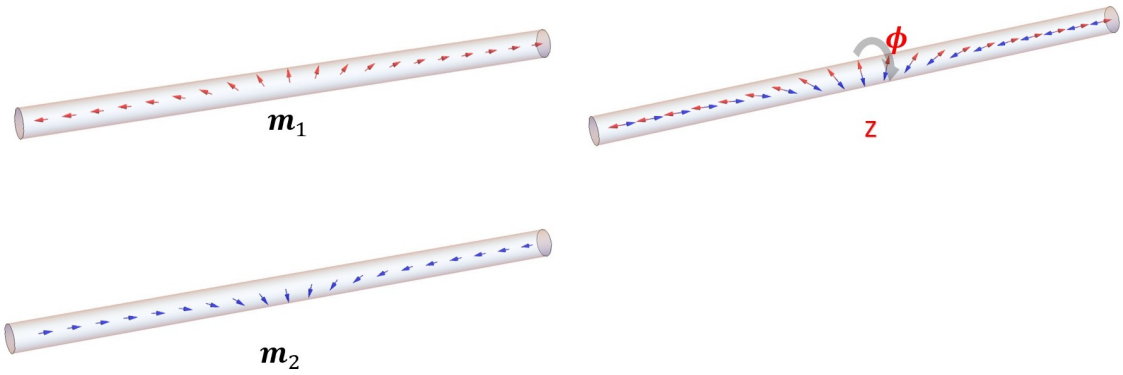

Figure 3.1: On the left we show the constituent sublattice magnetizations $\mathbf{m}_{1,2}$. These sublattices combine to form the antiferromagnet. A typical soliton in one dimension is a domain wall shown on the right. The domain wall is a soliton interpolating between the two unidirectional ground states of the one dimensional antiferromagnet.

from the Holstein-Primakoff mean field theory procedure. Later, we delve into the external perturbations that can couple to these hexagonal lattice systems and the kind of terms in the effective field theory engendered by the perturbations.

The two chapters are primarily based on work done in three papers. The gauge fields in antiferromagnets was done in collaboration with Se Kwon Kim and Oleg Tchernyshyov [61]. The spin wave theory of hexagonal antiferromagnet was sparked in a collaboration with Prof. Broholm's neutron scattering group. The experiment and related modelling is present in [62]. A broader theoretical perspective is presented in [63].

Solitonic dynamics in ferromagnets is dominated by gyroscopic effects generated by their angular momentum density. Thus, to propel a ferromagnetic vortex in the x direction of the xy plane, one applies a force in the y direction as we showed in Chapter 1, Eq.(1.26). Similarly, applying a force to a domain wall in a uniaxial ferromagnet

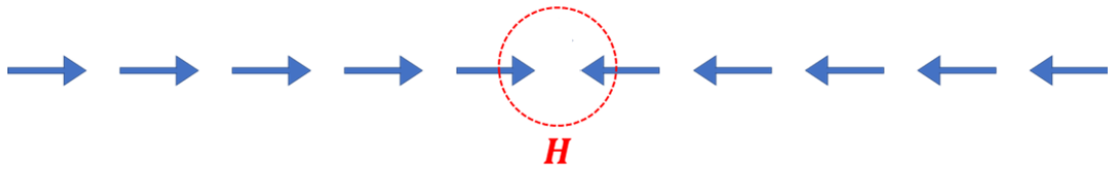

Figure 3.2: Here we show a head-to-head domain wall in an uniaxial ferromagnet. It is clear that at the location of the domain wall the moments point in and act as a sink for the magnetization. Now in a material we have $\mathbf{B} = \mathbf{H} + 4\pi\mathbf{M}$, since $\boldsymbol{\nabla} \cdot \mathbf{B} = 0$. A sink of magnetization $\mathbf{M}$, acts as a source for $\mathbf{H}$, $\boldsymbol{\nabla} \cdot \mathbf{H} = -4\pi\boldsymbol{\nabla} \cdot \mathbf{M}$. This is the origin of stray magnetic monopolar fields in ferromagnetic solitons.

primarily generates its precession. To propel it forward, one has to apply a torque to it. This is not the situation in antiferromagnets where a net angular momentum density is usually a secondary effect from local anisotropy and fights with a much larger exchange interaction.

For spintronics related applications, there are some potential advantages to antiferromagnets mainly an absence of long-range stray magnetic fields (see Fig. 3.2) and associated harmful crosstalk, the suppression of gyroscopic effects, and generally faster dynamics [64]. At the same time, there are new challenges. How does one apply a force to an antiferromagnetic soliton? An external magnetic field couples to the net magnetic moment, which is strongly suppressed in an antiferromagnet. Spin torque couples to the wrong channel, generating rotational, rather than translational, motion of an antiferromagnetic domain wall [65]. Here we attempt to resolve this question and arrive at generic conditions which result in propulsion of antiferromagnetic solitons.

A continuum theory of a collinear antiferromagnet with two sublattices operates

with two slowly varying (in space) fields $S\mathbf{m}_1(\mathbf{r})$ and $S\mathbf{m}_2(\mathbf{r})$, where S is as usual the spin size and $\mathbf{m}_1$, $\mathbf{m}_2$ are unit vector fields. In a state of equilibrium, $\mathbf{m}_1(\mathbf{r}) = -\mathbf{m}_2(\mathbf{r})$. More generally, the two sublattice fields are expressed in terms of dominant staggered magnetization $\mathbf{n} = (\mathbf{m}_1 - \mathbf{m}_2)/2$ and small uniform magnetization $\mathbf{m} = \mathbf{m}_1 + \mathbf{m}_2$. The constraints $|\mathbf{m}_1|^2 = 1$ and $|\mathbf{m}_2|^2 = 1$ translate into

$$\mathbf{m} \cdot \mathbf{n} = 0, \quad |\mathbf{n}|^2 = 1 - |\mathbf{m}|^2/4 \approx 1; \tag{3.2}$$

the last approximation is valid as long as $|\mathbf{m}|^2 \ll 1$.

3.2 The kinetic term and spin wave spectrum

We demonstrate the calculation of the spin wave spectrum for a two sublattice antiferromagnet on a square lattice with squares of side length a. The only interaction present is the nearest neighbour Heisenberg exchange J. The kinetic term for the antiferromagnet emerges from the Berry phases of the two sublattice magnetizations $\mathbf{m}_{1,2}$. The net phase for the unit cell can be expressed as:

$$\mathcal{L} = \mathcal{J}(\mathbf{a}_1.\dot{\mathbf{m}}_1 + \mathbf{a}_2.\dot{\mathbf{m}}_2), \tag{3.3}$$

here $\mathcal{J} = S/(2a^2)$ is the density of angular momentum in two dimensions with

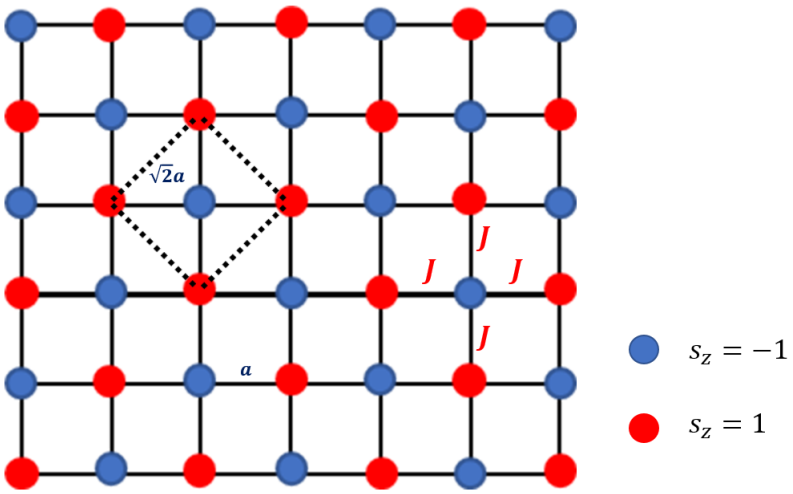

Figure 3.3: This figure shows the two dimensional two sublattice antiferromagnet. Red sites have their spins out of plane and blue spins have spins into the plane. The unit cell for each sublattice is marked in dashed lines. The exchanges are isotropic and are marked.

S as the moment (spin) length. While choosing the vector potentials for the two sublattices, $\mathbf{a}_{1,2}$, we choose different gauges, such that the Dirac string of the two monopoles lie on opposite hemispheres of the magnetization sphere. This ensures that neither $\mathbf{m_{1/2}}$ is near a Dirac string. The convenient choice is $\mathbf{a}_1(\mathbf{m}) = \mathbf{a}(\mathbf{m})$ and $\mathbf{a}_2(\mathbf{m}) = \mathbf{a}(-\mathbf{m})$.

In the equilibrium state when $\mathbf{m_1} = -\mathbf{m_2}$ the Berry phases of the two sublattices cancel exactly. This can be seen for the standard gauge choice of the vector potential $a_\theta = 0$ and $a_\phi = \frac{\cos\theta \pm 1}{\sin\theta}$. The Dirac string carries a 'flux' of $+4\pi$ either through the north or south pole. If we put the string through the south pole for $\mathbf{m}_1$ and through the north pole for $\mathbf{m}_2$ we have in equilibrium $\mathcal{L} = \mathcal{J}\left[\mathbf{a}(\mathbf{n}) - \mathbf{a}(-(-\mathbf{n}))\right] \cdot \dot{\mathbf{n}} = 0$.

The lowest non-vanishing kinetic terms are obtained by expanding the vector

potentials using $|\mathbf{m}|$ as a small parameter. Individually, $\mathbf{a}_1 \cdot \dot{\mathbf{m}}_1 = \mathbf{a}_1(\mathbf{m}/\mathbf{2} + \mathbf{n}) \cdot (\dot{\mathbf{m}}/2 + \dot{\mathbf{n}})$ and $\mathbf{a}_2 \cdot \dot{\mathbf{m}}_2 = \mathbf{a}_2(\mathbf{m}/\mathbf{2} - \mathbf{n}) \cdot (\dot{\mathbf{m}}/2 - \dot{\mathbf{n}})$. Expanding to quadratic order in $|\mathbf{m}|$ and $|\dot{\mathbf{n}}|$ the kinetic term, eq. (3.3) yields the following:

$$\begin{aligned} \mathcal{L} &= (\mathbf{a}_1(\mathbf{n}) + \mathbf{a}_2(-\mathbf{n})) \cdot \frac{\dot{\mathbf{m}}}{2} \\ &+ (\mathbf{a}_1(\mathbf{n}) - \mathbf{a}_2(-\mathbf{n})) \cdot \dot{\mathbf{n}} \\ &+ \frac{m_i}{2}\left(\frac{\partial \mathbf{a}_1(\mathbf{n})}{\partial n_i} - \frac{\partial \mathbf{a}_2(-\mathbf{n})}{\partial n_i}\right) \cdot \frac{\dot{\mathbf{m}}}{2} \\ &+ \frac{m_i}{2}\left(\frac{\partial \mathbf{a}_1(\mathbf{n})}{\partial n_i} + \frac{\partial \mathbf{a}_2(-\mathbf{n})}{\partial n_i}\right) \cdot \dot{\mathbf{n}} \end{aligned} \tag{3.4}$$

We have the identity $\frac{\partial \mathbf{a}_1(\mathbf{n})}{\partial n_i} - \frac{\partial \mathbf{a}_2(-\mathbf{n})}{\partial n_i} = 0$, from the definition of the vector potentials. This cancels the second and third terms. Now in the first term we transfer the time derivative to $\mathbf{a}$ using an integration by parts and combine with the corresponding vector potential term from the last line to get:

$$m_i \dot{n}_k \left(\frac{\partial a_k(\mathbf{n})}{\partial n_i} - \frac{\partial a_i(\mathbf{n})}{\partial n_k}\right) = \dot{\mathbf{n}} \cdot (\mathbf{n} \times \mathbf{m}), \tag{3.5}$$

where we have used $\boldsymbol{\nabla}_{\mathbf{n}} \times \mathbf{a} = -\mathbf{n}$. The potential energy is obtained from the

Heisenberg exchange:

$$\begin{aligned} U &= JS^2 \sum_{<i,j>} \mathbf{m}_i \cdot \mathbf{m}_j, \\ &= \frac{JS^2}{2} \sum_{\alpha} (\mathbf{m}_1 + \mathbf{m}_2)^2_\alpha \\ &= \int dV \; \frac{JS^2}{2} \left(\frac{2\mathbf{m}^2}{a^2} + (\partial_i \mathbf{n})^2 + \frac{(\partial_i \mathbf{m})^2}{2} \right), \end{aligned} \tag{3.6}$$

where J is the Heisenberg exchange strength and in the second line we have dropped the constant term. In the second line we have expressed the summation over nearest neighbours in terms of summation over two site magnetic unit cells α. We can see that the uniform magnetization picks up an energy contribution from the exchange interaction at the zeroth order in gradients and is hence a hard mode. The Neel field $\mathbf{n}$ only appears through gradients and is the typical example of a soft mode in antiferromagnetic systems.

The procedure to obtain the effective field theory is similar to the planar ferromagnet: we integrate out the hard field and express the theory in terms of the soft field and this process generates an inertia for the soft mode. Since $\mathbf{m}$ is hard we shall drop its gradient terms. Let us carry this out explicitly:

$$\mathcal{L} = \frac{S}{2a^2} \; \dot{\mathbf{n}} \cdot (\mathbf{n} \times \mathbf{m}) - \frac{JS^2}{2} \left(\frac{2\mathbf{m}^2}{a^2} + (\partial_i \mathbf{n})^2 \right). \tag{3.7}$$

Now we can solve for the hard field $\mathbf{m} = (\dot{\mathbf{n}} \times \mathbf{n})/(4JS)$. Plugging this solution back

into the Lagrangian we get a field theory for the soft Neel field $\mathbf{n}$:

$$\mathcal{L} = \frac{\rho}{2}\dot{\mathbf{n}}^2 - \frac{JS^2}{2}\left(\boldsymbol{\nabla}\mathbf{n}\right)^2, \tag{3.8}$$

with $\rho = 1/(8Ja^2)$. Here we have used $(\dot{\mathbf{n}} \times \mathbf{n})^2 = \dot{\mathbf{n}}^2$ as $\mathbf{n} \cdot \dot{\mathbf{n}} = 0$ from the unit vector constraint of $\mathbf{n}$.

The ordered state spontaneously breaks the degrees of freedom associated with the staggered magnetization vector $\mathbf{n}(\theta, \phi)$. Hence in this case there are two Goldstone modes, one for each continuous degree of freedom, dispersing linearly according to $\omega = ck$, with $c = \pm(2\sqrt{2}JS)$.

3.3 Moving antiferromagnetic solitons

We shall now look into the two sublattice antiferromagnet where the only spatial dependence of the staggered magnetization field $\mathbf{n}$ is at the location of defects, taking the remaining system to be ordered at any particular instant of time. Also since we explicitly couple to external magnetic fields we switch to magnetic moment densities from spin densities the two are related by $M = \gamma S$. The theory we work with:

$$\mathcal{L} = \mathcal{J}\dot{\mathbf{n}} \cdot (\mathbf{n} \times \mathbf{m}) - \left(\frac{\mathcal{M}^2}{2\chi}\right)\mathbf{m}^2 - \mathcal{U}_{\text{ext}}[\boldsymbol{\zeta}, \mathbf{n}, \mathbf{m}], \tag{3.9}$$

where we have absorbed the Heisenberg exchange strength into a spin susceptibility χ and $\mathcal{J} = \mathcal{M}/\gamma$ and γ is the gyromagnetic ratio. $\boldsymbol{\zeta}$ in the theory is an external field. Our main objective is to see how various external perturbations modify the Lagrangian density, in particular how they couple to the soft mode $\mathbf{n}$. Once we have an understanding of these couplings we shall study their effects on solitons in the staggered magnetization order. We shall outline the manner in which these solitons can be effectively moved in space by coupling to the order parameter. In particular we want to see how we can effectively displace uniaxial domain walls and planar vortices in $\mathbf{n}$.

As in the case of the ferromagnet we can study the dynamics of the antiferromagnet under an external magnetic field and a spin current in a perturbative regime. These external vector fields couple either to the uniform magnetization $\mathbf{m}(\mathbf{r}, t)$ or the staggered magnetization $\mathbf{n}(\mathbf{r}, t)$ in the Lagrangian. This is broadly guided by symmetries like time reversal and mirror planes of the spin Hamiltonian.

Fields which couple to $\mathbf{m}$ produce a gauge coupling to $\dot{\mathbf{n}}$, on integrating out $\mathbf{m}$. This is the case with perturbations like an external magnetic field $\mathbf{H}(\mathbf{r}, t)$ or a spin transfer torque characterized by the drift velocity $\mathbf{u}(\mathbf{r}, t)$. We shall show that such terms require a spatial or temporal variation of the external vector field to produce solitonic motion. Additionally these terms can be applied in a combination that generates an emergent gyrotropic effect on an antiferromagnetic soliton.

The coupling to $\mathbf{n}$ gives rise to terms like $(\boldsymbol{\zeta} \cdot \mathbf{n})^n$ where $n = 1, 2$ in the cases

we studied. Here $\boldsymbol{\zeta}$ represents an external field sourced from a combination of terms like the Dzyaloshinski-Moriya interaction, external magnetic fields or combinations. This term acts like a potential energy density. Expressed in terms of the collective coordinates, this generates a force that can change the position of the domain wall. Note here that an antiferromagnetic soliton by virtue of Eq. (3.8) is inertial, i.e. a push/force propels an antiferromagnetic domain wall instead of rotating it unlike the ferromagnetic case. We show that Dzyaloshinski-Moriya interactions generate such terms and can be exploited to move solitons.

3.3.1 Magnetic field

We start with the effect of the external magnetic field $\mathbf{H}$. The external magnetic field enters the Lagrangian as a Zeeman coupling to the uniform magnetization $\mathcal{U} = -\mathcal{M}\mathbf{H}\cdot\mathbf{m}$ [66]. This produces the Lagrangian density:

$$\mathcal{L}[\mathbf{m},\mathbf{n}] = \mathcal{J}\dot{\mathbf{n}}\cdot(\mathbf{n}\times\mathbf{m}) - \left(\frac{\mathcal{M}^2}{2\chi}\right)|\mathbf{m}|^2 + \mathcal{M}\mathbf{H}\cdot\mathbf{m}, \tag{3.10}$$

A straightforward minimisation with respect to $\mathbf{m}$ gives $\mathbf{m} = \left(\frac{\chi\mathcal{J}}{\mathcal{M}^2}\right)\dot{\mathbf{n}}\times\mathbf{n} + \left(\frac{\chi}{\mathcal{M}}\right)\mathbf{H}$ which violates the constraint $\mathbf{m}\cdot\mathbf{n} = 0$. To ensure the perpendicularity we resolve $\mathbf{h}$ into a component perpendicular to $\mathbf{n}$, $\mathbf{h}_\perp = \mathbf{n}\times(\mathbf{h}\times\mathbf{n})$ which enters the Zeeman coupling $\mathbf{m}\cdot\mathbf{h}_\perp$ to produce a term $(\mathbf{n}\times\mathbf{H})\cdot(\mathbf{n}\times\mathbf{m})$. Now on solving for $\mathbf{m}$ we obtain $\mathbf{m} = \left(\frac{\chi\mathcal{J}}{\mathcal{M}^2}\right)(\dot{\mathbf{n}}\times\mathbf{n}) + \left(\frac{\chi}{\mathcal{M}}\right)(\mathbf{n}\times\mathbf{H})\times\mathbf{n}$. Substituting this into the Lagrangian

we obtain:

$$\mathcal{L}(\mathbf{n}) = \frac{\rho(\dot{\mathbf{n}} - \gamma\mathbf{h}\times\mathbf{n})^2}{2} - \mathcal{U}(\mathbf{n}). \tag{3.11}$$

The Lagrangian is identical to that of a particle in a rotating frame with an angular velocity $\gamma|\mathbf{h}|$. It is clear that an external magnetic field will cause a texture in $\mathbf{n}$ to precess. There is an additional contribution to the energy in the form of $\mathcal{U}_H = -\frac{M^2}{2a}(\mathbf{n}\times\mathbf{H})^2$ which adds to the crystal anisotropy term in the energy functional.

Let us take a closer look at each of the terms in Eq.(3.11). The term $\rho\dot{\mathbf{n}}^2/2$ is the kinetic energy of staggered magnetization and $\rho = \chi/\gamma^2$ is the density of inertia [67, 68]. This term endows antiferromagnetic solitons with a mass. Suppose a soliton is parametrized by a set of collective coordinates $\mathbf{q} = \{q_1, q_2, \ldots\}$ such as the position of a domain wall, the coordinates of a vortex core etc. The variation of $\mathbf{n}$ in time is mediated by the change of these collective coordinates: $\dot{\mathbf{n}} = \dot{q}_i\partial\mathbf{n}/\partial q_i$. The soliton's kinetic energy is then $M_{ij}\dot{q}_i\dot{q}_j/2$, where $M_{ij} = \rho\int dV\, \frac{\partial\mathbf{n}}{\partial q_i}\cdot\frac{\partial\mathbf{n}}{\partial q_j}$ is the inertia tensor [69].

The potential term $\rho|\gamma\mathbf{h}\times\mathbf{n}|^2/2$ in Eq. (3.11) expresses local anisotropy favouring the direction of $\mathbf{n}$ orthogonal to the effective field $\mathbf{h}$. This term modifies the potential landscape $U(\mathbf{q})$ of a soliton:

$$U[\mathbf{q}, \mathbf{h}(\mathbf{r})] = U[\mathbf{q}, 0] - \int dV\, \frac{\rho|\mathbf{h}\times\mathbf{n}|^2}{2}. \tag{3.12}$$

It is notable that the cross term $\rho\gamma\mathbf{h}\cdot(\dot{\mathbf{n}}\times\mathbf{n})$ in Eq. (3.11) is linear in the time

derivative $\dot{\mathbf{n}}$ and thus quantifies the effective geometric phase for the dynamics of staggered magnetization. In the Lagrangian of a soliton, it turns into $A_i\dot{q}_i$, a coupling to an external gauge field

$$A_i(\mathbf{q}) = \int dV\, \rho\gamma\mathbf{h} \cdot \left(\frac{\partial \mathbf{n}}{\partial q_i} \times \mathbf{n} \right). \tag{3.13}$$

The equations of motion for an antiferromagnetic soliton have the form of Newton's second law for a particle of unit electric charge in this gauge field:

$$M_{ij}\ddot{q}_j = -\partial U/\partial q_i + E_i + F_{ij}\dot{q}_i - M_{ij}\dot{q}_j/T. \tag{3.14}$$

The "magnetic field" $F_{ij} = -F_{ji}$ is the curl of the gauge potential:

$$F_{ij} = \frac{\partial A_j}{\partial q_i} - \frac{\partial A_i}{\partial q_j} = -2 \int dV\, \rho\gamma\mathbf{h} \cdot \left(\frac{\partial \mathbf{n}}{\partial q_i} \times \frac{\partial \mathbf{n}}{\partial q_j} \right). \tag{3.15}$$

For the collective coordinates X_α representing rigid translations $x_\alpha \mapsto x_\alpha + X_\alpha$ of a magnetic soliton, the "magnetic field" $F_{\alpha\beta}$ is related to the gyrovector $\mathbf{G}$: $G_\alpha = \frac{1}{2}\epsilon_{\alpha\beta\gamma}F_{\beta\gamma}$; $F_\alpha = F_{\alpha\beta}\dot{X}_\alpha = \epsilon_{\alpha\beta\gamma}\dot{X}_\beta G_\gamma$ is the gyrotropic force [70]. The "electric field"

$$E_i = -\int dV\, \rho\gamma\dot{\mathbf{h}} \cdot \left(\frac{\partial \mathbf{n}}{\partial q_i} \times \mathbf{n} \right) \tag{3.16}$$

arises if $\mathbf{h}$ depends explicitly on time.

The "electromagnetic fields" satisfy Jacobi identities

$$\frac{\partial E_j}{\partial q_i} - \frac{\partial E_i}{\partial q_j} + \frac{\partial F_{ij}}{\partial t} = 0, \quad \frac{\partial F_{ij}}{\partial q_k} + \frac{\partial F_{jk}}{\partial q_i} + \frac{\partial F_{ki}}{\partial q_j} = 0. \tag{3.17}$$

the analogs of Maxwell's $\nabla \times \mathbf{E} + \dot{\mathbf{B}} = 0$ and $\nabla \cdot \mathbf{B} = 0$. In fact, we can define local versions of the "electromagnetic fields" as it was previously done for a ferromagnet [71],

$$\begin{aligned} A_\alpha &= \rho\gamma \mathbf{h} \cdot (\partial_\alpha \mathbf{n} \times \mathbf{n}), \\ E_\alpha &= -\rho\gamma \dot{\mathbf{h}} \cdot (\partial_\alpha \mathbf{n} \times \mathbf{n}), \\ B_\alpha &= -\epsilon_{\alpha\beta\gamma}\, \rho\gamma \mathbf{h} \cdot (\partial_\beta \mathbf{n} \times \partial_\gamma \mathbf{n}). \end{aligned} \tag{3.18}$$

The emergent fields couple to an electric current and are, in principle, measurable as in the ferromagnetic case [72].

The last term on the right-hand side of Eq. (3.14) is a viscous force with the mode-independent relaxation time $T = \rho/(2\alpha\mathcal{J})$, where α is Gilbert's dimensionless damping constant [73].

Easy axis antiferromagnet and the domain wall: We shall now use the simplest soltion at our disposal: a domain wall in a one dimensional easy axis antiferromagnet, see Fig. 3.1 to illustrate the effects of an external magnetic field. The

Heisenberg exchange for the local magnetization gives rise to the energy density:

$$\mathcal{U}(\mathbf{n}) = \frac{A}{2}\left|\frac{\partial \mathbf{n}}{\partial z}\right|^2 + \frac{K}{2}|\mathbf{e}_3 \times \mathbf{n}|^2. \tag{3.19}$$

Here $A > 0$ characterizes the strength of exchange, $K > 0$ is the easy axis anisotropy, and $\mathbf{e}_3 = (0, 0, 1)$. This system has two uniform ground states $\mathbf{n} = \pm\mathbf{e}_3$, linear excitations in the form of spin waves with the dispersion $\omega^2 = (K + Ak^2)/\rho$, and nonlinear solitons in the form of domain walls which interpolate between the two ground states. Static domain walls in $\mathbf{n} = (\sin\theta(z)\cos\phi, \sin\theta(z)\sin\phi, \cos\theta(z))$ have width $\lambda = \sqrt{A/K}$ and are parametrized in spherical angles $\theta(z)$ and $\phi(z)$ as follows:

$$\cos\theta(z) = \pm\tanh\frac{z - Z}{\lambda}, \quad \phi(z) = \Phi. \tag{3.20}$$

Position Z and azimuthal angle Φ represent the two zero modes of the system associated with the global symmetries of translation and rotation see Fig. 3.1. Weak or local external perturbations do not alter the shape of the soliton significantly and mostly induce the dynamics of Z and Φ.

The Lagrangian of a domain wall at this level contains kinetic energy: $L = M\dot{Z}^2/2 + I\dot{\Phi}^2/2$, where $M = 2\rho/\lambda$ is the mass and $I = M\lambda^2$ is the moment of inertia. Thus a domain wall behaves like a point mass constrained to move on the surface of a cylinder of radius λ. This link to a particle in a rotating frame was earlier noted in Eq. (3.11).

In the simplest case, the linear in $\mathbf{m}$ term in Eq. (3.10) comes from the external magnetic field $\mathbf{H}$, so that $\mathbf{h} = \mathbf{H}$. The gauge potential (3.13) for a domain wall (3.20) is:

$$A_Z = \pm\pi\rho\gamma(H_x \sin\Phi - H_y \cos\Phi), \quad A_\Phi = -2\rho\lambda\gamma H_z. \tag{3.21}$$

For a particle on the surface of a cylinder, these describe a "magnetic field" embedded in three dimensions,

$$\mathbf{B} = \frac{M\gamma}{2}(\pm\pi H_x, \pm\pi H_y, -4H_z). \tag{3.22}$$

When $\mathbf{B}$ is time-dependent, it induces an "electric field" $\mathbf{E}$ with the following axial and azimuthal components on the surface of the cylinder:

$$\mathbf{E}\cdot\mathbf{e}_3 = \pm\frac{\pi M\lambda\gamma}{2}\dot{\mathbf{H}}\cdot\mathbf{e}_\phi, \quad \mathbf{E}\cdot\mathbf{e}_\phi = M\lambda\gamma\dot{\mathbf{H}}\cdot\mathbf{e}_3, \tag{3.23}$$

where $\mathbf{e}_\phi = (-\sin\Phi, \cos\Phi, 0)$ is a unit vector in the azimuthal direction. The net "electromagnetic" force in the axial direction is

$$F_Z^{\rm em} = E_Z + F_{Z\Phi}\dot{\Phi} = \frac{d}{dt}\left(\pm\frac{\pi M\lambda\gamma}{2}\mathbf{H}\cdot\mathbf{e}_\phi\right). \tag{3.24}$$

A sustained "electromagnetic" force can be generated if the real magnetic field $\mathbf{H}$ (more precisely, its azimuthal component $\mathbf{H}\cdot\mathbf{e}_\phi$) rises linearly in time. This

is not a practical way to propel a domain wall. The "electromagnetic" force from an oscillating external field $\mathbf{H}(t)$ averages out to zero over time. To overcome this problem, Gomonay *et al* [74] proposed a ratchet propulsion mechanism combining periodic field pulses with an asymmetric profile $\mathbf{H}(t)$ and static friction. If the field is ramped up and down at different rates, the friction force, opposing the motion of the domain wall, has different magnitudes during the rise and fall of the field pulse $\mathbf{H}(t)$. As a result, even though the average "electromagnetic" force vanishes, the friction force does not.

The peculiar result for the "electromagnetic" force (3.24) is not specific to the example of a domain wall. Generally, if a soliton has a zero mode q_a associated with a global symmetry and the effective field $\mathbf{h}$ respects this symmetry, the corresponding "electromagnetic" force is given by the "electric field" alone:

$$F_a^{\rm em} = \frac{\delta}{\delta q_a}\int dt\, A_i \dot{q}_i = -\frac{dA_a}{dt} + \frac{\partial A_i}{\partial q_a}\dot{q}_i = -\frac{dA_a}{dt} \tag{3.25}$$

(translations in q_a do not change gauge potentials A_i). The long-time average of the force is 0, unless $A_a(t)$ keeps growing in time.

This situation is entirely equivalent to charging an LC circuit where over a cycle the energy is transferred back and forth between the inducator (L) and capacitor (C) without any dissipation. The only way to extract energy from the system is to add a resistance R (friction) [75]. It would be interesting to explore whether a

spatially nonuniform and time-dependent oscillating magnetic field $\mathbf{H}(\mathbf{r}, t)$ can be used to accelerate solitons.

3.3.2 Spin Transfer Torque

Another important external perturbation is the spin torque from an electric current in a metallic antiferromagnet. Spins of electrons moving in an inhomogeneous magnetic background undergo precession and thus exchange angular momentum with the soliton. Here we focus on adiabatic spin torque that results when electron spins follow the local direction of magnetization. We rely on a simple hopping model for the electron in which a conduction electron couples to only one of the antiferromagnetic sublattices [76].

For a ferromagnetic system the spin transfer torque is incorporated through the addition of a gradient term in the Landau-Lifshitz equation:

$$\mathcal{J}\dot{\mathbf{m}} = \mathbf{h}_{\text{eff}} \times \mathbf{m} - \mathcal{J}(\mathbf{u} \cdot \boldsymbol{\nabla})\mathbf{m} + \alpha\mathcal{J}\mathbf{m} \times \dot{\mathbf{m}}, \tag{3.26}$$

where $\mathbf{u}$ characterizes the coupling of the electron current to the local moments and is proportional to the electron drift velocity. The adiabatic spin transfer torque can be incorporated through a simple modification of the kinetic term in the Lagrangian: the time derivative ∂_t is replaced with the convective derivative $\partial_t + \mathbf{u} \cdot \nabla$ [77]. For the antiferromagnet the effect of spin torque is computed for each sublattice inde-

pendently. This leads to a kinetic term proportional to $\mathbf{m} \cdot [(\partial_t + \mathbf{u} \cdot \nabla)\mathbf{n} \times \mathbf{n}]$. On integrating out $\mathbf{m}$ this leads to a Lagrangian for the Neel field:

$$\mathcal{L}(\mathbf{n}) = \frac{\rho(\dot{\mathbf{n}} + (\mathbf{u} \cdot \nabla)\mathbf{n})^2}{2} - \mathcal{U}(\mathbf{n}). \tag{3.27}$$

Here $\mathbf{u}$ is the drift velocity of electrons related to the electric current $\mathbf{j} = en\mathbf{u}$; n is the concentration of electrons. In this case the theory is identical to a particle on a uniformly translating reference frame with a velocity $\mathbf{u}$. Although this does imply that solitons will 'translate' in the presence of an adiabatic spin current the net displacement will be reversed as soon as the current is switched off.

The Lagrangian density for the full system (3.10) acquires a term $\mathcal{J}\mathbf{m} \cdot [(\mathbf{u} \cdot \nabla)\mathbf{n} \times \mathbf{n}]$, from which we read off the effective magnetic field $\mathbf{h} = \gamma^{-1}(\mathbf{u} \cdot \nabla)\mathbf{n} \times \mathbf{n}$. The induced uniform magnetization $\mathcal{M}\mathbf{m} = \gamma\rho(\mathbf{u} \cdot \nabla)\mathbf{n} \times \mathbf{n}$ agrees with the standard phenomenology of adiabatic spin torque [76].

Returning to our model of an easy-axis antiferromagnet in one dimension, we compute the gauge potential (3.13) with $\gamma\mathbf{h} = u\,\partial_z\mathbf{n} \times \mathbf{n}$ to obtain

$$A_Z = -Mu, \quad A_\Phi = 0. \tag{3.28}$$

The "magnetic field" $F_{Z\Phi} = \partial_Z A_\Phi - \partial_\Phi A_Z = 0$, whereas the "electric field" $E_Z = -\dot{A}_Z = M\dot{u}$ is once again proportional to the time derivative of an external perturbation. Thus adiabatic spin torque alone cannot be used to propel a domain wall

[76].

3.3.3 Dzyaloshinski-Moriya Interaction

We will now examine the effect of adding the antisymmetric exchange or DM interaction [14, 15] to the Lagrangian. This interaction exists in an antiferromagnet with broken inversion symmetry intrinsically or at interfaces like sample edges and extended domain walls. The interaction is characterized by the energy density $\mathcal{U}_{\rm DMI} = \mathbf{D}\cdot(\mathbf{S}_i\times\mathbf{S}_j) = \frac{\mathbf{D}\mathcal{M}^2}{\gamma^2}\cdot(\mathbf{m}_i\times\mathbf{m}_j)$ where the direction of the DM vector $\mathbf{D}$ is dictated by the Moriya rules[15]. Their net effect is to induce a weak ferromagnetism in the material, which then couples to external torques and fields. The emergence of a ferromagnetic moment also implies the existence of a non zero gyrotropic force in these systems. In the presence of a DM interaction the theory takes the form:

$$\mathcal{L}[\mathbf{m},\mathbf{n}] = \mathcal{J}\dot{\mathbf{n}}\cdot(\mathbf{n}\times\mathbf{m}) - \left(\frac{\mathcal{M}^2}{2\chi}\right)|\mathbf{m}|^2 - \left(\frac{\mathcal{M}^2}{\gamma^2}\right)\mathbf{D}\cdot(\mathbf{n}\times\mathbf{m}) - U[\mathbf{n}], \qquad (3.29)$$

This adds an extra term to the solution for the staggered magnetization $\mathbf{m} = \left(\frac{\chi\mathcal{J}}{\mathcal{M}^2}\right)\dot{\mathbf{n}}\times\mathbf{n} - \frac{\chi}{\gamma^2}(\mathbf{D}\times\mathbf{n})$. On integrating out the uniform magnetization we obtain:

$$\mathcal{L} = \frac{\rho(\dot{\mathbf{n}} - (\mathcal{M}/\gamma)\mathbf{D})^2}{2} - \mathcal{U}(\mathbf{n}, D). \qquad (3.30)$$

where there is a new 'easy-axis' anisotropy term $\mathcal{U}[\mathbf{n}, D] \propto (\mathbf{n} \cdot \mathbf{D})^2$ from the DM vector. The coupling with the kinetic term gives rise to a vector potential of the form $A_i^{DMI} = \frac{J}{a} \int \frac{\partial \mathbf{n}}{\partial q_i} \cdot \mathbf{D}$. Just as in the previous cases of the magnetic field and the spin current the gyrotropic force generated by this averages to zero over a full cycle, unless we have a $\mathbf{D}$ that varies in time.

3.3.4 Crossed Interactions

Evidently, single perturbations are ineffective in moving antiferromagnetic solitons over a closed cycle. The way out of this conundrum is to combine these perturbations. The theme of these combinations is similar, one of the perturbations either a magnetic field $\mathbf{H}(\mathbf{r}, t)$ or a DM interaction $\mathbf{D}(\mathbf{r}, t)$ is used to locally (at the location of the soliton) induce a small magnetic moment (a source of Berry curvature) which the other perturbation, say the spin current $\mathbf{u}(\mathbf{r}, \mathbf{t})$, latches on to and generates a displacement of the soliton.

DM interaction and external magnetic field: If these two types of terms are simultaneously present in the system the Lagrangian density takes the form:

$$\mathcal{L} = \frac{\rho(\dot{\mathbf{n}} + \gamma(\mathbf{n} \times \mathbf{h}) - (\mathcal{M}/\gamma)\mathbf{D})^2}{2} - \mathcal{U}(\mathbf{n}, \mathbf{D}, \mathbf{h}). \tag{3.31}$$

The cross term of interest is:

$$\mathcal{U}_{\text{DM-h}} = -\rho\mathcal{M}\ \mathbf{n}\cdot(\mathbf{D}\times\mathbf{h}). \tag{3.32}$$

This term acts as a 'Zeeman' term but for the staggered magnetization with an effective magnetic field $\mathbf{h}_{\text{eff}} = (\mathbf{D}\times\mathbf{h})$. Note that in the presence of a DM interaction the extra uniform magnetization that is induced is $\mathbf{m} \propto (\mathbf{D}\times\mathbf{n})$. It is this extra induced ferromagnetic moment that 'Zeeman' couples with the external magnetic field.

This coupling expressed in collective coordinates acts like a potential energy for the domain wall and will produce force on the wall itself. However, to cause a net displacement in the position of the wall we require: $(\mathbf{D}\times\mathbf{h})_{\text{easy-axis}} \neq 0$, such that the force is in the correct channel. Here the easy axis points along the length of the domain wall. This requires in particular a DM vector that is not aligned along the easy axis. In our example domain wall this implies $D_z = 0$.

Crossed magnetic field and spin current: This situation is theoretically more interesting. We shall first delve on how we can locally induce a Berry phase density in an antiferromagnet using an external magnetic field. We follow up by using this density in the context of an antiferromagnetic vortex to generate a Magnus force which up till now was restricted to the realm of ferromagnetic vortices.

The interplay of adiabatic spin torque and an external magnetic field occurs

through the potential term in the Lagrangian density $\rho|\gamma\mathbf{h}\times\mathbf{n}|^2/2$ with the effective field $\gamma\mathbf{h}=\gamma\mathbf{H}+(\mathbf{u}\cdot\nabla)\mathbf{n}\times\mathbf{n}$, namely through the part $\rho\gamma\mathbf{H}\cdot(u_\alpha\partial_\alpha\mathbf{n}\times\mathbf{n})$ that is linear in the applied field $\mathbf{H}$ and the drift velocity $\mathbf{u}$. Its contribution to the stress tensor is

$$\sigma_{\alpha\beta}=\epsilon_{\alpha\mu}\epsilon_{\beta\nu}u_\mu\rho\gamma\mathbf{H}\cdot(\partial_\nu\mathbf{n}\times\mathbf{n}) \tag{3.33}$$

in 2 spatial dimensions.

This effect can be written out in terms of the collective coordinate set $\{q_1,q_2,...\}$. Generically, we require a conjugate pair for this effect to work (q_α,q_β). The magnetic field produces a gyrotropic tensor $G_{q_\alpha q_\beta}$ locally which the adiabatic spin current couples to. For a domain wall we are limited to the choice (Z,Φ). A magnetic field along the long axis $\hat{z}$ will cause a precession in both sublattices without inducing any Berry curvature, killing the effect.

Luckily we are rescued by the two dimensional (planar) systems where the two conjugate collective coordinates of vortices are (X,Y), the locations of the vortex core. We shall use this example to detail how this set of crossed fields can be used to generate a Magnus force for an antiferromagnetic vortex.

The Magnus force on the vortex core is obtained by integrating stress around a contour containing the core, $F_\alpha=-\oint\sigma_{\alpha\beta}\,dS_\beta$, where $dS_\beta=\epsilon_{\beta\lambda}dx_\lambda$ is an "area"

element normal to the contour segment dx_λ:

$$\begin{aligned} F_\alpha &= -\epsilon_{\alpha\mu} u_\mu \oint dx_\nu \, \rho\gamma \mathbf{H} \cdot (\partial_\nu \mathbf{n} \times \mathbf{n}) \\ &= \epsilon_{\alpha\mu} u_\mu \rho\gamma H \oint dx_\nu \, \partial_\nu \phi = -F_{\alpha\mu} u_\mu, \end{aligned} \tag{3.34}$$

as expected. In three dimensions for an antiferromagnetic vortex line, this translates into:

$$\mathbf{F} = 2\pi n \rho\gamma H \int \mathbf{u} \times d\mathbf{r}, \tag{3.35}$$

3.3.5 Antiferromagnetic vortices and (re)emergence of Berry curvature

Consider a Heisenberg antiferromagnet in two spatial dimensions with easy-plane ($K < 0$) anisotropy with potential energy density

$$\mathcal{U}(\mathbf{n}) = \frac{A}{2} |\nabla \mathbf{n}|^2 + \frac{K}{2} |\mathbf{e}_3 \times \mathbf{n}|^2. \tag{3.36}$$

It has uniform ground states $\mathbf{n} = (\cos\phi, \sin\phi, 0)$. Topological solitons are vortices $\mathbf{n}(\mathbf{r} - \mathbf{R})$, where $\mathbf{R} = (X, Y)$ is the location of the center of the vortex. A vortex centred at the origin, $\mathbf{n}(\mathbf{r})$, is parametrized in spherical angles as

$$e^{i\phi(\mathbf{r})} = \left(\frac{x + iy}{|x + iy|} \right)^n, \quad \cos\theta(\mathbf{r}) = \pm f_n(r/\lambda). \tag{3.37}$$

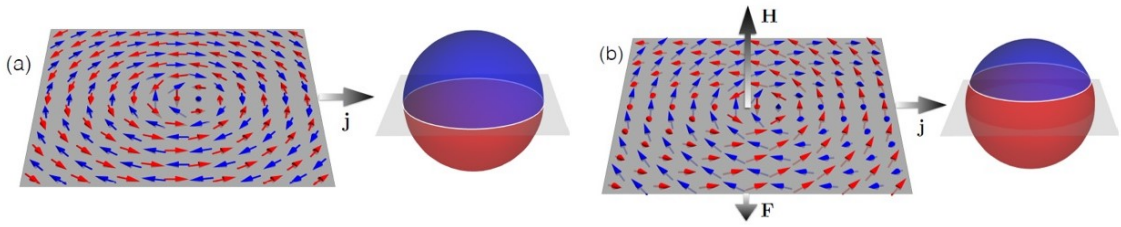

Figure 3.4: A vortex in an easy-plane antiferromagnet in zero magnetic field (a) and in a field $\mathbf{H}$ pointing along the hard axis normal to the plane (b). A combination of the field and an in-plane electric current $\mathbf{j}$ gives rise to a Magnus force $\mathbf{F} \propto \mathbf{j} \times \mathbf{H}$. Sublattice magnetizations $\mathbf{m}_1$ and $\mathbf{m}_2$ are shown in blue and red. Right panels show portions of the unit sphere covered by the magnetization fields $\mathbf{m}_1(\mathbf{r})$ and $\mathbf{m}_2(\mathbf{r})$.

Here $n \in \mathbb{Z}$ is the vortex winding number (vorticity). The function $f(\xi)$ is a profile of the out-of-plane magnetization at the vortex core with $f_n(0) = 1$ and $f_n(\infty) = 0$; $\lambda = \sqrt{A/|K|}$ is the radius of the core. The vortex mass $M = \pi\rho \ln(\Lambda/\lambda)$ depends logarithmically on the core radius λ and on a long-distance cutoff Λ, which can be the size of the system or the screening length due to the presence of other vortices.

A magnetic field $\mathbf{H} = H\mathbf{e}_3$ along the hard axis breaks the time-reversal symmetry of the antiferromagnet and allows for non-vanishing gyrotropic coefficients

$$G_{XY} = -G_{YX} = \int d^2r\, (-2\rho\gamma\mathbf{H}) \cdot (\partial_x\mathbf{n} \times \partial_y\mathbf{n}). \tag{3.38}$$

This expression follows from Eq. (3.15) under the assumption of a rigid soliton $\mathbf{n}(\mathbf{r} - \mathbf{R})$, for which $\partial_X = -\partial_x$ and $\partial_Y = -\partial_y$. To bring out the topological nature of this quantity, we recast the integrand as a curl $\partial_x a_y - \partial_y a_x$ of the vector $a_\alpha = \rho\gamma\mathbf{H}\cdot(\partial_\alpha\mathbf{n}\times\mathbf{n})$ and use Stokes' theorem to transform the area integral (3.38) into a line integral $\oint dx_\alpha\, \rho\gamma\mathbf{H} \cdot (\partial_\alpha\mathbf{n} \times \mathbf{n})$ over the boundary. Away from the vortex core, $\mathbf{n}$ is in the easy

plane, $\theta = \pi/2$, and $\mathbf{H} \cdot (\partial_\alpha \mathbf{n} \times \mathbf{n}) = -H\partial_\alpha \phi$. Hence the gyrotropic coefficients of a vortex,

$$G_{XY} = -G_{YX} = -\rho\gamma H \oint dx_\alpha \, \partial_\alpha \phi = -2\pi n \rho \gamma H. \tag{3.39}$$

This result was first obtained by [78].

The topological nature of the gyrotropic coefficients (3.39) clearly comes into focus if we view a vortex in the two antiferromagnetic sublattices separately, as if they were two independent ferromagnets. In the absence of an applied field, sublattice magnetizations $\mathbf{m}_1(\mathbf{r})$ and $\mathbf{m}_2(\mathbf{r})$ point in opposite directions and cover the northern and southern hemispheres, Fig. 3.4(a). This endows them with equal and opposite skyrmion numbers $q = \pm n/2$ and gyrotropic coefficients $F_{XY} = 4\pi q \mathcal{J} = \pm 2\pi n \mathcal{J}$ [77, 79]. The net gyrotropic coefficient is zero. In an applied magnetic field, both magnetizations tilt out of the easy plane toward the north pole by a small angle $\delta\theta = \frac{\chi H}{2\mathcal{M}} = \frac{\rho\gamma H}{2\mathcal{J}}$. Now $\mathbf{m}_1$ covers slightly less than the northern hemisphere and $\mathbf{m}_2$ slightly more than the southern hemisphere, Fig. 3.4(b). The respective skyrmion charges are $q = \pm\frac{n}{2} - \frac{n\rho\gamma H}{4\mathcal{J}}$. The net gyrotropic coefficient is then $F_{XY} = -2\pi n \rho \gamma H$.

In a two-dimensional ferromagnet, the gyrotropic tensor $F_{\alpha\beta}$ quantifies not only the Lorentz force $F_\alpha = F_{\alpha\beta}\dot{X}_\beta$ acting on a moving vortex, but also the Magnus force $F_\alpha = -F_{\alpha\beta}u_\beta$ exerted on the vortex core by a spin-polarized current of electrons flowing at the drift velocity $\mathbf{u}$ [77]. It is reasonable to expect the same from our antiferromagnet.

In a weak magnetic field, the velocity of the vortex $\mathbf{v}$ is set by the balance between

the Magnus force and the viscous force $-M\mathbf{v}/T$, so that $\mathbf{v}$ is orthogonal to $\mathbf{u}$ and their magnitudes are related by $v \approx \gamma HTu$. In a strong field, the gyrotropic force becomes dominant and $\mathbf{v}$ approaches $\mathbf{u}$. The crossover field being $H_{\rm cr} \approx 1/(\gamma T)$. In an insulating antiferromagnet Cr_2O_3, $\gamma = 1.76 \times 10^{11}$ s^{-1} T^{-1} and $T = 60$ ps [80], so $H_{\rm cr} \approx 0.1$ T. In metallic antiferromagnets, the relaxation time T is expected to be shorter and the crossover field higher. The spin drift velocity u is of the order of 5 m/s for a current density $j = 10^{11}$ A/m^2 [81]

3.4 Discussion

Thus we see that the antiferromagnetic soliton can have a gyrotropic response in situations where we can couple to the hard uniform magnetization field $\mathbf{m}$. This effect is relatively weak for the external magnetic field as it couples through a Zeeman term whose energy scale is of the order of 0.1meV. This has to compete with a very large Heisenberg exchange ($J \sim 10meV$) to induce a local skyrmion density. This can be seen explicitly in the coefficient of the Magnus force $\rho\gamma|\mathbf{H}| = (\chi/\gamma)|\mathbf{H}|$. Now $\chi \propto (1/J)$ where J is the exchange strength, so the coefficient is controlled by $(|\mathbf{H}|/J)$.

However, this method does provide a route to the electrical detection of these antiferromagnetic vortices which are notoriously hard to detect due to the absence of any induced local stray angular momentum density. There remains a largely unexplored area of the crossed DM interaction and magnetic field, especially in cases

where there is spatial dependence in either.

Chapter 4

Three sublattice antiferromagnets

4.1 Introduction

In this chapter we shall develop a generic field theory for three sublattice antiferromagnets with a local D_3 point group symmetry. In contrast to our main focus of the previous chapter, where we studied the dynamics of antiferromagnetic solitons, here we are interested in the theory governing the dynamics of spin waves.

Spin waves are gentle osicllations about a classical ground state. In most cases, barring the exception of frustrated antiferromagnets with small spin lengths (spin - $\frac{1}{2}$) spin wave theory is remarkably accurate[82]. The ordered moments are expressed in terms of classical vector fields:

$$\mathbf{S} = S\ (\sin\theta\sin\phi, \sin\theta\cos\phi, \cos\theta) \tag{4.1}$$

where S is the local spin/magnetization-length and $\theta(t, \boldsymbol{r})$ and $\phi(t, \boldsymbol{r})$ are slowly varying fields. Deviations are expressed as small displacements from the ground state order $\theta_0 \to \theta_0 + \delta\theta(t, \mathbf{r})$ and $\phi_0 \to \phi_0 + \delta\phi(t, \mathbf{r})$.

The spin waves are conveniently expressed in the basis of normal modes of the spin system. These modes form a symmetry governed irreducible representation for the spin degrees of freedom (rotational) in a magnetic unit cell [83]. The normal modes in a system where Heisenberg exchange is the dominant interaction, provide an intuitive picture of the spin wave excitations. In addition they provide insight into how the spin order couples to internal anisotropies and external perturbations, based on symmetry arguments.

As noted before in antiferromagnets the exchange interaction enforces a zero net spin per unit cell, $\sum_i \mathbf{S}_i = 0$, where the summation is over sublattices. Normal modes that violate this condition induce a net spin per plaquette, recall the uniform magnetization field $\mathbf{m}(\mathbf{r})$ in the two sublattice case.

These induced moments are penalized by the exchange interaction and are hence energetically costly. They will be henceforth referred to as 'hard' modes. We will be focused on soft modes that preserve the condition of zero net spin. They enter the energy density $\mathcal{U}(\mathbf{s})$ in the form of gradients. The presence of materials anisotropies such as local easy axes and DM interactions introduce finite energy corrections (at the constant level) to the soft modes and we shall show how. However, in a vast majority of cases the exchange strength is the dominant interaction by at least an

order of magnitude in the energy scales. We shall study the gaps induced by the anisotropies and substantiate this point later in the chapter.

In the ensuing chapter we shall construct the spin-wave theory for generic hexagonal antiferromagnets with three magnetic sublattices. A field theory for an antiferromagnet on the triangular lattice was developed previously by Dombre and Read [84, 85] in search for a topological term in the quantum field theory as found in one dimension by Haldane [86]. Our primary motivation, however, is to construct a framework from which one can calculate the spectrum of spin waves for a broad class of antiferromagnets with a hexagonal symmetric lattice and dominant nearest neighbor Heisenberg exchange interactions. The triangular-lattice [87] and kagome [88] antiferromagnets with exchange between nearest neighbors only are special cases with accidental degeneracy of the spin-wave spectra.

Some features unique to the three-sublattice antiferromagnet emerge from this theory. Firstly, there are now three Goldstone modes as compared to two for the two-sublattice case. This happens because the the Néel order parameter, staggered magnetization $\mathbf{n}$, for the two-sublattice case breaks the $SO(3)$ symmetry of the spin vectors only partially, down to $SO(2)$ rotations about the Néel vector. The three-sublattice magnetic order breaks the symmetry fully, resulting in three Goldstone modes. Secondly, from the perspective of point-group symmetry, the three Goldstone modes can be grouped into a singlet and a doublet. The field theory for this doublet is analogous to the continuum theory of elasticity in two dimensions.

In addition to providing a framework we shall present a more detailed view of the stacked kagome lattice antiferromagnets Mn_3X where X = Sn, Ge. The stacked kagome system is structurally more complicated and involves two separate kagome layers. However, in each layer the spins order into a 120° pattern of the three sublattice triangle. The strongest exchange is the nearest neighbor in plane interaction, this is augmented by further neighbor interplanar couplings which rise from the metallic character of these compounds. Our theory fares decently in this arena, we derive analytical expressions for the spin wave velocities for small wave numbers ($\mathbf{k} \to 0$) and the spectral gaps at $\mathbf{k} = 0$ which we use in fitting the inelastic neutron data. We also take a deeper look at the energetics of the spin wave bands under the influence of external perturbations like local anisotropies, DM interactions, and magnetic fields. Our motivation is to form a protocol with regard to how external probes can couple to the system and effect transport and magnetic properties.

4.2 Lattice and geometry

In this section, we review the geometry of the spins and their normal modes in three-sublattice antiferromagnets. This forms the first step towards the construction of a general theory of spin waves for these lattices, which we shall extend to the more complex situation of Mn_3X.

The simplest examples of this class of magnets are the Heisenberg model on a tri-

angular lattice or on a kagome network of corner sharing triangles, Fig. 4.1. Although their spectra differ significantly—the kagome antiferromagnet with nearest-neighbor interactions has many spin waves with zero frequency—there are features common to many models.

Among these robust universal features are three Goldstone modes: spin waves with a linear dispersion, $\omega \sim ck$, in the long-wavelength limit. Their existence is related to the spontaneous breaking of the spin-rotation symmetry. They are affected by the presence of anisotropic spin interactions. However, because Heisenberg exchange is typically the dominant form of interactions for spins, this symmetry exists in at least an approximate form and the picture of three Goldstone modes with a linear dispersion is a good starting point. The general setting is an antiferromagnet with Heisenberg exchange interactions on a two-dimensional lattice with a triangle as a building block, see Fig. 4.2(a). We assume that classical ground states have a magnetic unit cell with three coplanar spins $\mathbf{S}_1$, $\mathbf{S}_2$, and $\mathbf{S}_3$ such that

$$\mathbf{S}_1 + \mathbf{S}_2 + \mathbf{S}_3 = 0. \tag{4.2}$$

This provides the triangle inequality between the three spin vectors of equal magnitude which will be crucial in establishing our analogy between the spin wave theory of these magnetic states and the continuum theory of elasticity.

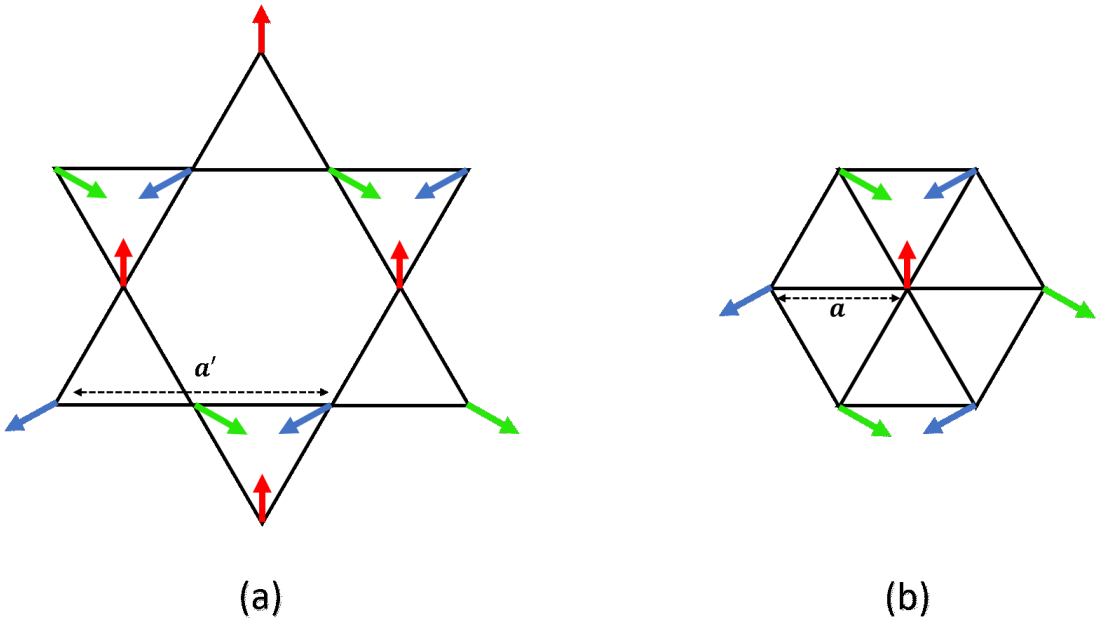

Figure 4.1: The two prototype triangular lattices, the kagome lattice of corner sharing triangles (a) and the triangular lattice (b). We show a 120° ordered state on both where sites with the same spin color or orientation belong to the same spin sublattice.

4.2.1 Local geometry of the normal modes

The geometry of the ground state and the lattice is shown in Fig. 4.2(a). Spatial rotations through the angle $+2\pi/3$ in the $x-y$ plane produce a cyclic exchange of the spin variables:

$$\begin{pmatrix} \mathbf{S}'_1 \\ \mathbf{S}'_2 \\ \mathbf{S}'_3 \end{pmatrix} = \begin{pmatrix} 0 & 0 & 1 \\ 1 & 0 & 0 \\ 0 & 1 & 0 \end{pmatrix} \begin{pmatrix} \mathbf{S}_1 \\ \mathbf{S}_2 \\ \mathbf{S}_3 \end{pmatrix} . \tag{4.3}$$

Note that the spins $\mathbf{S}_i$ are permuted but there is no rotation in spin space. A mirror reflection $x \to -x$, $y \to y$ exchanges spins 1 and 2:

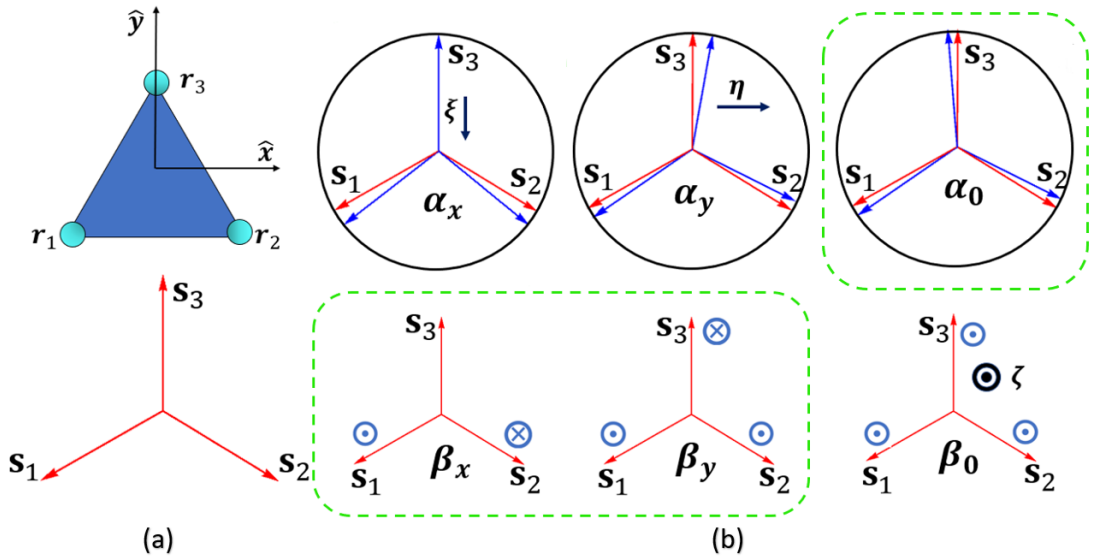

Figure 4.2: On the left we have the geometry of a single triangular plaquette with an example 120° ground state. The spins carry the same labels as the site i.e spin $\mathbf{S}_i$ is at site $\mathbf{r}_i$ (a). The normal modes (b) for the spin structure with the in plane α modes, the red arrow indicates the ground state, while the blue arrows indicate the distorted state. The out of plane β modes are shown at the bottom. The three soft modes, $(\alpha_0, \boldsymbol{\beta})$, are indicated by a dashed box. These modes obey the condition $\mathbf{S_1} + \mathbf{S_2} + \mathbf{S_3} = 0$. The secondary black arrows (ξ, η, ζ) label the axes attached to the moments induced by the hard modes $(\alpha_x, \alpha_y, \beta_0)$.

$$\begin{pmatrix} \mathbf{S}'_1 \\ \mathbf{S}'_2 \\ \mathbf{S}'_3 \end{pmatrix} = \begin{pmatrix} 0 & 1 & 0 \\ 1 & 0 & 0 \\ 0 & 0 & 1 \end{pmatrix} \begin{pmatrix} \mathbf{S}_1 \\ \mathbf{S}_2 \\ \mathbf{S}_3 \end{pmatrix}. \tag{4.4}$$

Because we are dealing with a ground state where the order itself does not have a spatial variation and is defined within a single magnetic unit cell (the spin waves are

variations on top of the order), it will suffice to consider the three spins on a triangle,

$$\mathbf{S}_i = S(\sin\theta_i \cos\phi_i, \sin\theta_i \sin\phi_i, \cos\theta_i) \tag{4.5}$$

with $i = 1, 2, 3$ representing the three sublattices. It is convenient to express these angles in terms of six normal modes α_0, α_x, α_y, β_0, β_x, and β_y, see Fig. 4.2(b):

$$\begin{aligned}
\begin{pmatrix} \phi_1 \\ \phi_2 \\ \phi_3 \end{pmatrix} &= q \begin{pmatrix} \frac{2\pi}{3} \\ \frac{4\pi}{3} \\ 0 \end{pmatrix} - qR \begin{pmatrix} \alpha_x \\ \alpha_y \\ \alpha_0 \end{pmatrix}, \\
\begin{pmatrix} \theta_1 \\ \theta_2 \\ \theta_3 \end{pmatrix} &= \begin{pmatrix} \frac{\pi}{2} \\ \frac{\pi}{2} \\ \frac{\pi}{2} \end{pmatrix} + R \begin{pmatrix} \beta_x \\ \beta_y \\ \beta_0 \end{pmatrix},
\end{aligned} \tag{4.6}$$

where R is the orthogonal matrix.

$$R = \begin{pmatrix} \frac{1}{\sqrt{2}} & \frac{1}{\sqrt{6}} & \frac{1}{\sqrt{3}} \\ -\frac{1}{\sqrt{2}} & \frac{1}{\sqrt{6}} & \frac{1}{\sqrt{3}} \\ 0 & -\frac{2}{\sqrt{6}} & \frac{1}{\sqrt{3}} \end{pmatrix}. \tag{4.7}$$

We measure the ground state spin angles from $\mathbf{S}_3$ as the reference. Here $q = \pm 1$ accounts for the chirality of the ground state: $q = 1$ is the chiral ground state while

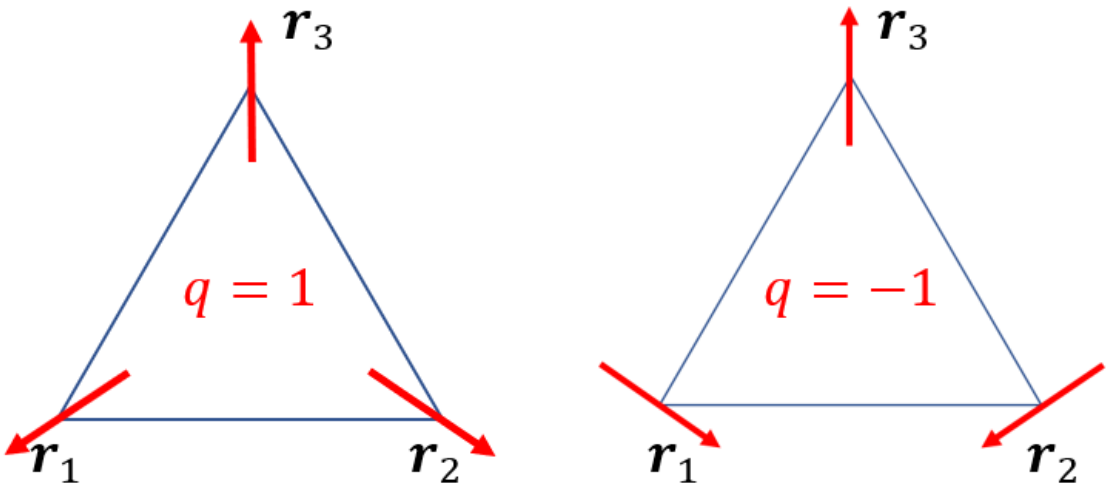

Figure 4.3: The two ground state chiralities are shown. For the $q = 1$ state if we proceed in an anticlockwise sense around the triangle $\mathbf{r}_1 \to \mathbf{r}_2 \to \mathbf{r}_3 \to \mathbf{r}_1$ the spins wind in an anticlockwise sense. For the $q = -1$ state for the same route around the triangle the spins wind in a clockwise sense.

$q = -1$ is the anti-chiral ground state, see Fig. 4.3. The ground state chosen by the system is decided by the sign of the out of plane DM exchange. For Mn_3X the DM vector is out of plane and chooses the anti-chiral state. Note that the ground state retains a $O(2)$ degree of freedom in the xy plane captured by the α_0 mode. Under spatial transformations allowed by D_3 symmetry group of the equilateral triangle (rotations by $\pm 2\pi/3$ and mirror reflections), α_0 and β_0 stay unchanged. We therefore call them scalar modes.

Modes α_x and α_y form a doublet transforming as 2 components of a polar vector.

Under the $+2\pi/3$ rotation (4.3),

$$\begin{pmatrix} \alpha'_x \\ \alpha'_y \end{pmatrix} = \begin{pmatrix} -\frac{1}{2} & -\frac{\sqrt{3}}{2} \\ \frac{\sqrt{3}}{2} & -\frac{1}{2} \end{pmatrix} \begin{pmatrix} \alpha_x \\ \alpha_y \end{pmatrix}. \tag{4.8}$$

Under the reflection (4.4),

$$\begin{pmatrix} \alpha'_x \\ \alpha'_y \end{pmatrix} = \begin{pmatrix} -1 & 0 \\ 0 & 1 \end{pmatrix} \begin{pmatrix} \alpha_x \\ \alpha_y \end{pmatrix}. \tag{4.9}$$

The same applies to the modes (β_x, β_y) which also form a doublet.

Thus we can resolve the normal modes into two singlets α_0 and β_0 which are scalar and two doublets $\boldsymbol{\alpha} = (\alpha_x, \alpha_y)$ and $\boldsymbol{\beta} = (\beta_x, \beta_y)$ which transform as vectors in the xy plane.

4.2.2 Hard and soft modes

Modes α_x, α_y, and β_0 create a net spin on a triangle. They allow us to define three mutually orthogonal spin axes ξ, η, and ζ, respectively, Fig. 4.2(b). The other three modes, β_x, β_y, and α_0, generate rotations about the spin directions $-\xi$, $-\eta$, and ζ, respectively.

By creating a net spin on a triangle, modes α_x, α_y, and β_0 increase its exchange energy $J(\mathbf{S}_1 + \mathbf{S}_2 + \mathbf{S}_3)^2/2$. These modes are therefore hard. The remaining modes

β_x, β_y, and α_0 are soft.

4.3 Field theory for the soft modes

Here we derive the spin wave field theory for the generic triangular unit antiferromagnet. The kinematic term originates from the local spin Berry phase for each of the three spins $\mathcal{S}\mathbf{a}(\mathbf{m}) \cdot \dot{\mathbf{m}}$, which we can write using the standard gauge choice as $\mathcal{S}(\cos(\theta) - 1)\dot{\phi}$. Note that the spins lie in the plane with minimal canting so it does not matter which pole we thread the Dirac string through. For a spin confined to the xy plane $\theta \simeq \pi/2$, this reduces to: $(\pi/2 - \theta_i)\dot{\phi}_i$ on each sublattice, $i = 1, 2, 3$. For the triangle this leads to a Lagrangian, expressed in terms of the normal modes:

$$\mathcal{L}_B = \mathcal{S} \sum_{i=1}^{3} (\pi/2 - \theta_i)\dot{\phi}_i = \mathcal{S}(\dot{\alpha}_0\beta_0 - \boldsymbol{\alpha} \cdot \dot{\boldsymbol{\beta}}), \tag{4.10}$$

where $\mathcal{S}$ is the spin density at a site. The potential energy for the triangle is calculated by expanding the dominant nearest neighbor Heisenberg interaction

$$U = \frac{JS^2}{2}(\mathbf{s}_1 + \mathbf{s}_2 + \mathbf{s}_3)^2, \tag{4.11}$$

in terms of the normal modes. At the zeroth order in gradients, the potential energy depends solely on the hard modes and is given by:

$$\mathcal{U} = \frac{\mathcal{A}}{2}(\alpha_x^2 + \alpha_y^2 + 2\beta_0^2) + \mathcal{U}_g(\nabla\alpha_0, \nabla\beta_x, \nabla\beta_y), \tag{4.12}$$

where $\mathcal{A}$ is a lattice-dependent constant. The single triangle Lagrangian now reads:

$$\mathcal{L} = \mathcal{S}(\dot{\alpha}_0\beta_0 - \boldsymbol{\alpha}\cdot\dot{\boldsymbol{\beta}}) - \frac{\mathcal{A}}{2}(\alpha_x^2 + \alpha_y^2 + 2\beta_0^2) - \mathcal{U}_g \tag{4.13}$$

From this we can solve for the hard modes, using their equations of motion:

$$S\dot{\beta}_x = -\mathcal{A}\alpha_x, \quad S\dot{\beta}_y = -\mathcal{A}\alpha_y, \quad S\dot{\alpha}_0 = \mathcal{A}\beta_0. \tag{4.14}$$

Plugging the solutions back in we get to a kinetic energy for the soft modes:

$$\mathcal{K} = \frac{\rho_\alpha}{2}\dot{\alpha}_0^2 + \frac{\rho_\beta}{2}(\dot{\beta}_x^2 + \dot{\beta}_y^2), \quad \rho_\alpha = \frac{S^2}{2\mathcal{A}}, \quad \rho_\beta = \frac{S^2}{\mathcal{A}}. \tag{4.15}$$

To complete the theory, and account for the dispersion at finite wave numbers we need to add the contributions to the potential energy density from the soft modes $\mathcal{U}_g(\nabla\alpha_0, \nabla\beta_x, \nabla\beta_y)$. This is obtained by expanding the exchange interaction in terms of gradients (to second order) of the soft modes, after setting the hard mode amplitudes to zero. For the hard modes we have a contribution from the exchange

interaction at the zeroth order in gradients. Since we are interested in long distance behaviour, in the gradient expansion we keep terms to the lowest order in gradients and drop the spatial variations of the hard modes. There are restrictions imposed on the kinds of terms generated, namely the α_0 transforms as a scalar and the $\boldsymbol{\beta}$ doublet like a vector. We also generate six-fold terms allowed by the hexagonal symmetry D_3 of the lattice.

What emerges from this at the quadratic order in soft mode gradients is a wave-equation in 2+1 dimensions for the α_0 mode (recall the ϕ field in the XY ferromagnet) and a theory analogous to a continuum theory of elasticity in 2-d for the $\boldsymbol{\beta}$ doublet. The gradients of the displacement fields, $\mathbf{u}(\mathbf{r})$, in elasticity ($\partial_i u_j$) are replaced by the gradients of the $\boldsymbol{\beta}$ doublet ($\partial_i \beta_j$). We outline both in what follows, ending with additions to the simple elasticity theory from higher order (in gradients) terms that are allowed by the D_3 symmetry.

4.3.1 Singlet

The singlet mode α_0 has simple dynamics. Its Lagrangian density consists of a kinetic energy with mass density ρ_α and a potential energy quadratic in the gradients of α_0:

$$\mathcal{L} = \frac{\rho_\alpha}{2}\dot{\alpha}_0^2 - \frac{\kappa}{2}\partial_i\alpha_0\,\partial_i\alpha_0. \tag{4.16}$$

Here $\kappa \propto \mathcal{A}$, introduced in Eq. (4.12) with the constant of proportionality which depends on the local lattice environment. Summation is assumed over doubly repeated Cartesian indices $i = x, y$.

As often happens in highly symmetric solids, the effective Lagrangian (4.16) obeys not just the discrete symmetries of the point group D_3 but also the full rotational symmetry SO(2). Spin waves have a linear dispersion $\omega = ck$ with the speed $c = \sqrt{\kappa/\rho_\alpha}$.

4.3.2 Doublet

The continuum theory for the doublet is more involved as the doublet field $\boldsymbol{\beta}$ itself transforms like a vector under rotations. The Lagrangian of this field has the following form:

$$\mathcal{L} = \frac{\rho_\beta}{2}\dot{\beta}_i\dot{\beta}_i - \frac{C_{ijkl}}{2}\beta_{ij}\beta_{kl} - \frac{\tilde{C}_{ijkl}}{2}\tilde{\beta}_{ij}\tilde{\beta}_{kl}. \tag{4.17}$$

Here we have introduced symmetrized and anti-symmetrized gradients,

$$\beta_{ij} \equiv \frac{1}{2}(\partial_i\beta_j + \partial_j\beta_i), \quad \tilde{\beta}_{ij} \equiv \frac{1}{2}(\partial_i\beta_j - \partial_j\beta_i). \tag{4.18}$$

The inertia density ρ_β is generally different from its counterpart ρ_α for the singlet mode. The stiffness coefficients are fourth-rank tensors with the following symmetry properties: C_{ijkl} is symmetric and $\tilde{C}_{ijkl}$ is antisymmetric under the exchanges $i \leftrightarrow j$ and $k \leftrightarrow l$; both tensors are symmetric under the exchange $(ij) \leftrightarrow (kl)$.

The structure of the Lagrangian (4.17) is highly reminiscent of the theory of elasticity in two dimensions. Here β_i identifies with the lattice displacement, β_{ij} with strain, and $\tilde{\beta}_{ij}$ with rotation of the lattice. In a solid, rotations do not increase the elastic energy, so $\tilde{C}_{ijkl} = 0$ for lattice vibrations. For spin waves, $\tilde{C}_{ijkl} \neq 0$ in general.

As with the elastic constants, the highly symmetric hexagonal environment drastically reduces the number of independent potential coefficients. Both fourth-rank tensors can be expressed in SO(2)-invariant forms:

$$\begin{aligned} C_{ijkl} &= \lambda\delta_{ij}\delta_{kl} + \mu(\delta_{ik}\delta_{jl} + \delta_{il}\delta_{jk}), \\ \tilde{C}_{ijkl} &= \tilde{\mu}\epsilon_{ij}\epsilon_{kl} = \tilde{\mu}(\delta_{ik}\delta_{jl} - \delta_{il}\delta_{jk}). \end{aligned} \tag{4.19}$$

Here δ_{ij} is the Kronecker delta and ϵ_{ij} is the antisymmetric Levi-Civita symbol, $\epsilon_{xy} = -\epsilon_{yx} = +1$. The Lamé parameters λ and μ determine the bulk modulus $\lambda + \mu$ (in 2 dimensions) and the shear modulus μ. For the spin system these moduli are all proportional to the Heisenberg exchange strength(s) as we shall see in our examples. To continue the analogy with a solid, we will refer to $\tilde{\mu}$ as the rotation modulus. The explicit form of the Lagrangian for the $\boldsymbol{\beta}$ modes is

$$\mathcal{L} = \frac{\rho_\beta}{2}\dot{\beta}_i^2 - \frac{\lambda}{2}\,\partial_i\beta_i\,\partial_j\beta_j - \frac{\mu+\tilde{\mu}}{2}\partial_i\beta_j\partial_i\beta_j - \frac{\mu-\tilde{\mu}}{2}\partial_i\beta_j\partial_j\beta_i. \tag{4.20}$$

Spin waves for the $\boldsymbol{\beta}$ modes with longitudinal and transverse polarizations have

the propagation speeds

$$c_{||} = \sqrt{\frac{\lambda + 2\mu}{\rho_\beta}}, \quad c_\perp = \sqrt{\frac{\mu + \bar{\mu}}{\rho_\beta}}. \tag{4.21}$$

4.3.3 Six-fold symmetric terms

The continuum spin-wave Lagrangians (4.16) and (4.20) exhibit full $SO(2)$ rotational invariance. In a hexagonal solid, this symmetry is only approximate and is explicitly broken if we include terms of higher orders in the gradients. These higher order terms are required to obey the local six-fold symmetry of rotations and inversion (D_3 point group).

The six-fold symmetric terms can be constructed as follows. Take three unit vectors $\mathbf{n}_1$, $\mathbf{n}_2$, and $\mathbf{n}_3$ making angles of 120° with one another. For arbitrary vectors $\mathbf{a}$, $\mathbf{b}$, and $\mathbf{c}$, the sum

$$\sum_{i=1}^{3} (\mathbf{a} \cdot \mathbf{n}_i)(\mathbf{b} \cdot \mathbf{n}_i)(\mathbf{c} \cdot \mathbf{n}_i) \tag{4.22}$$

is invariant under 120° rotations. Furthermore, the square of this quantity is invariant under 60° rotations.

For the α_0 mode, the only vector available is the gradient ∇ (or the wave-vector $\mathbf{k}$), so we take $\mathbf{a} = \mathbf{b} = \mathbf{c} = \nabla$. A quantity invariant under 60° rotations is

$$\mathcal{L}_6 = -\frac{\sigma_\alpha}{8} \left[\left(\partial_x^3 - 3\partial_x \partial_y^2 \right) \alpha_0 \right]^2 . \tag{4.23}$$

Adding this term to the Lagrangian of the α_0 mode alters the magnon dispersion, warping the cone $\omega = ck$ as follows:

$$\omega^2 = c^2k^2 + \frac{\sigma_\alpha}{\rho_\alpha}k^6 \cos^2 3\phi, \tag{4.24}$$

where ϕ is the angle at which the magnon propagates in the xy plane, $\mathbf{k} = (k\cos\phi, k\sin\phi)$. The warping is strongly suppressed near the center of the Brillouin zone.

For the $\boldsymbol{\beta}$ modes, we have two vectors to play with, ∇ and $\boldsymbol{\beta}$. The relevant invariant is

$$\mathcal{L}_6 = -\frac{\sigma_\beta}{2}\left[(\partial_x^2 - \partial_y^2)\beta_x - 2\partial_x\partial_y\beta_y\right]^2. \tag{4.25}$$

For nondegenerate longitudinal and transverse modes ($c_{||} \neq c_\perp$), the magnon dispersions are warped as follows:

$$\begin{aligned} \omega^2 &= c_{||}^2k^2 + \frac{\sigma_\beta}{\rho_\beta}k^4 \cos^2 3\phi, \\ \omega^2 &= c_\perp^2k^2 + \frac{\sigma_\beta}{\rho_\beta}k^4 \sin^2 3\phi. \end{aligned} \tag{4.26}$$

The warping for the $\boldsymbol{\beta}$ modes comes at a lower order in the gradient expansion and is therefore more pronounced than for the α_0 mode. Note that if either of the velocities $(c_{||}, c_\perp)$ are zero this makes the six-fold pattern very prominent.

4.4 Testing the theory on the triangular and kagome lattices

Let us now explicitly construct the field theory for the nearest neighbor triangular antiferromagnet and the kagome antiferromagnet, see Fig. 4.1. The point of difference here is the spin density per sublattice site. For the triangular lattice each site has a coordination number of six while for the kagome the coordination number is four. These densities have to be calculated separately for each new lattice type.

For any individual lattice system we start with the kinetic energy derived in Eq. (4.15). The inertia for the soft modes ρ_α and ρ_β and the parameter $\mathcal{A}$ need to be determined for each lattice type. For the soft mode contribution to the potential energy density $\mathcal{U}$ we do a gradient expansion of the exchange interaction in the soft modes with the amplitudes of the hard modes set to zero. This is combined with the kinetic energy to form the full Lagrangian density $\mathcal{L} = \mathcal{L}_{\rm kin} - \mathcal{U}_g(\nabla\alpha_0, \nabla\beta_x, \nabla\beta_y)$.

4.4.1 Triangular antiferromagnet

In the nearest-neighbor Heisenberg model on the triangular lattice [85, 87], the magnetic unit cell has the area $A = (3\sqrt{3}/2)a^2$ where a is the nearest neighbor distance, see Fig 4.1(b). The spin density is: $\mathcal{S} = 2S/(3\sqrt{3}a^2)$ and the energy density

parameter $\mathcal{A} = (\sqrt{3}JS^2)/a^2$ This results in the inertia:

$$\rho_\beta = \frac{\mathcal{S}^2}{\mathcal{A}} = \frac{4}{27\sqrt{3}\ Ja^2} = 2\rho_\alpha. \tag{4.27}$$

In addition gradient expansion yields the energy density:

$$\mathcal{U}_g = \frac{JS^2}{4\sqrt{3}} \left[(\nabla\alpha_0)^2 + (\nabla\beta_x)^2 + (\nabla\beta_y)^2 \right], \tag{4.28}$$

One can identify the constants $\kappa = JS^2/\sqrt{3}$ for the α_0 singlet and for the $\boldsymbol{\beta}$ doublet $\lambda = 0$, and $\mu = \tilde{\mu} = JS^2/(2\sqrt{3})$.

The α_0 mode has the speed $c = \frac{3\sqrt{3}}{2}JSa$. The $\boldsymbol{\beta}$ modes are degenerate and have speeds $c_{||} = c_\perp = c/\sqrt{2}$, see Eq. (4.21) and Fig. 4.4(c). The degeneracy is associated with the special values of the Lamé coefficients, $\lambda = 0$ and $\mu = \tilde{\mu}$, and reflects a higher, SO(2) $\times$ SO(2) symmetry of the Lagrangian,

$$\mathcal{L} = \frac{1}{2}\rho_\beta \dot{\beta}_i \dot{\beta}_i - \mu\, \partial_i\beta_j\, \partial_i\beta_j, \tag{4.29}$$

where one SO(2) rotates spatial coordinates and the other transforms components of the $\boldsymbol{\beta}$ doublet.

4.4.2 Kagome antiferromagnet

For the nearest-neighbor kagome antiferromagnet [88] the magnetic unit cell area is $A = (\sqrt{3}/2)a'^2$ where a' is the lattice parameter and is equal to twice the nearest neighbor distance. The spin density is given by $\mathcal{S} = 2S/(\sqrt{3}a'^2)$, see Fig. 4.1(b). This gives the energy density parameter $\mathcal{A} = (2\sqrt{3}JS^2)/a'^2$. From this we can extract the inertia for the two modes:

$$\rho_\beta = \frac{\mathcal{S}^2}{\mathcal{A}} = \frac{2}{3\sqrt{3}Ja'^2} = 2\rho_\alpha. \tag{4.30}$$

The soft mode gradient expansion of the exchange interaction yields the following energy density:

$$\mathcal{U}_g = \frac{JS^2}{8\sqrt{3}}\left[(\nabla\alpha_0)^2 + 2(\nabla\cdot\boldsymbol{\beta})^2\right]. \tag{4.31}$$

The constants for the kagome lattice are hence $\kappa = JS^2/4\sqrt{3}$ for the α_0 singlet and for the $\boldsymbol{\beta}$ doublet $\lambda = JS^2/2\sqrt{3}$, and $\mu = \tilde{\mu} = 0$.

The α_0 mode and the longitudinal part of the $\boldsymbol{\beta}$ mode have the speed $c_\alpha = c_{||} = \frac{\sqrt{3}}{2}JSa'$, whereas the transverse $\boldsymbol{\beta}$ mode has $c_\perp = 0$, see Fig. 4.4(a)[88]. The zero transverse speed is associated with the vanishing shear and rotation moduli, $\mu = \tilde{\mu} = 0$ in the dual elasticity theory. In this sense, the nearest-neighbor kagome antiferromagnet resembles a fluid.

The spin lattice has zero modes as a result of a highly degenerate ground state manifold rising from the so called 'weather-vane' modes which do not cost exchange

energy to excite (soft modes in our classification). These modes have been observed in [89, 90]. Note in particular, that the excitation they show in Fig. 1 (a) of [89] is the β_x soft mode shown in Fig. 4.2(b). For a wave propagating along $(0, k_y)$ where the planes of equal phase lie along $\hat{x}$ as shown in [89] Fig. 1 (a), $\boldsymbol{\beta}_{\perp} = (\beta_x, 0)$ and $\boldsymbol{\beta}_{||} = (0, \beta_y)$. So the kagome flat (non-dispersive) mode in this case is the β_x soft mode. In [89] the flat band lifts from zero energy due the DM interaction. This is also evident from our energy expressions in Eq. (4.52) and [62]. Both the experiments were carried out on powdered samples where effects of the local D_3 symmetry are suppressed and hence the six-fold quartic corrections to the dispersion are hard to discern.

This 'fluid' behaviour is in fact a direct analogy to the continuum elasticity theory of nearest neighbor kagome lattice, which is critical according to the Maxwell criteria for stability [91, 92]. The n.n kagome lattice is unstable to shear distortions with floppy modes which are lifted by an addition of a next nearest neighbor elastic coupling [93].

Similarly, for the spin system the addition of further neighbor exchanges, lifts the degeneracy between the α_0 and the longitudinal β mode and generates a finite velocity for the transverse β mode [88], see Fig. 4.4(b).

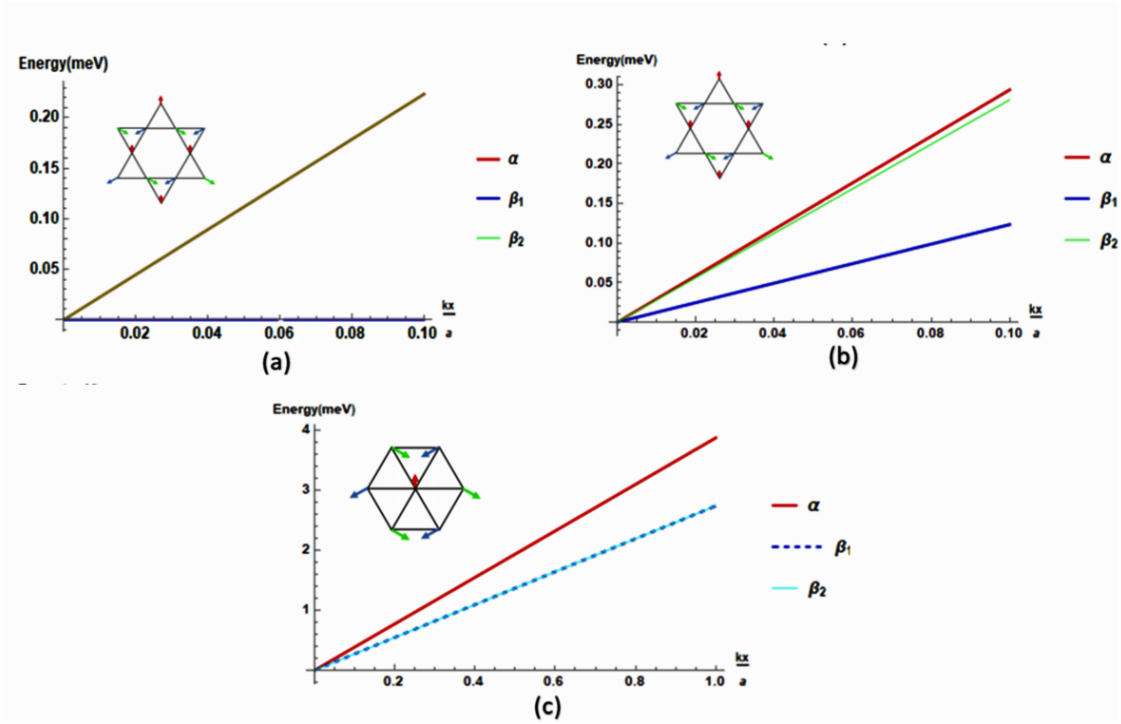

Figure 4.4: Dispersion of the three Goldstone modes $(\alpha_0, \boldsymbol{\beta})$ along k_x from the Γ point for kagome lattice on the left (a,b) and the triangular lattice on the right (c), for $J = 10$ meV and $S = 1$. For the kagome lattice, with n.n exchange (a) one of the β modes is flat and the other one degenerate with the α_0 mode. The two effects are lost for a further neighbor ferromagnetic exchange (b) $|J_{nnn}| = 0.5$ meV. For the triangular lattice (c) the two β modes are degenerate for n.n exchange.

4.5 Stacked Kagome

We shall now look into a layered AB stacked kagome system Mn_3Ge. It is not in direct analogy to the single layered triangular lattices we have so far elucidated on. However, the primary magnetic unit here is the three sublattice triangle with the magnetic sites interacting via a strong nearest neighbor antiferromagnetic Heisenberg exchange. This ensures a nearly 120° spin order in the ground state in each kagome plane.

From the inelastic neutron data [62], we notice the absence of any non-dispersive bands at finite energies. As seen in Sec. 4.4 this happens in the kagome with further neighbor interactions. In our theory we show that the minimal additional interactions required to produce this dispersion are interplanar.

In addition, the system has a fairly strong DM interaction with a $\mathbf{D} = D\hat{z}$ vector that points out of plane. This locks the spins into an antichiral order and minimizes canting out of the kagome planes. There is a small on-site easy axis anisotropy which cants the spins in plane, out of the 120° order, characterized by δ [94, 95, 96]. This energy scale is three orders of magnitude smaller than any other energy scale $\delta \ll (J_2, J_4)$. This is evident from our fits to spin wave dispersion data in [62], see Table. 4.1

Thus, we have on our hands a stacked triangular unit antiferromagnet, where the triangular ordering of spins produces the same Goldstone mode structure as we dealt with before. We apply our theory to this system, extracting analytical expressions for the spin-waves near the Γ point and the gaps at the Γ point. The model Hamiltonian, with all the energy terms, we are fitting to is:

$$\begin{aligned} \mathcal{H}_{JD\delta} = & \sum_{<i,j>} J_{ij}\ \mathbf{S}_i \cdot \mathbf{S}_j + \sum_{<i,j>} \mathbf{D}_{ij} \cdot (\mathbf{S}_i \times \mathbf{S}_j) \\ & - \sum_i \delta(\hat{\mathbf{n}}_i \cdot \mathbf{S}_i)^2. \end{aligned} \tag{4.32}$$

Here $JD\delta$ stands for a model containing Heisenberg exchanges, collectively J, a DM

interaction D and local anisotropy δ. The local anisotropy is six fold and at each site is directed towards the nearest Sn or Ge site, see Fig. 4.5(d).

An effective description of the system requires two sets of modes: $(\alpha_0, \boldsymbol{\alpha}, \beta_0, \boldsymbol{\beta})$ for the A layer and $(\alpha_0', \boldsymbol{\alpha}', \beta_0', \boldsymbol{\beta}')$ for the B layer, see Fig. 4.6. The theory is better expressed in terms of symmetric and antisymmetric combinations of the two sets, $\zeta^s = \frac{\zeta+\zeta'}{\sqrt{2}}$ and $\zeta^a = \frac{\zeta-\zeta'}{\sqrt{2}}$, where ζ stands for any of the α or β modes. To simplify the expressions a bit we absorb the unit cell volume $V = (\sqrt{3}a'^2 l)/2$ into the metric $\mathcal{L} \equiv V\mathcal{L}$. As indicated before a' is the lattice parameter in the kagome plane.

The primary unit is the David-star motif consisting of an up triangle in the lower (blue) layer and a down triangle of the upper (red) layer, see Fig. 4.6(a). The net Berry phase can be expressed in terms of the symmetric and antisymmetric modes:

$$\mathcal{L} = S(\dot{\alpha}_0^s \beta_0^s - \boldsymbol{\alpha}^s \cdot \dot{\boldsymbol{\beta}}^s) + S(\dot{\alpha}_0^a \beta_0^a - \boldsymbol{\alpha}^a \cdot \dot{\boldsymbol{\beta}}^a). \tag{4.33}$$

To obtain the potential energy density at the Γ point we have to consider three types of exchange interactions.

The dominant exchange is the intralayer nearest neighbor antiferromagnetic exchange characterized by the strength J_2. To reproduce the isotropic dispersion seen in [62] we need to add next neighbor interplanar couplings, see Fig. 4.6. The minimal set required is J_1 and J_4. The index i on the exchange strength J_i represents the actual distance between two neighbors.

The layer separation is small and hence the first neighbor is indeed interlayer J_1. Fits to data fix the value of J_1 to be $\ll J_{2,4}$ but we retain J_1 as it presents some novel features. In particular, J_1 affects the non dispersive band only at the quartic order and that too in a distinctly six-fold manner. J_3 produces the same qualitative dispersion as J_1 including the appearance of non dispersive bands. A fit to the data resolves $J_3 \to 0$. J_4 is the nearest exchange which lifts the flat band isotropically.

The interlayer exchange interactions J_1 and J_4 respect the D_3 symmetry of the triangle and the inversion symmetry with respect to the center of the star. J_4 connects sites with the same sublattice index, whereas J_1 connects different sublattices, see Fig. 4.6.

As before, we can convert the Berry phase into a kinetic energy by integrating out the hard modes. In this case there are six such modes. For the examples we worked out in Sec. 4.4, the modes we retained were the ones that were soft under exchange. We perform the same exercise here but with a bit more scrutiny. The energy $\mathcal{U}$ at the Γ point obtained from expansion of three exchange interactions:

$$\begin{aligned} \mathcal{U} &= C_1\left[(\boldsymbol{\alpha}^s)^2 + 2(\beta_0^s)^2\right] + C_2(\boldsymbol{\alpha}^a)^2 + C_3(\beta_0^a)^2 \\ &+ C_4\left[(\boldsymbol{\beta}^a)^2 + (\alpha_0^a)^2\right] + \mathcal{U}_g. \end{aligned} \tag{4.34}$$

The constants C_n are:

$$\begin{aligned} C_1 &= \left(\frac{3}{2}J_2 + \frac{3}{2}J_1\right) S^2. \\ C_2 &= \left(\frac{3}{2}J_2 + \frac{J_1}{2} - 4J_4\right) S^2. \\ C_3 &= (3J_2 - J_1 - 4J_4)\, S^2. \\ C_4 &= 2\,(J_1 - 2J_4)\, S^2. \end{aligned} \tag{4.35}$$

In the presence of the interlayer exchanges J_1 and J_4, all the antisymmetric modes pick up zeroth order in gradient energy contributions. Three gapless modes (Goldstones) remain: the symmetric modes $(\alpha_0^s, \boldsymbol{\beta}^s)$.

Note that the interlayer couplings can cause instabilities (negative gap energies) in the 120° order if we have a ferromagnetic (antiferromagnetic) exchange between sites of the opposite (same) sublattice. Here, for instance, if $\mathrm{sgn}(J_1) < 0$ or $\mathrm{sgn}(J_4) > 0$. For the experiment [62] the fits require an antiferromagnetic J_1 and a ferromagnetic J_4, this provides positive constant energies to all the antisymmetric modes and there are no instabilities leading to a theory:

$$\boldsymbol{\mathcal{L}} = \boldsymbol{\mathcal{L}}_B - \boldsymbol{\mathcal{U}}[\alpha_0^a, \boldsymbol{\beta}^a, \beta_0^s, \beta_0^a, \boldsymbol{\alpha}^s, \boldsymbol{\alpha}^a]. \tag{4.36}$$

From this we integrate out six modes$(\beta_0^s, \beta_0^a, \boldsymbol{\alpha}^s, \boldsymbol{\alpha}^a)$ using their equations of motion.

This results in a theory:

$$\begin{aligned}\mathcal{L} &= \frac{\rho_{\alpha^s}}{2}(\dot{\alpha}_0^s)^2 + \frac{\rho_{\boldsymbol{\beta}^s}}{2}(\dot{\boldsymbol{\beta}}^s)^2 + \frac{\rho_{\alpha^a}}{2}(\dot{\alpha}_0^a)^2 + \frac{\rho_{\boldsymbol{\beta}^a}}{2}(\dot{\boldsymbol{\beta}}^a)^2 \\ &- C_4\left[(\boldsymbol{\beta}^a)^2 + (\alpha_0^a)^2\right]. \end{aligned} \tag{4.37}$$

The inertia for the $\boldsymbol{\beta}^s$ modes is generated by integrating out the hard $\boldsymbol{\alpha}^s$ modes and the inertia for the α_0^s mode is generated by integrating out the hard β_0^s mode:

$$\rho_{\beta^s} = \frac{S^2}{2C_1} = \frac{1}{3(J_2 + J_1)} = 2\rho_{\alpha^s}. \tag{4.38}$$

Similarly the inertias for the antisymmetric modes are:

$$\rho_\beta^a = \frac{S^2}{2C_2}, \quad \rho_\alpha^a = \frac{S^2}{2C_3}. \tag{4.39}$$

These modes are not critical to our study as they are gapped in Mn_3Ge by C_4, see Eq. (4.37). This allows us the freedom to drop the space-time gradients of all the antisymmetric modes. The resulting kinetic energy density we work with is:

$$\mathcal{L}_{\text{kin}} \simeq \frac{\rho_{\alpha^s}}{2}(\dot{\alpha}_0^s)^2 + \frac{\rho_{\boldsymbol{\beta}^s}}{2}(\dot{\boldsymbol{\beta}}^s)^2. \tag{4.40}$$

In the presence of interlayer exchanges the antisymmetric modes are gapped, and we need not retain their kinetic terms in the gradient expansion.

We now calculate the interaction energy density generated by the gradient expansion of the Heisenberg exchanges in the soft modes $(\alpha_0^s, \boldsymbol{\beta}^s)$. We proceed one exchange interaction at a time, highlighting the features in each case.

4.5.1 Intralayer interactions

Heisenberg antiferromagnetic exchange between nearest neighbor sites confined to a single kagome plane, J_2 (see Fig. 4.6(a)) reproduces the kagome lattice example worked out earlier. This is the dominant exchange term in this compound. The energy density of the soft modes is:

$$\begin{aligned} \mathcal{U}_g &= \frac{J_2}{16} a^2 S^2 \left[(\nabla \alpha_0^s)^2 + (\nabla \alpha_0^a)^2 \right] \\ &+ \frac{J_2}{8} a^2 S^2 \left[(\nabla \cdot \boldsymbol{\beta}^s)^2 + (\nabla \cdot \boldsymbol{\beta}^a)^2 \right]. \end{aligned} \tag{4.41}$$

In the absence of interlayer coupling, the symmetric and antisymmetric modes are degenerate. This implies that the inertia for the symmetric and antisymmetric modes is the same, $\rho_\alpha^s = \rho_\alpha^a = \rho_\alpha$ and $\rho_\beta^s = \rho_\beta^a = \rho_\beta$.

We can read off the velocity of the $\alpha_0^{s,a}$ mode from Eq. (4.16), identifying $\kappa = \frac{J_2}{8} a^2 S^2$, $c_\alpha = \sqrt{\kappa/\rho_\alpha} aS = \sqrt{J_2/(8\rho_\alpha)} aS$.

For the $\boldsymbol{\beta}^{s,a}$ elasticity theory we can read off the elasticity moduli: $\lambda = \frac{J_2}{4} a^2 S^2$, $\mu = \tilde{\mu} = 0$ and hence the velocities:

$$\begin{aligned} c_{||} &= \sqrt{\frac{J_2}{4\rho_\beta}} aS \\ c_\perp &= 0. \end{aligned} \tag{4.42}$$

As is evident the 'solid' has zero shear modulus and hence carries a flat mode in the direction perpendicular to a propagating elastic wave. Since $\rho_\beta = 2\rho_\alpha$ the two dispersive modes propagate at the same speed $c_\alpha = c_{||}$

4.5.2 Interlayer interactions

To reproduce the dispersion observed in the experiment [62] we need to find exchange interactions that endow the flat $\beta_\perp$ mode with an isotropic dispersion. The nearest interactions that do the job are J_1 and J_4, shown in Fig. 4.6. Note that this is a minimal set of exchanges and in actuality represent an effective interlayer coupling that reproduces the correct dispersion.

The interactions themselves can be either ferro or antiferromagnetic. If an interaction connects opposite (same) sublattices on the two layers and is ferromagnetic (antiferromagnetic) then the interaction strength has to be smaller than the in plane Heisenberg coupling J_2 to produce the same ground state. The interlayer interaction potential $\mathcal{U}$ is given as:

$$\begin{aligned}\frac{\mathcal{U}_g}{S^2} &= (2J_1 - 4J_4)\left[(\alpha_0^a)^2 + (\boldsymbol{\beta^a})^2\right] + \frac{a^2}{6}\left(\frac{J_1}{8} - J_4\right)(\nabla\alpha_0^s)^2 \\ &- \frac{a^2 J_4}{8}(\partial_x\beta_x^s + \partial_y\beta_y^s)^2 + \frac{a^2}{24}(J_1 - 5J_4)(\partial_y\beta_x^s - \partial_x\beta_y^s)^2 \\ &- \frac{a}{\sqrt{3}}(J_1 + J_4)\left[\beta_x^a(\partial_y\beta_x^s + \partial_x\beta_y^s) + \beta_y^a(\partial_x\beta_x^s - \partial_y\beta_y^s)\right].\end{aligned} \tag{4.43}$$

where we have dropped the gradients of the massive antisymmetric modes, α_0^a and $\boldsymbol{\beta}^a$.

In the presence of these interlayer interactions our 'elastic' theory analogy seems to fail due to terms, linear in field derivatives $\beta_i^a\partial_j\beta_k^s$ or $\beta_i^s\partial_j\beta_k^a$. Inversion transformations about the common triangle center (center of the David's star motif) reduces the form of allowed terms to : $\beta_i^a\partial_j\beta_k^s$ which are invariant under inversions, since $\boldsymbol{\beta}^a \to -\boldsymbol{\beta}^a$, $\boldsymbol{\beta}^s \to \boldsymbol{\beta}^s$ and $\nabla \to -\nabla$ leaving the combination unchanged, see Fig. 4.6.

These terms do not fit directly into the mould of an elasticity theory, and the kinetic term $\mathcal{K} \propto (\dot{\boldsymbol{\beta}}^a)^2$, keeps us from integrating out the massive antisymmetric modes to re-obtain an elastic theory. However, with the assumption that the antisymmetric modes are sufficiently gapped by an ferromagnetic J_4 and an antiferromagnetic J_1, we can do a perturbation theory in these linear terms for their contribution to the velocities of the symmetric modes. In this limit we return to an elasticity theory involving the $\boldsymbol{\beta}^s$ modes.

The linear gradient interactions are also responsible for inducing a 6-fold pattern in

the dispersions at the quartic level ($\simeq k^4$), see Eq. (4.47). This is especially apparent for an antiferromagnetic J_1 interaction. However, in the presence of a ferromagnetic J_4 this six-fold behaviour is alleviated by the more isotropic nature of J_4. This is important as the dispersion in the sample data is isotropic around the Γ point, see Fig. 4.7.

4.5.2.1 In-plane velocities

We can now list the velocities of all the gapless modes in the presence of both in-plane and out-of-plane interactions. In the presence of (J_1, J_2, J_4) the velocities are:

$$\begin{aligned} c^s_\alpha &= \sqrt{\frac{1}{\rho_{\alpha^s}}\left(\frac{J_2}{8} - \frac{J_4}{3} + \frac{J_1}{24}\right)}a'S \\ c^s_{||} &= \sqrt{\frac{1}{\rho_{\beta^s}}\left(\frac{J_2}{4} - \frac{5J_4}{24} - \frac{J_1}{12} - \frac{3J_1J_4}{8(J_1-2J_4)}\right)}a'S \\ c^s_\perp &= \sqrt{\frac{1}{\rho_{\beta^s}}\left(-\frac{3J_4}{8} - \frac{3J_1J_4}{8(J_1-2J_4)}\right)}a'S, \end{aligned} \tag{4.44}$$

where a' is the lattice parameter for a single kagome layer. Note that with just a J_1 out of plane interaction ($J_4 = 0$) the perpendicular mode ($c^s_\perp$) that was flat under J_2 remains flat to linear order and develops flat directions in q-space at the quadratic level, see Fig. 4.7(a). The situation with J_4 as the out of plane interaction is isotropic.

4.5.2.2 Out-of-plane velocities

For the α_0 mode the dispersion is given by $\rho_\alpha \omega_\alpha^2 = (\frac{J_1}{4} - \frac{J_4}{2})(k_z l)^2$. For the $\beta_{x,y}$ modes the c-dispersion is $\rho_\beta \omega_\beta^2 = (\frac{J_1}{4} - \frac{J_4}{2})(k_z l)^2$. These lead to the out of plane velocities:

$$c_\alpha = \sqrt{\frac{J_1 - 2J_4}{4\rho_{\alpha^s}}} lS \tag{4.45}$$
$$c_\beta = \sqrt{\frac{J_1 - 2J_4}{4\rho_{\beta^s}}} lS,$$

where l is the separation between unit cells in the c-direction. Now since $\rho_{\beta^s} = 2\rho_{\alpha^s}$ the relation between the velocity of the two types of modes is $c_{\alpha^s} = \sqrt{2} c_{\beta^s}$ in the k_z-direction.

4.5.3 Symmetry features of the interplane interactions

The interplane interactions expressed using the symmetric vector field $\boldsymbol{\beta}^s$ and the antisymmetric vector field $\boldsymbol{\beta}^a$ contain the following terms :

1. A mass term for the field $\boldsymbol{\beta}^a$.

2. Direct quadratic interactions: $\partial_i \boldsymbol{\beta}^a \cdot \partial_j \boldsymbol{\beta}^a$ and $\partial_i \boldsymbol{\beta}^s \cdot \partial_j \boldsymbol{\beta}^s$ ('elasticity' theory).

3. Crossed interaction terms between $\boldsymbol{\beta}^a$ and $\boldsymbol{\beta}^s$ which are linear in derivatives

$\beta_i^a \partial_j \beta_k^s$. The cross terms have to follow the inversion symmetry criteria for the exchanges.

The interlayer exchanges are shown in Fig. 4.6 and their gradient expanded forms are shown in Eq. (4.43). Let us take a closer look at the linear term which is common to both expressions:

$$\mathcal{U}_{\text{linear}} \propto \left[\beta_x^a(\partial_y \beta_x^s + \partial_x \beta_y^s) + \beta_y^a(\partial_x \beta_x^s - \partial_y \beta_y^s)\right]. \tag{4.46}$$

We motivated a generic construction of a six-fold term in Eq. (4.22). In that construction if we take the vectors $\mathbf{a} = (-\beta_y^a, \beta_x^a)$, $\mathbf{b} = \nabla$, and $\mathbf{c} = (\beta_x^s, \beta_y^s)$ we generate the cross term in Eq. (4.46).

In section 4.3, we noted that such a structure has a 120° symmetry. For the case of the interlayer coupling this turns into a 60° symmetry. This happens because in Eq. (4.46), a 60° degree rotation interchanges the three unit vectors $\mathbf{e}_i$ with a flipped sign and flips the primed and unprimed modes, which leads to $\boldsymbol{\beta}^a \to -\boldsymbol{\beta}^a$ and $\boldsymbol{\beta}^s \to \boldsymbol{\beta}^s$. The two flips of sign cancel to produce a 60° symmetry, see Fig. 4.8.

This 6-fold symmetry is explicit in the dispersions. Keeping only two antiferromagnetic interactions J_1 and J_2 with $\mathbf{k} = k\ (\cos\phi_k, \sin\phi_k)$ the two gapless modes have dispersions:

$$\begin{aligned}\rho_\beta \omega^2_{\beta_1} &= \left(\frac{J_1+J_2}{384}\right)(1+\cos(6\phi_k))\,k^4 \\ \rho_\beta \omega^2_{\beta_2} &= \left(\frac{J_2}{4}-\frac{J_1}{12}\right)k^2 \\ &- \frac{1}{1152}(3J_2-5J_1+3(J_2+J_1)\cos(6\phi_k))k^4\end{aligned} \tag{4.47}$$

Both the gapless β modes display a six fold feature at the quartic level, see Fig. 4.7(a),(b). One of these dispersions (the β_2^s mode) is modified by J_2 at the quadratic level making it isotropic near the Γ point. However note that as $J_1 \to 3J_2$ the quadratic part goes to zero and six-fold features will become prominent, Fig. 4.7(b).

The other mode is the 'six-fold flat mode' which results from the interlayer interaction J_1 lifting the flat mode associated with the frustrated J_2-only kagome lattice, in a non-isotropic fashion at the quartic order in k.

In contrast and as apparent in Eq. (4.44), J_4 has quadratic contributions to both the gapless $\boldsymbol{\beta}^s$ modes resulting in an isotropic dispersion of the former flat mode, see Fig. 4.7(c),(d).

4.6 Gapping the Goldstones

The Goldstone modes are gapped by three anisotropies normally present in the chiral kagome compounds Mn_3X. Of these three, two of them: the easy plane anisotropy, characterized by K_z and the DM interaction, characterized by the vectors $\mathbf{D}_{ij}$ keep the $U(1)$ symmetry in the xy plane intact. As a result they do not gap the α_0^s mode and do not split the degeneracy of the $\boldsymbol{\beta}^s$ doublet. That is accomplished by a fairly weak local anisotropy characterized by δ. The local anisotropy axis is directed towards the nearest Sn/Ge site (at the center of the hexagon), see Fig. 4.5 (d). This breaks the $U(1)$ and gaps the α_0^s mode and splits the $\boldsymbol{\beta}^s$ doublet. The energetic separation resulting from the DM (or K_z) is an important feature of the spectrum. In its absence the local easy axis term mixes the α_0^s and $\boldsymbol{\beta}^s$ manifolds.

The interactions are given by:

$$\begin{aligned} \mathcal{U}_{\text{easy-plane}} &= K_z \sum_{n=1}^{3} (\mathbf{S}_n \cdot \mathbf{e}_z)^2 \\ \mathcal{U}_{\text{DM}} &= \frac{1}{2} \sum_{m=1}^{3} \sum_{n=1}^{3} \mathbf{D}_{mn} \cdot (\mathbf{S}_m \times \mathbf{S}_n) \\ \mathcal{U}_{\text{easy-axis}} &= -\delta \sum_{n=1}^{3} (\mathbf{S}_n \cdot \mathbf{e}_n)^2 \end{aligned} \tag{4.48}$$

where the DM vectors $\mathbf{D}_{mn} = -\mathbf{D}_{nm} = \pm D\mathbf{e}_z$ are normal to the easy plane and favour one of the two possible "vorticities" of spins on a triangle. In both Mn_3Sn and Mn_3Ge, "antivortex" states are preferred: as we move counterclockwise around

a triangle, the spins rotate clockwise.

In "antivortex" states, the local anisotropy $U_{\text{easy-axis}}$ is frustrated: the three magnetization $\mathbf{S}_i$ cannot all point along the respective easy directions. As a compromise, only one of the three sublattices is fully happy, resulting in six possible ground states for each compound.

We can express the interactions in Eq. (4.48) in terms of the symmetric normal modes $(\alpha_0^s, \boldsymbol{\alpha}^s, \beta_0^s, \boldsymbol{\beta}^s)$. The antisymmetric modes are gapped by a strong J_4.

$$\begin{aligned}
\mathcal{U}_{\text{easy-plane}} &= \frac{k_z}{2} S^2 \left[(\beta_0^s)^2 + (\boldsymbol{\beta}^s)^2 \right], \qquad (4.49)\\
\mathcal{U}_{\text{DM}} &= \frac{D}{2} S^2 \left[3\sqrt{3}(\boldsymbol{\alpha}^s)^2 + 2\sqrt{3}(\boldsymbol{\beta}^s)^2 \right],\\
\mathcal{U}_{\text{easy-axis}} &= \delta\sqrt{3} S^2 \left[\alpha_x^s \cos\left(\frac{2}{\sqrt{3}}\alpha_0^s\right) - \alpha_y^s \sin\left(\frac{2}{\sqrt{3}}\alpha_0^s\right) \right]\\
&- \frac{\delta}{4} S^2 \left[2(\alpha_x^s)^2 - 2(\alpha_y^s)^2 + (\beta_x^s)^2 - (\beta_y^s)^2 + 2\sqrt{2}\beta_0^s\beta_y^s \right] \cos\left(\frac{2}{\sqrt{3}}\alpha_0^s\right)\\
&- \frac{\delta}{2} S^2 \left[2\alpha_x^s\alpha_y^s + \beta_x^s\beta_y^s + \sqrt{2}\beta_0^s\beta_y^s \right] \sin\left(\frac{2}{\sqrt{3}}\alpha_0^s\right).
\end{aligned}$$

The full energy density at the Γ point:

$$\mathcal{U}_{\text{full}} = \mathcal{U}_{\text{exchange}} + \mathcal{U}_{\text{DM}} + \mathcal{U}_{\text{easy-axis}} + \mathcal{U}_{\text{easy-plane}} \qquad (4.50)$$

From here we proceed to calculate the gaps at the Γ point. We shall treat all the energies barring the exchange as perturbations on top of exchange. The first step is to minimize $\mathcal{U}_{\text{full}}$ and solve for the modes which are hard under exchange in terms of

the soft modes: $\alpha_x^s = \alpha_x^s(\boldsymbol{\beta}^s, \alpha_0^s)$ and same for α_y^s, and β_0^s. Then consider the theory:

$$\begin{aligned} \mathcal{L} &= \mathcal{L}_{\text{kin}} - (\mathcal{U}_{\text{DM}} + \mathcal{U}_{\text{easy-axis}} + \mathcal{U}_{\text{easy-plane}}), \\ \mathcal{L} &= \mathcal{L}^s_{\text{kin}} - \mathcal{U}_{\text{perturbation}}(\boldsymbol{\beta}^s, \alpha_0^s), \end{aligned} \tag{4.51}$$

where we only retain the symmetric part of $\mathcal{L}_{\text{kin}}$ shown in Eq. (4.40 as $\mathcal{L}^s_{\text{kin}}$. This theory can be now used to solve for the Γ point gaps in the Goldstone modes.

$$\begin{aligned} E_\alpha &= \sqrt{\frac{1}{\rho_{\alpha^s}}\left(\frac{3\delta^3}{J_{eff}^2}\right)}S, \\ E_{\beta_y} &= \sqrt{\frac{1}{\rho_{\beta^s}}\left(2\left(\sqrt{3}D + \frac{\delta}{2}\right) + \frac{\delta}{6J_{eff}}(4\sqrt{3}D - \delta)\right)}S, \\ E_{\beta_x} &= \sqrt{\frac{1}{\rho_{\beta^s}}\left(2\left(\sqrt{3}D + \frac{\delta}{2}\right) - \frac{\delta}{6J_{eff}}(4\sqrt{3}D - \delta)\right)}S, \end{aligned} \tag{4.52}$$

where $J_{eff} = J_2 + J_1$. We have also dropped the easy plane anisotropy K_z as the DM interaction itself provides an easy plane anisotropy which suffices to fit the experimental data.

We can fit the three gaps, Eq.(4.52) and the three velocities and Eq.(4.44), Eq.(4.45) using six parameters $(J_1, J_2, J_4, DM, \delta, \rho_{\alpha^s})$, see Fig. 4.5 (a,b,c). The fit values are reported in Table. 4.1.

	J_1S^2	J_2S^2	J_4S^2	DS^2	δS^2
refined value (meV)	0(6)	34(7)	$-17(5)$	0.02(1)	$\leq$0.01

Table 4.1: Microscopic parameters of the spin Hamiltonian refined for Mn_3Ge. A positive (negative) sign for the exchange parameters corresponds to AFM (FM) interactions. Note that J_1 and J_4 are inter-plane interactions (see Fig.4.6), while J_2, D and δ are intra-plane interactions.

4.7 Coupling to external fields

The study of the normal modes and their natures reveal effective ways of coupling to the magnetic order. External probes like magnetic fields couple to the spins locally, or the net spin of the plaquette and engender terms which are D_3 symmetric. These couplings are expressed in the basis of the normal modes, which represent the spin degrees of freedom. Given that the normal modes are D_3 symmetric by construction and decouple into a pair of singlets and a pair of doublets we can limit the terms that can be produced based on symmetry properties alone.

For instance, for an external magnetic field the Zeeman coupling is between two time reversal odd vectors: the magnetic field $\mathbf{B}_{\text{ext}}$ and a net spin per plaquette. The only vectors available at the linear order in fields, which are also time reversal odd are, $\mathbf{B}_{\text{ext}}$, and $\boldsymbol{\alpha}$. Hence the Zeeman term will be of the form $\mathbf{B}_{\text{ext}} \cdot (\mathcal{R}\boldsymbol{\alpha})$ where $\mathcal{R}$ is a 2-d rotation matrix, which accounts for the global $O(2)$ freedom of the spins in the xy plane.

4.7.1 Net spin in the ground state

As an explicit example of this let us look into the origin of the small ferromagnetic moment in the ground state of these compounds. We derive a Landau functional from which the size of the ferromagnetic moment resulting from spin canting due to δ can be obtained. Consider a *single kagome layer* with coplanar spins arranged in 120° order in an anticlockwise sense, and an in plane magnetic field. The energy terms we have to consider are: nearest neighbor exchange J, easy-axis anisotropy δ, and a Zeeman term.

In each of the six allowed 'antivortex' ground states the two spins that are not along the local easy axis try to align along the easy axis giving rise to a small ferromagnetic moment. This can be expressed in terms of the hard modes $\boldsymbol{\alpha}$.

$$\begin{aligned} m_x &= -\sqrt{\frac{3}{2}} S \left[\alpha_x \cos(\phi_0) - \alpha_y \sin(\phi_0)\right] \\ m_y &= \sqrt{\frac{3}{2}} S \left[\alpha_x \sin(\phi_0) + \alpha_y \cos(\phi_0)\right], \end{aligned} \tag{4.53}$$

where $\sqrt{3}\phi_0 = \alpha_0$. Note that in [62] the ground state is at $\alpha_0 \to 0$ in each triangle. Now the size of the moment depends on the values of the doublet $\boldsymbol{\alpha}$ in the ground state. To get that we start by writing down the energy density in terms of all six

modes:

$$\begin{aligned} \mathcal{U}_{\text{exchange}} &= \frac{3J}{2} S^2(\boldsymbol{\alpha})^2 \\ \mathcal{U}_{\text{Zeeman}} &= \sqrt{\frac{3}{2}} hgS \left[\alpha_x \cos(\phi_0 + \psi_h) - \alpha_y \sin(\phi_0 + \psi_h)\right] \\ \mathcal{U}_{\text{easy-axis}} &= \sqrt{\frac{3}{2}} S^2 \delta \left[\alpha_x \cos(2\phi_0) - \alpha_y \sin(2\phi_0)\right]. \end{aligned} \tag{4.54}$$

Here we have used the magnetic field $\mathbf{H} = h(\cos(\psi_h), \sin(\psi_h))$ and g is the gyromagnetic ratio. We can minimize the total energy $\mathcal{U}_{\text{total}} = \mathcal{U}_{\text{exchange}} + \mathcal{U}_{\text{Zeeman}} + \mathcal{U}_{\text{easy-axis}}$ and solve for $\boldsymbol{\alpha}$. Plugging this back into Eq. (4.53) we obtain the induced moments as:

$$\begin{aligned} m_x &= S\frac{\delta \cos(\phi_0)}{2J} + g\frac{h\cos(\psi_h)}{2J} \\ m_y &= S\frac{\delta \sin(\phi_0)}{2J} + g\frac{h\sin(\psi_h)}{2J}. \end{aligned} \tag{4.55}$$

Note the extra induced ferromagnetic moment from the anisotropy δ, above the paramagnetic component. Fro $\phi_0 = 0$ we have $\mathbf{m}_{\text{fm}} = (S\frac{\delta}{2J}, 0)$ as the ground state in [62] suggests.

4.8 Discussion

We have presented a field theory for spin waves in a hexagonal antiferromagnet with three magnetic sublattices in terms of normal modes of a spin triangle. The zero

net spin condition imposed on each triangular plaquette leads to a spin wave theory which has three Goldstone modes each with a different velocity, in the generic case. The theory decomposes into a field theory for a singlet α_0 and a doublet $\boldsymbol{\beta}$. The theory for the doublet maps to a continuum theory for elasticity with the spin wave velocities as 'sound' velocities.

We use the familiar settings of the Heisenberg antiferromagnet on the triangular and kagome lattice to demonstrate the features of the field theory. In this case, the two examples are slight outliers because of their highly symmetric lattice environment.

The triangular lattice has the $\boldsymbol{\beta}$ modes as degenerate, and in the kagome we have a degeneracy between the α_0 singlet and one of the $\boldsymbol{\beta}$ modes while the other one is zero throughout the Brillouin Zone, see Fig. 4.4. We show that the flat mode of the kagome can be anticipated from the elasticity analogy: the mechanical kagome lattice (phonons) with nearest neighbor interaction has zero shear and this property is manifest in our spin wave analog as the flat mode.

Although the spin wave analyses around the 120° ground state of both the triangular Heisenberg antiferromagnet and the kagome antiferromagnet are well documented [85, 87] their description in terms of three sub lattice field theory is absent from the literature to the best of our knowledge.

Additionally, in the case of a local D_3 symmetric environment we provide a generic construction scheme for six fold symmetric terms. This is particularly useful in presence of local anisotropies which break the $O(2)$ symmetry in the plane but keep the

six fold symmetry intact. We use this theory to describe the spin wave spectrum of Mn_3Ge, extending it to the bi-layer situation with interlayer couplings. The analytical expressions for the spin waves and the gaps are used to extract the parameters of the Mn_3Ge Hamiltonian.

The study of the normal modes and their natures reveal effective ways of coupling to the magnetic order. External probes like magnetic fields couple to the spins locally, or the net spin of the plaquette and engender terms which are D_3 symmetric. These couplings are expressed in the basis of the normal modes, which represent the spin degrees of freedom. Given that the normal modes are D_3 symmetric by construction and decouple into a pair of singlets and a pair of doublets we can limit the terms that can be produced based on symmetry properties alone.

For instance, for an external magnetic field the Zeeman coupling is between two time reversal odd vectors: the magnetic field $\mathbf{B}_{\text{ext}}$ and a net spin per plaquette. The only vectors available at the linear order in fields, which are also time reversal odd are, $\mathbf{B}_{\text{ext}}$, and $\boldsymbol{\alpha}$. Hence the Zeeman term will be of the form $\mathbf{B}_{\text{ext}} \cdot (\mathcal{R}\boldsymbol{\alpha})$ where $\mathcal{R}$ is a 2-d rotation matrix, which accounts for the global $O(2)$ freedom of the spins in the xy plane.

Since the magnetism in these materials is intricately linked to the conduction bands of the electrons, through an *s-d* coupling [97], certain features like the location of the Weyl points and, the magnitude of the anomalous Hall response [97, 96] can be manipulated through the local magnetic order. This is a promising avenue of future

work in these materials.

The emergent elasticity theory is also interesting from a more general point of view than just the present scenario, allowing a comparison of this case with other emergent elasticity theories like in Skyrmion crystals[98]. It also leaves open avenues of investigation along the lines of the duality theory developed in [47] and [99], especially since in Mn_3Ge the non collinear ground state allows a spin-phonon coupling, which might make a melting transition particularly interesting.

A detailed study of the soft modes, as provided here, is of use in spintronics where they can couple to external perturbations [100]. In the effective theory for a two sublattice antiferromagnet presented in [61], it was noted that space-time dependent external perturbations introduce gauge fields which can be used to interact with and drive solitons. A similar construction can be envisioned for the three-sublattice case where the solitons in question can be domain walls between the six-fold ground states [101].

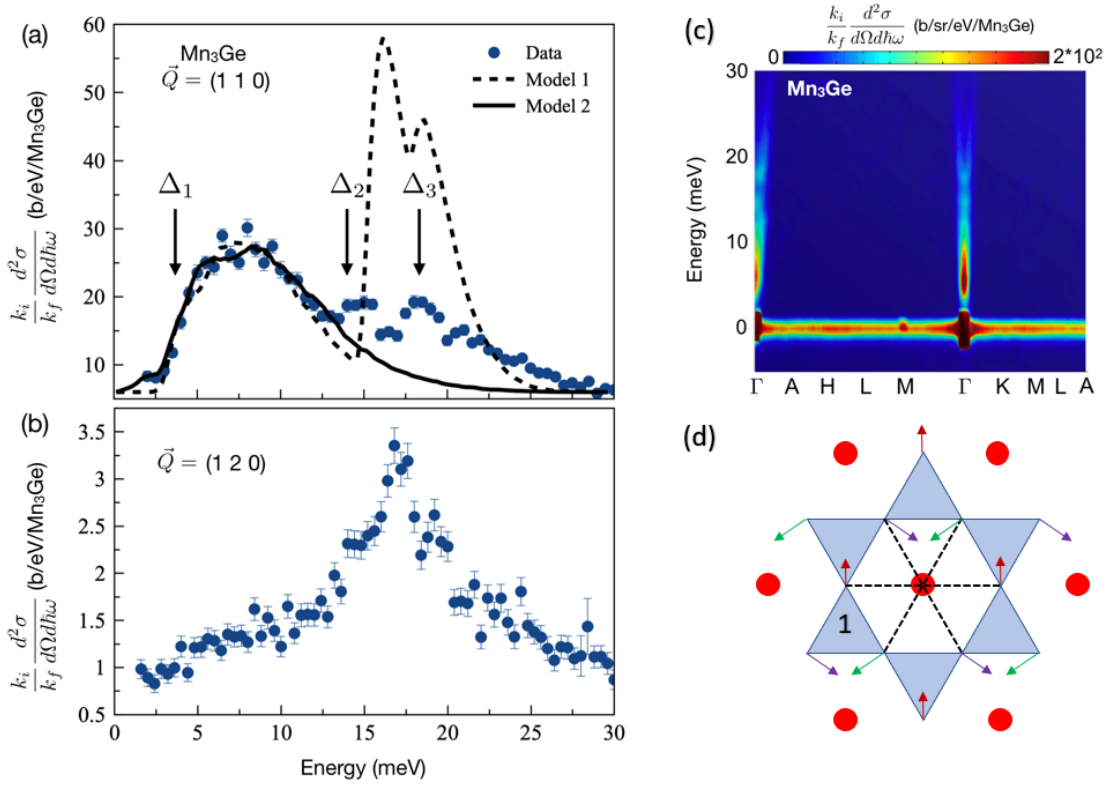

Figure 4.5: Panels (a), (b) and (c) refer to the inelastic neutron scattering experiment in Mn_3Ge [62]. In panel (a) we show the fit to the data using two sets of parameters $(J_1, J_2, J_4, D, \delta, K_z)$. Of the two models, model 1 assumes that the two smaller peaks at 15 and 18 meV are the $\boldsymbol{\beta}^s$ manifold peaks. This requires fairly large values of DM and easy axis anisotropy (δ). The second model interprets the peaks at 15-18meV as optical phonons hybridizing with the magnons. Here it turns out that the local anisotropy is very small and the $\boldsymbol{\beta}^s$ manifold is nearly degenerate and is almost pushed onto the α_0^s mode. The second model is better supported by the intensity of the peaks and by the data from panel (b) which indicates a high phonon contribution to the intensity around 15-18 meV. Panel (d) shows the local environment of the kagome layer in Mn_3X. The easy axes are marked in black dashed lines. For Mn_3Sn the spins want to align with the easy axes while for Mn_3Ge they want to align perpendicular to the easy axes. As is evident with the antichiral state only one in three sublattices can satisfy this requirement this gives rise to six equivalent ground states: each sublattice and its time reversed partner contributing once.

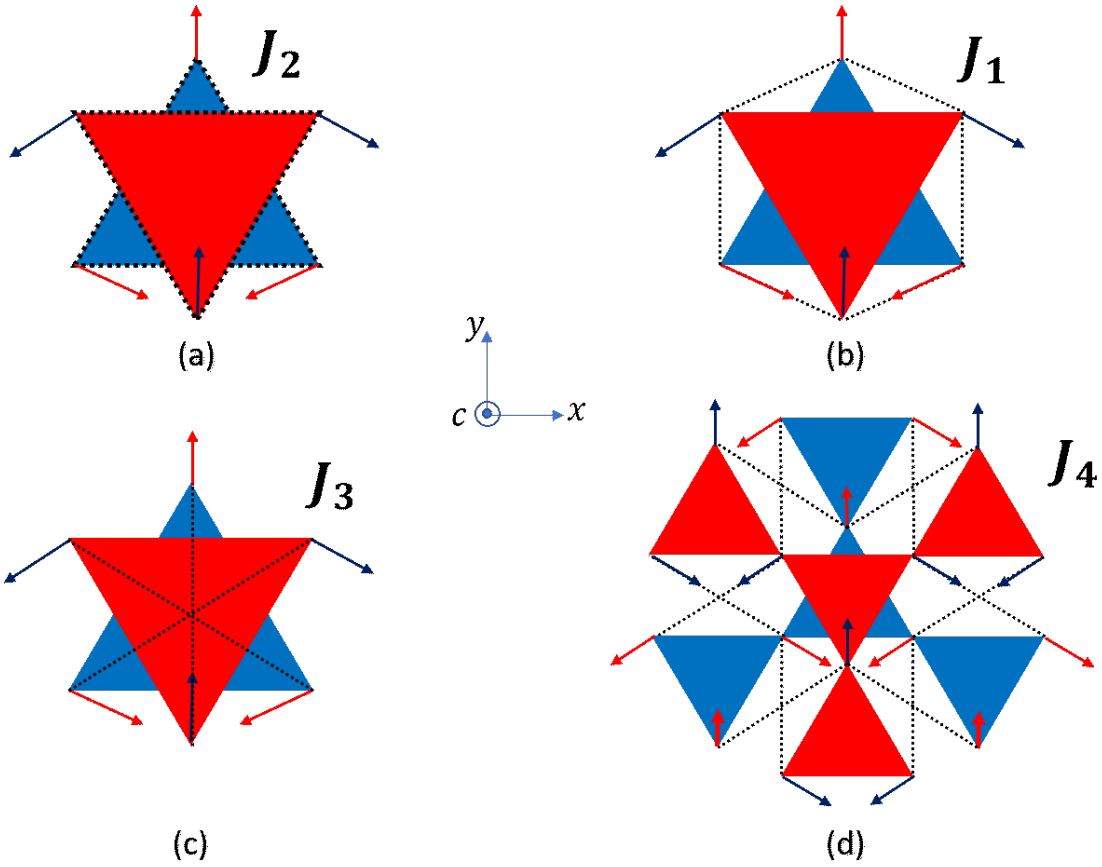

Figure 4.6: Heisenberg exchange interactions in Mn_3Ge, shown as dashed lines: intralayer exchange J_2 (a) and interlayer exchanges J_1 (b), J_3 (c), and J_4 (d).

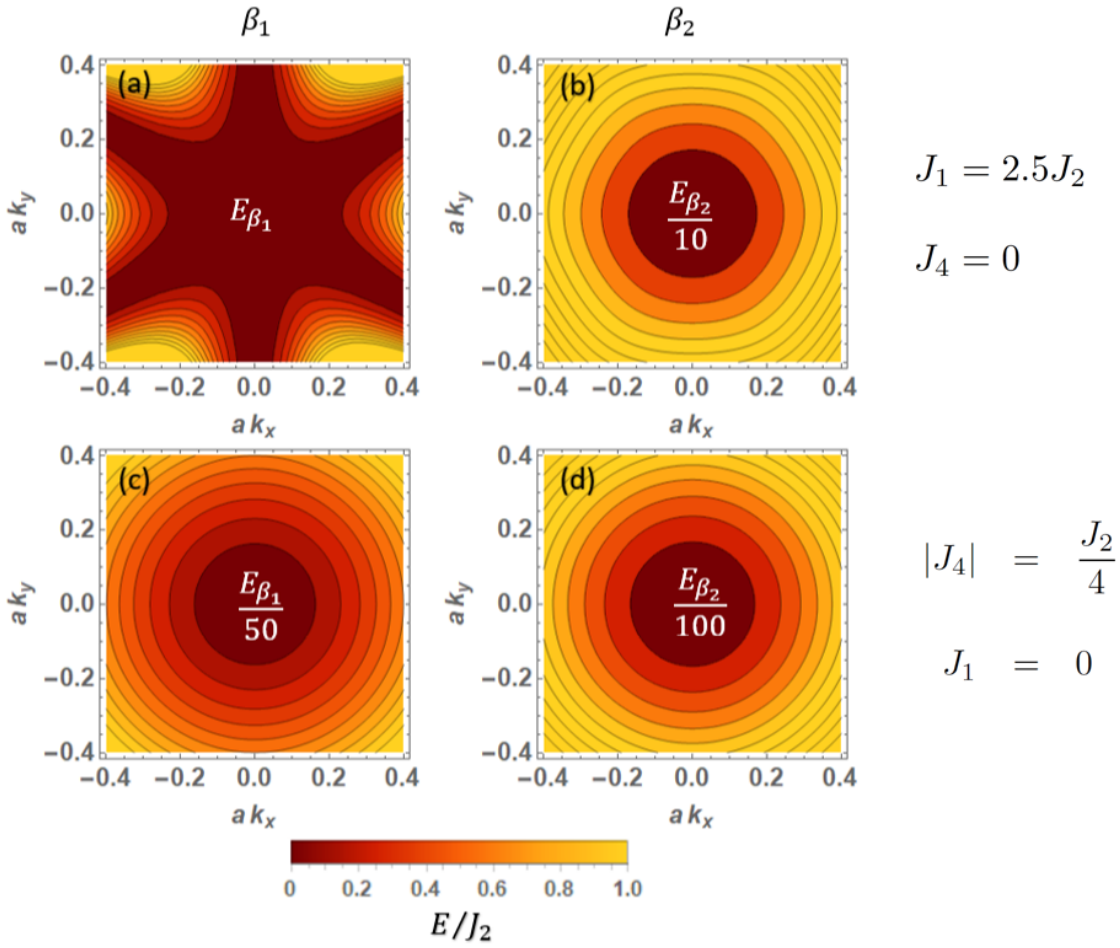

Figure 4.7: Color plots for the dispersions of the $\boldsymbol{\beta}$ doublet with an antiferromagnetic (J_2, J_1) and ferromagnetic J_4. **Upper panels**: show the dispersions for the β^s modes with $J_1 = 2.5\ J_2$, and $J_4 = 0$. We can clearly see the six fold pattern in both cases. *Left* : The dispersion for the $c_\perp^S$ mode the flat lines represent directions in the k-space for which $c_\perp^S = 0$. *Right*: The dispersion for the $c_{||}^S$ mode. There are no flat directions but a six fold pattern is prominent. **Lower panels**: show the dispersions for β^s modes with $J_2 = 4|J_4|$, and $J_1 = 0$ with $c_\perp^S$ mode on the left and $c_{||}^S$ mode on the right. Both modes are isotropic and there are no flat directions.

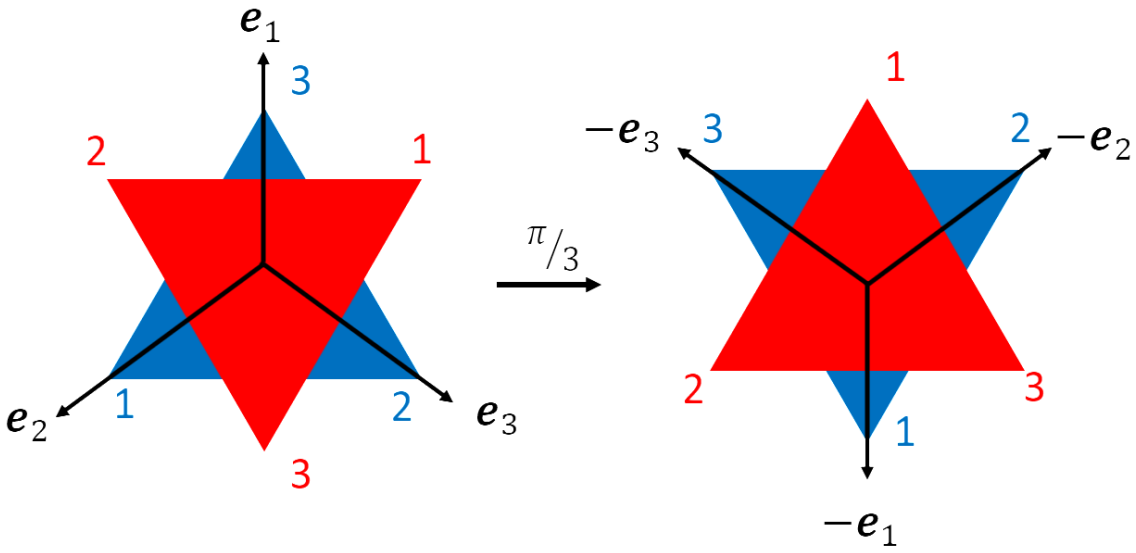

Figure 4.8: This figure shows how a 120° symmetric term converts to a 60° term for the central David's star motif in Mn_3X. Here we choose the three unit vectors $\mathbf{e}_1$, $\mathbf{e}_2$, $\mathbf{e}_3$ along highly symmetric directions for purposes of illustration. It is clear that after a $\frac{\pi}{3}$ rotation the blue and red (up and down) modes are interchanged and the unit vector axes are reversed. Note that the cyclic permutation of labels caused by the rotation is absorbed into the summation over the labels in Eq. (4.22).

Chapter 5

Discussion

In this thesis we have discussed the field theories of magnetically ordered systems. We started with the planar ferromagnet defined on the xy plane. We showed that this system can be mapped to a theory of electromagnetism in two spatial and one time dimension. We also show how the magnetic vortices under the same mapping become electric charges with a magnetic flux attached to their cores. This charge-flux mapping leads to the notion of a modified quantum statistics of these dual particles where they can interpolate between a boson and a fermion depending on the spin-length (integer or half-integer) of the magnetic lattice.

We then moved onto a discussion of the two sublattice antiferromagnetic system. Here we showed that the a gauge like addition to the Lagrangian can be made by introducing an external magnetic field or a finite DM interaction. This creates a local magnetization density in the antiferromagnet producing a gyrotropic tensor density.

We also show how using this induced gyrotropic term we can produce a Magnus force on an antiferromagnetic vortex using a spin current. This, as far as we know, is the first example of this phenomena.

Lastly we discuss in detail the three sublattice antiferromagnet. Here we construct the spin wave theory for the general three sublattice antiferromagnet with 120° ordered spins. The theory contains three Goldstone modes which are grouped into a scalar mode and a vector (in xy space) mode. Intriguingly we notice that the theory for the vector mode maps to an emergent theory of elasticity in (t, x, y). We use our theory to obtain the analytical expressions for the spin wave velocities in Mn_3Ge. This was used in conjunction with inelastic neutron scattering data to fit the spin Hamiltonian for Mn_3Ge. We end by proving a general outlook of how external probes can couple to the system and distort the order.

Bibliography

[1] Lucretius, *The Nature of Things*. Penguin Classics, 2007.

[2] J. C. Maxwell, *A Treatise on Electricity and Magnetism*. Oxford University Press Warehouse, 1881.

[3] E. Fradkin and M. Stone, "Topological terms in one- and two-dimensional quantum heisenberg antiferromagnets," *Phys. Rev. B*, vol. 38, pp. 7215–7218, Oct 1988. [Online]. Available: https://link.aps.org/doi/10.1103/PhysRevB.38.7215

[4] R. Shankar, *Quantum Field Theory And Condensed Matter: An Introduction*. Cambridge: Cambridge University Press, 2017.

[5] S. S. P. Parkin, M. Hayashi, and L. Thomas, "Magnetic domain-wall racetrack memory," *Science*, vol. 320, no. 5873, pp. 190–194, 2008.

[6] A. A. Thiele, "Steady-state motion of magnetic domains," *Phys. Rev. Lett.*, vol. 30, pp. 230–233, Feb 1973.

[7] N. Majlis, *The quantum theory of magnetism*. World Scientific, 2000.

[8] W. Heisenberg, "Mehrkrperproblem und resonanz in der quantenmechanik," *Z. Phys*, vol. 38, pp. 411–426, 1926.

[9] P. A. M. Dirac, "Quantum mechanics of many-electron systems," *Proc. Roy. Soc (London) A*, vol. 123, pp. 714–733, 1929.

[10] H. A. Kramers, "L'interaction Entre les Atomes Magnétogènes dans un Cristal Paramagnétique," *Physica*, vol. 1, no. 1, pp. 182–192, Jan. 1934.

[11] P. W. Anderson, "Antiferromagnetism. theory of superexchange interaction," *Phys. Rev.*, vol. 79, pp. 350–356, Jul 1950.

[12] ——, "The resonating valence bond state in la_2cuo_4 and superconductivity," *Science*, vol. 235, no. 4793, pp. 1196–1198, 1987.

[13] J. D. Jackson, *Classical Electrodynamics*, 2nd ed. New York: Wiley, 1975.

[14] I. Dzyaloshinsky, "A thermodynamic theory of "weak" ferromagnetism of antiferromagnetics," *Journal of Physics and Chemistry of Solids*, vol. 4, no. 4, pp. 241 – 255, 1958.

[15] T. Moriya, "Anisotropic superexchange interaction and weak ferromagnetism," *Phys. Rev.*, vol. 120, pp. 91–98, Oct 1960.

[16] X. Z. Yu, Y. Onose, N. Kanazawa, J. H. Park, J. H. Han, Y. Matsui, N. Nagaosa,

and Y. Tokura, "Real-space observation of a two-dimensional skyrmion crystal," *Nature*, vol. 465, no. 7300, pp. 901–904, Jun 2010.

[17] N. D. Mermin, "The topological theory of defects in ordered media," *Rev. Mod. Phys.*, vol. 51, pp. 591–648, Jul 1979.

[18] D. J. Clarke, O. A. Tretiakov, G.-W. Chern, Y. B. Bazaliy, and O. Tchernyshyov, "Dynamics of a vortex domain wall in a magnetic nanostrip: Application of the collective-coordinate approach," *Phys. Rev. B*, vol. 78, p. 134412, Oct 2008.

[19] O. Tchernyshyov, "Conserved momenta of a ferromagnetic soliton," *Annals of Physics*, vol. 363, pp. 98 – 113, 2015.

[20] S. Dasgupta and O. Tchernyshyov, "Energy-momentum tensor of a ferromagnet," *Phys. Rev. B*, vol. 98, p. 224401, Dec 2018. [Online]. Available: https://link.aps.org/doi/10.1103/PhysRevB.98.224401

[21] L. LANDAU and E. LIFSHITZ, "3 - on the theory of the dispersion of magnetic permeability in ferromagnetic bodiesreprinted from physikalische zeitschrift der sowjetunion 8, part 2, 153, 1935." pp. 51 – 65, 1992.

[22] T. L. Gilbert, "A phenomenological theory of damping in ferromagnetic materials," *IEEE Transactions on Magnetics*, vol. 40, no. 6, pp. 3443–3449, 2004.

[23] M. J. Donahue and D. G. Porter, "Oommf user's guide, version

1.0," NIST, Tech. Rep. NISTIR 6376, 1999. [Online]. Available: https://math.nist.gov/oommf

[24] A. Ghosh, K. S. Huang, and O. Tchernyshyov, "Annihilation of domain walls in a ferromagnetic wire," *Phys. Rev. B*, vol. 95, p. 180408, May 2017.

[25] J. Slonczewski, "Current-driven excitation of magnetic multilayers," *Journal of Magnetism and Magnetic Materials*, vol. 159, no. 1, pp. L1 – L7, 1996.

[26] L. Berger, "Emission of spin waves by a magnetic multilayer traversed by a current," *Phys. Rev. B*, vol. 54, pp. 9353–9358, Oct 1996.

[27] A. Altland and B. Simons, *Condensed matter field theory*, 2nd ed. Cambridge: Cambridge University Press, 2010.

[28] N. Nagaosa and Y. Tokura, "Topological properties and dynamics of magnetic skyrmions," *Nature Nanotechnology*, vol. 8, no. 12, pp. 899–911, Dec 2013.

[29] S. Dasgupta, S. Zhang, I. Bah, and O. Tchernyshyov, "Quantum statistics of vortices from a dual theory of the xy ferromagnet," *Phys. Rev. Lett.*, vol. 124, p. 157203, Apr 2020. [Online]. Available: https://link.aps.org/doi/10.1103/PhysRevLett.124.157203

[30] J. M. Kosterlitz, "The critical properties of the two-dimensional xy model," *J. Phys. C*, vol. 7, pp. 1046–1060, 1974.

[31] M. E. Peskin, "Mandelstam-'t hooft duality in abelian lattice models," *Ann. Phys.*, vol. 113, pp. 122–152, 1978.

[32] M. P. A. Fisher and D. H. Lee, "Correspondence between two-dimensional bosons and a bulk superconductor in a magnetic field," *Phys. Rev. B*, vol. 39, pp. 2756–2759, Feb 1989.

[33] R. Y. Chiao, A. Hansen, and A. A. Moulthrop, "Fractional statistics of the vortex in two-dimensional superfluids," *Phys. Rev. Lett.*, vol. 54, pp. 1339–1342, Apr 1985.

[34] A. Hansen, A. A. Moulthrop, and R. Y. Chiao, "n-dependent fractional statistics of n vortices," *Phys. Rev. Lett.*, vol. 55, pp. 1431–1434, Sep 1985.

[35] F. D. M. Haldane and Y.-S. Wu, "Quantum dynamics and statistics of vortices in two-dimensional superfluids," *Phys. Rev. Lett.*, vol. 55, pp. 2887–2890, Dec 1985.

[36] T. Shinjo, T. Okuno, R. Hassdorf, K. Shigeto, and T. Ono, "Magnetic vortex core observation in circular dots of permalloy," *Science*, vol. 289, p. 930, 2000.

[37] A. Wachowiak, J. Wiebe, M. Bode, O. Pietzsch, M. Morgenstern, and R. Wiesendanger, "Direct observation of internal spin structure of magnetic vortex cores," *Science*, vol. 298, pp. 577–580, 2002.

[38] A. A. Thiele, "Steady-state motion of magnetic domains," *Phys. Rev.*

Lett., vol. 30, pp. 230–233, Feb 1973. [Online]. Available: https://link.aps.org/doi/10.1103/PhysRevLett.30.230

[39] D. L. Huber, "Dynamics of spin vortices in two-dimensional planar magnets," *Phys. Rev. B*, vol. 26, pp. 3758–3765, Oct 1982.

[40] S.-B. Choe, Y. Acremann, A. Scholl, A. Bauer, A. Doran, J. Stöhr, and H. A. Padmore, "Vortex Core-Driven Magnetization Dynamics," *Science*, vol. 304, pp. 420–422, apr 2004.

[41] O. A. Tretiakov and O. Tchernyshyov, "Vortices in thin ferromagnetic films and the skyrmion number," *Phys. Rev. B*, vol. 75, p. 012408, Jan 2007.

[42] F. Wilczek, "Magnetic flux, angular momentum, and statistics," *Phys. Rev. Lett.*, vol. 48, pp. 1144–1146, Apr 1982.

[43] ——, "Quantum mechanics of fractional-spin particles," *Phys. Rev. Lett.*, vol. 49, pp. 957–959, Oct 1982.

[44] A. V. Nikiforov and E. B. Sonin, "Dynamics of magnetic vortices in a planar ferromagnet," *Sov. Phys. JETP*, vol. 58, no. 2, pp. 373–378, Aug. 1983.

[45] F. Hellman, A. Hoffmann, Y. Tserkovnyak, G. S. D. Beach, E. E. Fullerton, C. Leighton, A. H. MacDonald, D. C. Ralph, D. A. Arena, H. A. Dürr, P. Fischer, J. Grollier, J. P. Heremans, T. Jungwirth, A. V. Kimel, B. Koopmans, I. N. Krivorotov, S. J. May, A. K. Petford-Long, J. M. Rondinelli, N. Samarth,

I. K. Schuller, A. N. Slavin, M. D. Stiles, O. Tchernyshyov, A. Thiaville, and B. L. Zink, "Interface-induced phenomena in magnetism," *Rev. Mod. Phys.*, vol. 89, p. 025006, Jun 2017.

[46] C. W. Misner, K. S. Thorne, and J. A. Wheeler, *Gravitation*. New York: Freeman, 1973.

[47] M. Pretko and L. Radzihovsky, "Fracton-elasticity duality," *Phys. Rev. Lett.*, vol. 120, p. 195301, May 2018. [Online]. Available: https://link.aps.org/doi/10.1103/PhysRevLett.120.195301

[48] D. Tong, "Lectures on gauge theory," lecture notes, 2018. [Online]. Available: http://www.damtp.cam.ac.uk/user/tong/gaugetheory.html

[49] N. Papanicolaou and T. N. Tomaras, "Dynamics of magnetic vortices," *Nucl. Phys. B*, vol. 360, no. 2-3, pp. 425–462, 1991.

[50] V. G. Bar'yakhtar, M. V. Chetkin, B. A. Ivanov, and S. N. Gadetskii, *Dynamics of Topological Magnetic Solitons*, ser. Springer Tracts in Modern Physics. Berlin: Springer, 1994, vol. 129.

[51] B. A. Ivanov, H. J. Schnitzer, F. G. Mertens, and G. M. Wysin, "Magnon modes and magnon-vortex scattering in two-dimensional easy-plane ferromagnets," *Phys. Rev. B*, vol. 58, pp. 8464–8474, Oct 1998.

[52] We owe this idea to one of the referees of this paper.

[53] A. Y. Galkin and B. A. Ivanov, "Semiclassical dynamics of vortices in 2D easy-plane ferromagnets," *J. Exp. Theor. Phys.*, vol. 104, no. 5, pp. 775–791, May 2007.

[54] B. A. Ivanov, E. G. Galkina, and A. Y. Galkin, "Quantum dynamics of vortices in small magnetic particles," *Low Temp. Phys.*, vol. 36, no. 8, pp. 747–751, Aug. 2010.

[55] R. Takashima, H. Ishizuka, and L. Balents, "Quantum skyrmions in two-dimensional chiral magnets," *Phys. Rev. B*, vol. 94, p. 134415, Oct 2016.

[56] H. Watanabe and H. Murayama, "Noncommuting momenta of topological solitons," *Phys. Rev. Lett.*, vol. 112, p. 191804, May 2014.

[57] O. Tchernyshyov, "Conserved momenta of a ferromagnetic soliton," *Ann. Phys.*, vol. 363, pp. 98–113, Oct. 2015.

[58] J. Preskill, "Quantum computation," lecture notes, 2004. [Online]. Available: http://theory.caltech.edu/~preskill/ph219/

[59] P. W. Anderson, "An approximate quantum theory of the antiferromagnetic ground state," *Phys. Rev.*, vol. 86, pp. 694–701, Jun 1952.

[60] F. D. M. Haldane, "Nonlinear field theory of large-spin heisenberg antiferromagnets: Semiclassically quantized solitons of the one-dimensional easy-axis néel state," *Phys. Rev. Lett.*, vol. 50, pp. 1153–1156, Apr 1983.

[61] S. Dasgupta, S. K. Kim, and O. Tchernyshyov, "Gauge fields and related forces in antiferromagnetic soliton physics," *Phys. Rev. B*, vol. 95, p. 220407, Jun 2017. [Online]. Available: https://link.aps.org/doi/10.1103/PhysRevB.95.220407

[62] Y. Chen, J. Gaudet, S. Dasgupta, G. G. Marcus, J. Lin, T. Chen, T. Tomita, M. Ikhlas, Y. Zhao, W. C. Chen, M. B. Stone, O. Tchernyshyov, S. Nakatsuji, and C. Broholm, "Antichiral spin order, its soft modes, and their hybridization with phonons in the topological semimetal mn_3ge," *Phys. Rev. B*, vol. 102, p. 054403, Aug 2020. [Online]. Available: https://link.aps.org/doi/10.1103/PhysRevB.102.054403

[63] S. Dasgupta and O. Tchernyshyov, "Theory of spin waves in a hexagonal antiferromagnet," *Phys. Rev. B*, vol. 102, p. 144417, Oct 2020. [Online]. Available: https://link.aps.org/doi/10.1103/PhysRevB.102.144417

[64] T. Jungwirth, X. Marti, P. Wadley, and J. Wunderlich, "Antiferromagnetic spintronics," *Nat. Nano.*, vol. 11, no. 3, pp. 231–241, 03 2016.

[65] S. K. Kim, Y. Tserkovnyak, and O. Tchernyshyov, "Propulsion of a domain wall in an antiferromagnet by magnons," *Phys. Rev. B*, vol. 90, p. 104406, Sep 2014.

[66] E. G. Tveten, A. Qaiumzadeh, O. A. Tretiakov, and A. Brataas, "Staggered dynamics in antiferromagnets by collective coordinates," *Phys. Rev. Lett.*, vol. 110, p. 127208, Mar 2013.

[67] F. D. M. Haldane, "Nonlinear field theory of large-spin heisenberg antiferromagnets: Semiclassically quantized solitons of the one-dimensional easy-axis néel state," *Phys. Rev. Lett.*, vol. 50, pp. 1153–1156, Apr 1983.

[68] A. M. Kosevich, B. A. Ivanov, and A. S. Kovalev, "Magnetic solitons," *Phys. Rep.*, vol. 194, no. 3-4, pp. 117–238, 1990.

[69] E. G. Tveten, A. Qaiumzadeh, O. A. Tretiakov, and A. Brataas, "Staggered dynamics in antiferromagnets by collective coordinates," *Phys. Rev. Lett.*, vol. 110, p. 127208, Mar 2013.

[70] A. A. Thiele, "Steady-state motion of magnetic domains," *Phys. Rev. Lett.*, vol. 30, pp. 230–233, Feb 1973.

[71] G. E. Volovik, "Linear momentum in ferromagnets," *J. Phys.: Condens. Matter*, vol. 20, no. 7, pp. L83–L87, 1987.

[72] S. A. Yang, G. S. D. Beach, C. Knutson, D. Xiao, Q. Niu, M. Tsoi, and J. L. Erskine, "Universal electromotive force induced by domain wall motion," *Phys. Rev. Lett.*, vol. 102, p. 067201, Feb 2009.

[73] S. K. Kim, Y. Tserkovnyak, and O. Tchernyshyov, "Propulsion of a domain wall in an antiferromagnet by magnons," *Phys. Rev. B*, vol. 90, p. 104406, Sep 2014.

[74] O. Gomonay, M. Kläui, and J. Sinova, "Manipulating antiferromagnets with

magnetic fields: Ratchet motion of multiple domain walls induced by asymmetric field pulses," *Appl. Phys. Lett.*, vol. 109, no. 14, p. 142404, 2016.

[75] S. E. Barnes and S. Maekawa, "Generalization of faraday's law to include nonconservative spin forces," *Phys. Rev. Lett.*, vol. 98, p. 246601, Jun 2007.

[76] K. M. D. Hals, Y. Tserkovnyak, and A. Brataas, "Phenomenology of current-induced dynamics in antiferromagnets," *Phys. Rev. Lett.*, vol. 106, p. 107206, Mar 2011.

[77] G. Tatara, H. Kohno, and J. Shibata, "Microscopic approach to current-driven domain wall dynamics," *Phys. Rep.*, vol. 468, no. 6, pp. 213–301, 2008.

[78] B. A. Ivanov and D. D. Sheka, "Dynamics of vortices and their contribution to the response functions of classical quasi-two-dimensional easy-plane antiferromagnet," *Phys. Rev. Lett.*, vol. 72, pp. 404–407, Jan 1994.

[79] O. A. Tretiakov, D. Clarke, G.-W. Chern, Y. B. Bazaliy, and O. Tchernyshyov, "Dynamics of domain walls in magnetic nanostrips," *Phys. Rev. Lett.*, vol. 100, p. 127204, Mar 2008.

[80] K. D. Belashchenko, O. Tchernyshyov, A. A. Kovalev, and O. A. Tretiakov, "Magnetoelectric domain wall dynamics and its implications for magnetoelectric memory," *Appl. Phys. Lett.*, vol. 108, no. 13, p. 132403, 2016.

[81] M. Zhu, C. L. Dennis, and R. D. McMichael, "Temperature dependence of

magnetization drift velocity and current polarization in $ni_{80}fe_{20}$ by spin-wave doppler measurements," *Phys. Rev. B*, vol. 81, p. 140407, Apr 2010.

[82] A. Aharoni, *Introduction to the Theory of Magnetism*, 1st ed. Oxford: Oxford University Press, 1996.

[83] H. Georgi, *Lie Algebras In Particle Physics*, 2nd ed. Boca Raton, Fl: CRC Press, 1999.

[84] T. Dombre and N. Read, "Absence of the hopf invariant in the long-wavelength action of two-dimensional quantum antiferromagnets," *Phys. Rev. B*, vol. 38, pp. 7181–7183, Oct 1988.

[85] ——, "Nonlinear σ models for triangular quantum antiferromagnets," *Phys. Rev. B*, vol. 39, pp. 6797–6801, Apr 1989.

[86] F. D. M. Haldane, "" physics" and quantum spin chains (abstract)," *J. Appl. Phys.*, vol. 57, no. 8, pp. 3359–3359, 1985.

[87] A. V. Chubukov, S. Sachdev, and T. Senthil, "Large-s expansion for quantum antiferromagnets on a triangular lattice," *J. Phys.: Condens. Mat.*, vol. 6, no. 42, pp. 8891–8902, Jan. 1999.

[88] A. B. Harris, C. Kallin, and A. J. Berlinsky, "Possible néel orderings of the kagomé antiferromagnet," *Phys. Rev. B*, vol. 45, pp. 2899–2919, Feb 1992.

[89] K. Matan, D. Grohol, D. G. Nocera, T. Yildirim, A. B. Harris, S. H. Lee, S. E. Nagler, and Y. S. Lee, "Spin waves in the frustrated kagomé lattice antiferromagnet kfe$_3$(OH)$_6$(so$_4$)$_2$," *Phys. Rev. Lett.*, vol. 96, p. 247201, Jun 2006.

[90] F. C. Coomer, A. Harrison, G. S. Oakley, J. Kulda, J. R. Stewart, J. A. Stride, B. Fåk, J. W. Taylor, and D. Visser, "Inelastic neutron scattering study of magnetic excitations in the kagome antiferromagnet potassium jarosite," *Journal of Physics: Condensed Matter*, vol. 18, no. 39, pp. 8847–8858, sep 2006. [Online]. Available: https://iopscience.iop.org/article/10.1088/0953-8984/18/39/015

[91] J. C. Maxwell, "L. on the calculation of the equilibrium and stiffness of frames," *Phil. Mag.*, vol. 27, no. 182, pp. 294–299, 1864.

[92] K. Sun, A. Souslov, X. Mao, and T. C. Lubensky, "Surface phonons, elastic response, and conformal invariance in twisted kagome lattices," *PNAS*, vol. 109, no. 31, pp. 12 369–12 374, 2012.

[93] X. Mao and T. C. Lubensky, "Coherent potential approximation of random nearly isostatic kagome lattice," *Phys. Rev. E*, vol. 83, p. 011111, Jan 2011.

[94] S. Tomiyoshi and Y. Yamaguchi, "Magnetic structure and weak ferromagnetism of mn3sn studied by polarized neutron diffraction," *J. Phys. Soc. Jpn*, vol. 51, no. 8, pp. 2478–2486, 1982.

[95] P. J. Brown, V. Nunez, F. Tasset, J. B. Forsyth, and P. Radhakrishna, "Determination of the magnetic structure of mn3sn using generalized neutron polarization analysis," *J. Phys.: Condens. Mat.*, vol. 2, no. 47, pp. 9409–9422, nov 1990.

[96] S. Nakatsuji, N. Kiyohara, and T. Higo, "Large anomalous Hall effect in a non-collinear antiferromagnet at room temperature," *Nature*, vol. 527, no. 7577, pp. 212–215, 2015.

[97] J. Liu and L. Balents, "Anomalous hall effect and topological defects in antiferromagnetic weyl semimetals: mn_3Sn/Ge," *Phys. Rev. Lett.*, vol. 119, p. 087202, Aug 2017.

[98] O. Petrova and O. Tchernyshyov, "Spin waves in a skyrmion crystal," *Phys. Rev. B*, vol. 84, p. 214433, Dec 2011. [Online]. Available: https://link.aps.org/doi/10.1103/PhysRevB.84.214433

[99] M. Pretko and L. Radzihovsky, "Symmetry-enriched fracton phases from supersolid duality," *Phys. Rev. Lett.*, vol. 121, p. 235301, Dec 2018. [Online]. Available: https://link.aps.org/doi/10.1103/PhysRevLett.121.235301

[100] E. V. Gomonay and V. M. Loktev, "Spintronics of antiferromagnetic systems (review article)," *Low Temp. Phys.*, vol. 40, no. 1, pp. 17–35, 2014.

[101] Y. Yamane, O. Gomonay, and J. Sinova, "Dynamics of noncollinear

antiferromagnetic textures driven by spin current injection," *Phys. Rev. B*, vol. 100, p. 054415, Aug 2019. [Online]. Available: https://link.aps.org/doi/10.1103/PhysRevB.100.054415

Vita

Sayak Dasgupta received his M.Sc. degree in physics from the Indian Institute of Technology, Kanpur in 2015, and enrolled in the Physics Ph.D. program at Johns Hopkins University. He received the Malcolm H. Laucheimer Endowed Graduate Fellowship in 2011 and the GMAG Student Travel Award for the 2019 March Meeting in Boston. His research focuses on the study of micromagnetic theory as applicable to antiferromagnetic solions and spin wave theory in antiferromagnets. Starting in September 2020, he will join a collaboration between Prof Marcel Franz at the University of British Columbia and Prof. Masaki Oshikawa at the University of Tokyo as an MPI-UBC-UTokyo post doctoral fellow. He will continue his work on strongly correlated systems in this position.